Aus der Medizinischen Universitätsklinik und Poliklinik Tübingen
Abteilung VIII, Medizinische Onkologie und Pneumologie

Improvement of Therapeutic Anti-Cancer Strategies by Combination of Oncolytic Vaccinia Virus GLV-1h68 with Epigenetic Modulating Agents

Inaugural-Dissertation
zur Erlangung des Doktorgrades
der Medizin

der Medizinischen Fakultät
der Eberhard Karls Universität
zu Tübingen

vorgelegt von

Köllhofer, Luisa Anne

2020

Dekan:	Professor Dr. I. B. Autenrieth
1. Berichterstatter:	Professor Dr. U. Lauer
2. Berichterstatter:	Professor Dr. F. Stubenrauch
Tag der Disputation:	12.12.2019

To my beloved parents

Table of contents

1. Introduction

1.1 Cancer

As reported by the World Health Organization (WHO) 8.8 million people died from cancer worldwide in 2015 and thus cancer is the second leading cause of death after cardiovascular diseases. The incidence of cancer rose from 12.7 million in 2008 to 14.1 million in 2012. It is presumed that the number of new cases will increase by more than 70% in the upcoming 2 decades, bringing the number of cancer cases close to 25 million [1].

Cancer is a disease caused by different genetic abnormalities, like gene mutations or chromosomal changes, which result in loss of function in tumor-suppressor genes or gain of function in oncogenes [2]. Furthermore, also epigenetic alterations have been considered as being causative for the onset of cancer [3].

The routine treatments of cancer are surgery, chemotherapy and radiotherapy, which can be used in a single or combined application. There are further treatment options for different cancer entities available, such as immunotherapy or hormonal therapy.

The development of new therapy options for cancer is an important and also necessary task of current medical research. Depending on the type of cancer, therapy options are often quite limited; thus it is indispensable to search for new therapy options, which have a better efficacy, an improved selectivity towards malignancies, good safety aspects and less adverse effects, respectively.

Virotherapy represents a promising new strategy for human cancer therapy. Oncolytic viruses are capable of infecting selectively cancer cells, leading to cell death while normal cells remain undamaged [4]. Oncolysis describes the lysis or breakdown of cells caused by chemical or physical action, in this case, viral replication within cancer cells. Consequently, the great production of virus progeny leads to cell lysis and viral spread, thereby rolling out a wave of new infection rounds into neighboring, hitherto uninfected cancer cells (Figure 2).

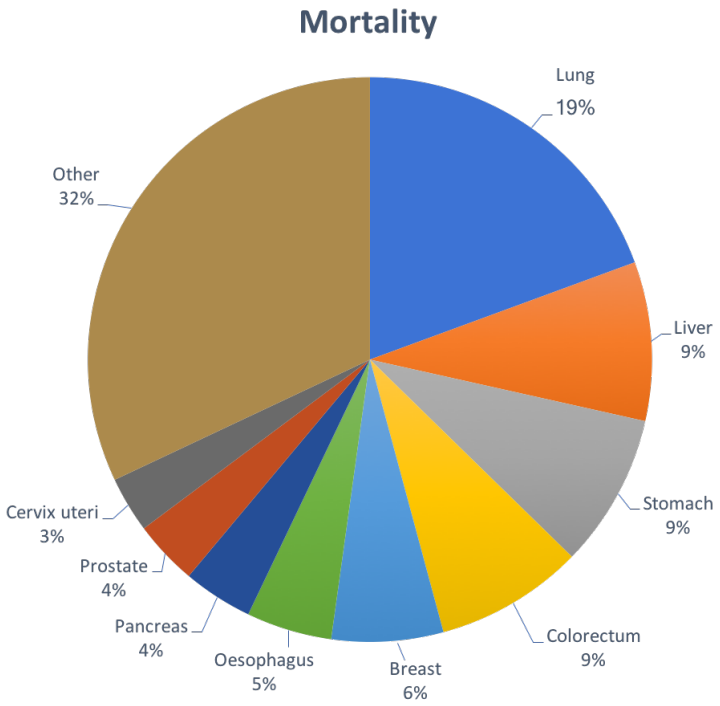

Figure 1. Cancer related deaths in 2012 worldwide in both sexes combined. Data based on the WHO world cancer report 2014 [1].

1.1.1 Colorectal cancer

Colorectal cancer (CRC) is the third most common cancer and third leading cause of cancer-related death among men and women, with a continuous increase in incidence after the age of 50 [5]. Predisposing factors are colorectal adenomas, family history with a first-degree relative, hereditary syndromes, such as familial adenomatous polyposis (100% risk by age of 40) or hereditary nonpolyposis colorectal cancer (80% progress to CRC), inflammatory bowel diseases for example ulcerative colitis or Crohn's disease. Dietary factors and lifestyle also play an important role. Among the risk factors for colorectal cancer are smoking, alcohol consumption and obesity [6, 7].

The preferred treatment option is the surgical resection of colorectal cancers and their metastases. The resection is complemented by adjuvant chemo-therapy. Biologicals, such as anti-VEGF (vascular endothelial growth factor) antibodies or anti-EGFR (epidermal growth factor receptor) antibodies can be

added to the chemotherapy for metastatic disease [8, 9]. According to the American cancer society, the average 5-year-survival rate between 2007 and 2013 was 64.9%, depending on the stage of cancer (American Cancer Society. Colorectal Cancer Facts & Figures 2017-2019).

1.1.2 Renal cell adenocarcinoma

Renal cell adenocarcinoma (RCC) is the most common cause for renal malignancies in adults. About 4 % are associated with hereditary disorders, but most of the cases are sporadic. Important risk factors include smoking, renal pelvic stones, acquired cystic disease of the kidney, obesity, hypertension and exposure to certain toxins, such as cadmium. The treatment of choice is the surgical resection of the tumor and metastases. The majority of small RCC can be cured by surgical resection [10]. RCCs are infamously resistant to chemo-therapeutic agents. This is due to the fact that tumor cells express MDR-1 (multidrug resistance protein-1). Thus, immunomodulatory or targeted therapy, e.g. Interferon-α, recombinant cytokines (interleukin-2), or tyrosine kinase inhibitors (sorafenib, sunitinib, pazopanib), are the treatment options for the metastatic disease [11]. The relative 5-year-survival rate is between 65 and 75%, depending on the histological subtype [12].

1.2 Oncolytic virotherapy

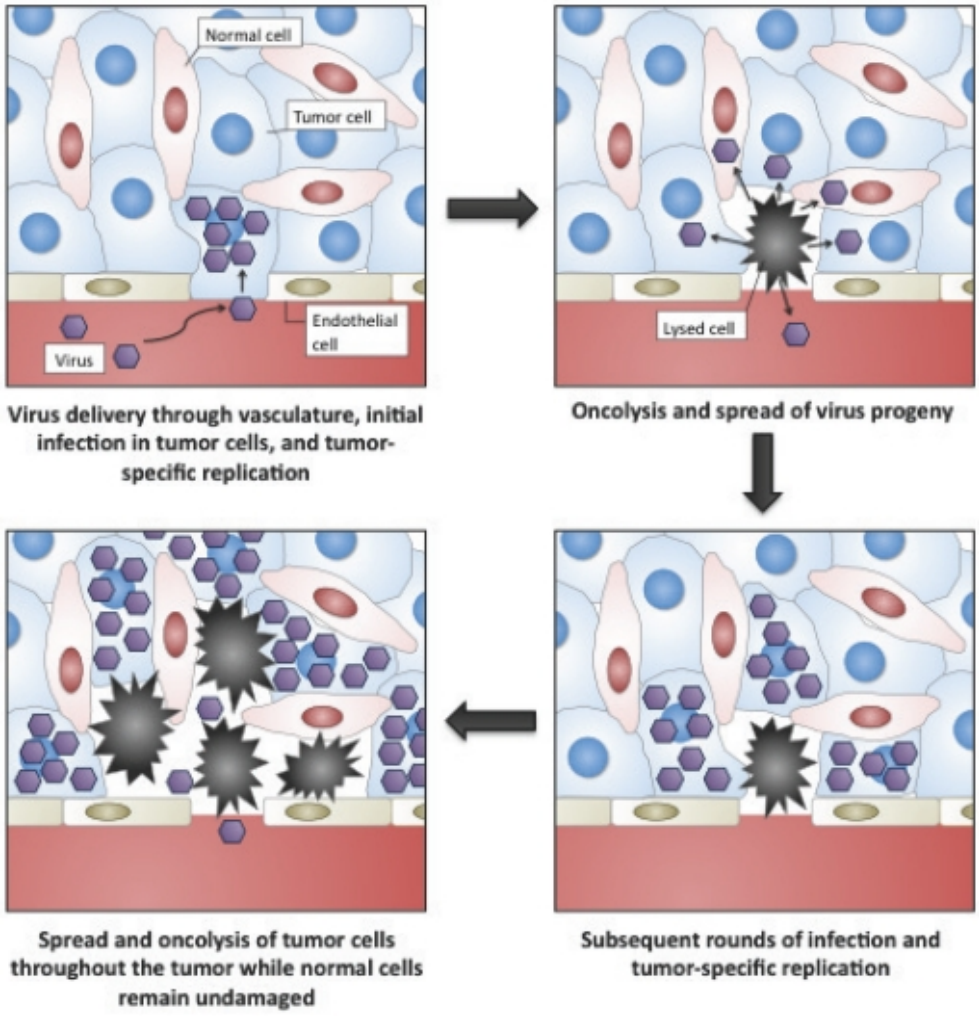

Figure 2. Oncolytic mechanism of virotherapeutics. The virus replicates selectively in cancer cells, then the virus progeny is released from the dying cancer cell and spreads and infects neighboring cancer cells while healthy cells remain undamaged. Figure taken from [13].

Starting in the 19th century, spontaneous tumor regression was observed after natural virus infections, mainly described in hematological diseases, such as leukemia and lymphomas [14, 15]. Further tumor regression was induced by viral vaccines, for instance smallpox and measles virus vaccination [16, 17].

Some of the oncolytic viruses, for example reovirus [18], Newcastle disease virus [19] and vesicular stomatitis virus [20] exhibit a natural tumor selectivity and at the same point aren't pathogenic or only lead to minor symptoms after infection in humans, since they are not the main host organism [21]. Furthermore, the human pathogen measles virus, which also has a natural

tumor selectivity was attenuated to be used as an oncolytic virus [22]. Lately, improvements in the field of virotherapy led to a better understanding of the mechanism of action of oncolytic virotherapy (OV).

Besides wild-type virus strains, genetically engineered oncolytic viruses were produced improving tumor selectivity, efficacy, safety aspects, and attenuating side effects. These engineered viruses also entered clinical trials [23]. The aim could be a perfectly fitting oncolytic virotherapeutic that addresses a specific tumor biology. By modification of vectors, which encode specific functional transgenes, virotherapy holds great promise in the future of cancer therapy.

1.2.1 Mechanisms of oncolytic virotherapy

To deliver the virotherapeutic into cancer patients, different routes of application can be used, e.g. intratumoral, intravenous, intrapleural or intraperitoneal. Nevertheless, systemic delivery is the preferred approach for treatment of metastases or inaccessible tumors since it offers access to all vascularized tumor sites, while healthy cells remain intact [24]. Oncolytic viruses exploit deregulated processes in malignant cells, such as a defective antiviral response [25]. However, oncolytic viruses require specific alterations in the host cell signaling pathways, for example mutations within the interferon (IFN) mediated pathway. IFNs protect cells against viral infections, restrain cell proliferation, regulate the expression of specific genes and trigger apoptosis [26]. Malignant cells often are resistant towards IFN signals and thus protect themselves against elimination [27]. Meanwhile, cancer cells become sensitive to viral infection when they lose their innate antiviral protection, such as the IFN pathway. This is one reason for the cancer selectivity of oncolytic viruses [28, 29]. Furthermore, tumor cells are attacked by different immune cells, first dendritic cells, which detect viral antigens, then CD8+ T and NK cells are recruited and activated by the infected tumor cells and viral particles [30, 31].

Indeed, the activation of the adaptive immune system is an essential response to virotherapeutics, since tumor bearing mice, which had a lack of CD8+ T or

NK cells and were treated with oncolytic vesicular stomatitis viruses (VSV) showed lower oncolytic efficacy compared to fully immune competent mice [20].

1.2.2 Advantages and disadvantages

Oncolytic viruses are capable of selectively replicating within tumor cells, leading to infection-related cell lysis by viral spread or apoptosis while normal cells remain undamaged [23].

Even if chemotherapy or radiotherapy is non-effective, viruses are still able to kill tumor cells since there is no cross-resistance [32, 33]. Furthermore, tumor stem cells that are barely affected by chemotherapeutics, on the contrary show sensibility towards virotherapeutics [34, 35].

Also safety aspects were proved in various clinical trials for minimum six different virus species [23, 36] that mainly didn't cause more than flu-like symptoms [23, 37].

Despite these promising results, the immune system is able to recognize the virus as foreign and combats the viral particles often before they are able to efficiently infect tumor cells [32]. Already low antibody titers can neutralize the viruses [38]. Consequently, recurrent applications induce rising titers of neutralizing antibodies and decrease the oncolytic reaction [39]. Intratumoral application sometimes does not show any benefit either [40].

Plenty of viruses were tested in clinical trials for the treatment of different solid tumors [40]. Unfortunately, some trials have shown that a monotherapy might not be sufficient to destroy tumor cells. Therefore, virotherapeutics were combined with different compounds, such as chemotherapeutics [41], radio-therapy [42] and epigenetically modulating agents [43, 44] to enhance the therapeutical oncolysis [23, 45].

1.2.3 Vaccinia Virus

Until the WHO defined smallpox as eradicated (1980), it was a dangerous infectious disease caused by variola virus. Smallpox has a high contagion potential since transmission occurs through airborne inhalation. After an incubation period of about 12 days flu-like symptoms, like fever or shivering, appear. After 3 - 4 days, characteristic red skin spots, so called enanthema occur, enlarge, rupture, and thus huge amounts of virus are released [46]. About 100 years ago, Edward Jenner noticed that people who caught cowpox didn't catch smallpox, hence they were protected from variola infection [47]. Consequently, the vaccination of humans against smallpox started. In 1967, the WHO made a worldwide obligation to vaccinate. The last known smallpox infection occurred in 1977 in Somalia [48].

Vaccinia virus (VACV) was originally isolated from infected cows, indeed later was mixed with isolates from horses to increase the potency [46]. At some point, these vaccines were replaced by another VACV, which is another pox-virus whose origin remains unknown [49].

Variola virus and vaccinia virus both belong to the Orthopoxvirinae into the biological family of Chordopoxvirinae. As a result of its usage as a vaccine for years, the tolerability and health effects could be characterized in detail [50]. The poxvirus is the largest known virus. The large double-stranded DNA (deoxyribonucleic acid) genome offers a variety of therapeutic and diagnostic possibilities as it allows the insertion of transgenes up to a size of 25 kb [51]. An enhanced tumor tissue tropism is induced by selective deletion of important genes, such as the depletion of thymidine kinase [52, 53]. Thymidine kinase is necessary for the viral infection of healthy cells, but it is not necessary for tumor cells. Thus, a thymidine kinase-deleted vaccinia virus mutant has the ability to replicate in and destroy selectively tumor cells [54].

VACV consists of distinct antigenic forms, such as an enveloped virus (EEV) form that envelopes itself in a host cell membrane that contains different complement control factors of the host's immune system and several exposed viral proteins. Consequently, vaccinia virus can easily escape the immune

system and spread within the host's bloodstream to reach distant tumors [55]. A systemic delivery of VACV is highly efficient [56, 57].

Poxviruses are exclusive among DNA viruses, because replication only occurs within the cytoplasm of the cell in so called viral factories. Thus, VACV does not integrate into the host genome, which is a further important safety aspect [58]. Since VACV has been used as a smallpox vaccine, its safety in humans as well as side effects are well-documented [59]. In case of unexpected side effects after VACV application, different antiviral agents are available, such as Cidofovir, ST-246 or specific tyrosine kinase inhibitors [60-62].

1.2.4.1 Vaccinia virus GLV-1h68

Vaccinia virus GLV-1h68 is a large, complex enveloped virus that belongs to the poxvirus family. It is derived from the LIVP strain (Lister strain from the Institute for Research on Viral Preparations, Moscow) [63]. The linear, double-stranded DNA genome has a size of about 190 kbp. The virus strain GLV-1h68 was attenuated by inserting 3 expression cassettes into the genome encoding for marker proteins: i) the Renilla luciferase-Aequorea GFP (green fluorescent protein) fusion protein (ruc-GFP) into the F14.5L locus, ii) *β*-galactosidase (l*acZ*) into the thymidine kinase (tk) locus J2R, and iii) *β*-glucuronidase (*gusA*) into the A56R hemagglutinin locus (Figure 3).

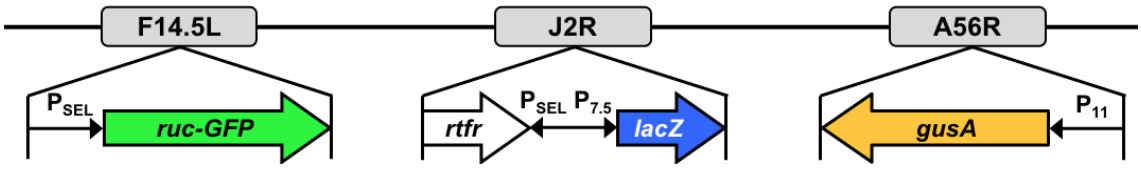

Figure 3. The three expression cassettes of GLV-1h68, which encode for marker proteins. Renilla luciferase-Aequorea GFP fusion protein (ruc-GFP) was inserted into the F14.5 locus. The *β*-galactosidase (l*acZ*) gene was inserted into the thymidine kinase (tk) locus J2R. The *β*-glucuronidase (*gusA*) gene was inserted into the A56R hemagglutinin locus. Modified from Zhang et al., 2007.

Thus, it contains an inactive thymidine kinase gene, shows reduced toxicity, and enhanced tumor-selective replication compared with its parental LIVP strain and

other strains, such as Western Reserve (WR). GLV-1h68 selectively infects tumor cells and has been proven to be non-toxic towards healthy cells. In nude mice GLV-1h68 caused regression and elimination of human breast tumor xenografts [63].

GLV-1h68 has been prepared and kindly provided by Genelux Corporation, San Diego, CA, USA.

1.2.4 Vaccinia virus resistant tumor cell lines

In spite of great achievements of oncolytic viruses for selectively killing cancer cells with moderate toxicity for healthy non-malignant tissues, virus-induced oncolysis is often limited by poor access of oncolytic viruses to tumor sites. Another limitation is caused by primary resistances against the available viro-therapeutics, which are mainly used in monotherapy. Thus, trying to combine virotherapeutics with drugs, such as chemotherapeutics, epigenetically modulating agents or radiotherapy might be a solution to overcome these primary resistances.

In preliminary work, the well characterized tumor cell panel of the National Cancer Institute in Bethesda, MD, USA (NCI-60 panel) was screened *in vitro* to identify cancer cell lines, which are primarily resistant towards the therapy with oncolytic vaccinia virus (unpublished data by Christian Raff, University Hospital Tübingen). Thus, three different cancer cell lines were chosen that have shown a high or partial resistance towards vaccinia virus: HCT-116 and HCT-15, which both are colon cancer cell lines and ACHN, a renal adenocarcinoma cell line. Additionally, a murine colon cancer cell line, Colon-26, was selected to test differences in resistance aspects compared to the above-mentioned three human cancer cell lines.

Depending on the remnant tumor cell mass after treatment with vaccinia virus at 96 hours post infection (hpi), high-grade resistance equals remaining tumor cell mass >75 %, partial resistance equals remaining tumor cell mass between 50-75 % and cell lines displaying tumor cell mass below 50 % at 96 hpi were

classified as susceptible to virus-induced oncolysis (using a multiplicity of infection (MOI) of 0.1, respectively; i.e., one virus particle per addressed tumor cell).

1.3 Epigenetics

1.3.1 The structure of the genome

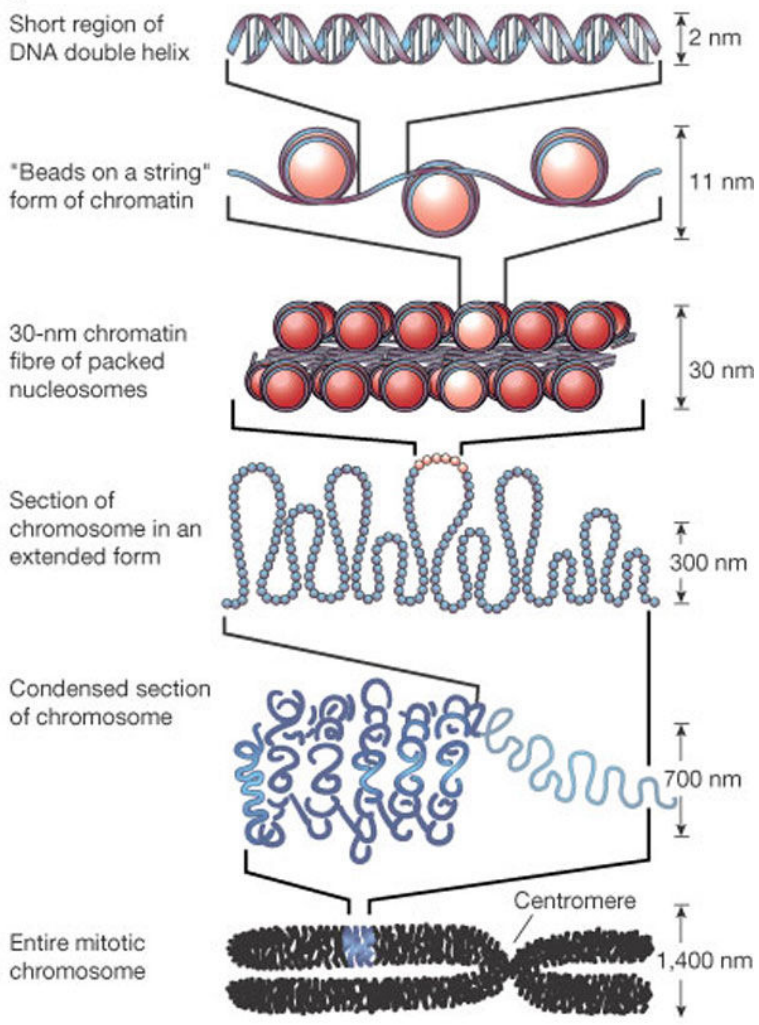

Figure 4. Schematic organization from the DNA double helix to the entire chromosome [64].

Chromatin consists of DNA (deoxyribonucleic acid), histone and nonhistone proteins, located within the nucleus of eukaryotic cells (Figure 4). Besides the storage of the genetic information are the main functions to condense the DNA,

control gene activity, and other cellular processes, for example DNA replication and repair. Chromatin has two different conformation states: heterochromatin, a silent conformation, and consequently a densely packed transcriptionally inert structure and euchromatin, a decondensed and transcriptionally active conformation. The arrangement of the chromatin is among other things regulated by different histones H1 - H4. The nucleosome, a subunit of chromatin, consists of an octamer of core histones (two H2A-H2B dimers and two H3-H4 dimers). About 147 base pairs of DNA are folded around this histone octamer. The DNA between two nucleosomes is called linker DNA and has a length of about 10-80 base pairs. Histone H1 binds to the linker DNA between the nucleosomes [64-67]. The tails of the histone proteins are reachable on the nucleosome surface for posttranslational alterations, which lead to changes in conformation and therefore interfere with gene accessibility and thus gene activation or silencing [68].

1.3.2 Epigenetic mechanisms

The term epigenotype or epigenetics was characterized by Conrad Waddington in 1942 [69]. The definition of epigenetics is “the study of the mechanism of temporal and spatial control of gene activity during the development of complex organisms” [70] or “the study of mitotically and/or meiotically heritable changes in gene function that cannot be explained by changes in DNA sequence” by Arthur Riggs [71].

The two main epigenetic changes are DNA methylation or demethylation and modifications of histones. Both have an impact on transcription and gene expression. Besides, histone modifications also induce long-term effects by defining heterochromatin conformation for the next cell generation [72, 73]. The combination of epigenetic modifications and genetic aberrations leads to alteration of gene expression and may result in the development of cancer. Quite often, genes with tumor suppressor activity are epigenetically silenced. [3].

1.3.3 DNA methylation

DNA methylation regulates the gene expression by adding a methyl group through DNA methyltransferases (DNMTs) at the 5' carbon position of a cytosine ring. Some cytosine rings are at cytosine-guanosine dinucleotide (CpGs) sites, so called CpG islands, close to the promoter region. If these CpG islands are methylated, different transcription factors have less access to the binding sites resulting in transcriptional silencing.

In human malignant cancer cells, abnormal DNA methylation patterns as well as increased expression of DNMTs were found. DNA promoter hypermethylation in tumor cells causes transcriptional silencing of different genes, e.g. tumor suppressor genes. Furthermore, hypomethylation in repetitive sequences leads to chromosomal alterations and genetic instability [74-77]. Different inhibitors of DNA methylation are under investigation for the treatment of various cancer entities.

1.3.4 Histone modification

Histone modifications are posttranslational epigenetic processes, which influence gene regulation without changing the DNA sequence [72]. Two important modifications are histone acetylation and histone methylation.

Acetylation and deacetylation of histone tails are regulated by histone acetyltransferases (HATs) and histone deacetylases (HDACs). HATs transfer acetyl groups to the lysine residues at the amino-terminal tail of histones, thus transcription factors as polymerases have access to the DNA and the transcription rate is increased. HDACs, the antagonists of HATs, remove acetyl groups from lysine residues of histone proteins, the chromatin condenses and represses the transcription of genes, which is also called gene silencing [78]. Errors in the regulation of these processes, as for instance inactive HATs or overexpression of HDACs seem to provoke cancer formation [79-81]. Lower levels of histone acetylation were shown in solid tumors, whereas an

upregulation of HDACs was found in prostate cancer, gastric cancer and colon cancer [82-84].

Hence, HDACs are target structures for tumor therapy. So far, 18 different HDACs were identified, which are subdivided into four classes (classes I - IV) depending on their homology to yeast histone deacetylases. Class I HDACs are homologous to the yeast RPD3 gene and mainly regulate cell proliferation and apoptosis. Class II HDACs are homologous to the Had1 gene and regulate amongst others cell migration and angiogenesis [85]. Class III HDACs have a homology to the Sir2 (silent information regulator 2) gene and regulate gene expression. Class IV HDACs combine features of class I and II [86].

As mentioned before, another histone modification is histone methylation. It mainly occurs on histones H3 and H4. Contrary to histone acetylation, which correlates primary with transcriptional activation, histone methylation can indicate either activation or repression of transcription, depending on the methylation sites and on the number of methyl groups added [87, 88].

1.3.5 Histone deacetylase inhibitors

Altered expression of HDACs and thus dysfunction of transcriptional processes is associated with different types of cancers. As described above, over-expression of diverse HDACs seems to increase cancer formation, e.g. over-expression of HDAC1 can lead to prostate and gastric cancer, overexpression of HDAC2 to colon cancer [82-84]. Hence, HDACs are promising targets for therapeutic interventions.

HDAC inhibitors (HDACi) represent an interesting class of potent anticancer compounds with activity against an immense spectrum of neoplasms at concentrations that are well tolerated and minimally toxic for the host [89]. Because of different chemical structures, HDACi are a heterogeneous family, divided into 6 groups: short-chain fatty acids, hydroxamates, benzamides, cyclic tetrapeptides, electrophilic ketones and miscellaneous [90]. Some HDACi only inhibit specific HDACs, other pan-HDACi have an effect on multiple HDAC

groups [91]. Generally, the HDAC inhibition leads to a relaxed chromatin structure and thus to an increased transcriptional activity of former silenced genes (Figure 5).

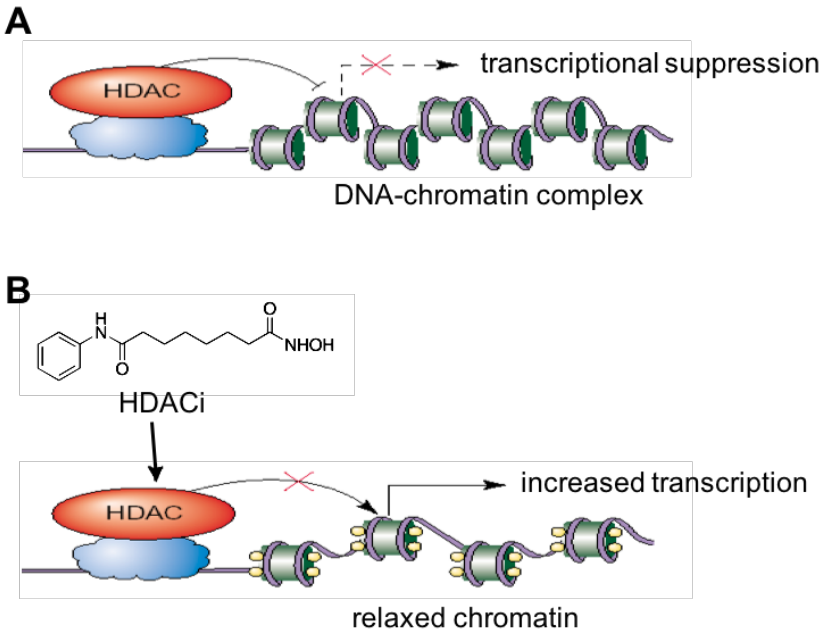

Figure 5. HDACi compounds such as SAHA can upregulate gene expression. A) HDACs bind to the histone proteins and suppress transcription. B) HDAC inhibitors, in this case SAHA, block HDAC enzymatic activity and thus induce increased transcriptional activity. Figure was modified from Kramer et al. [92].

HDACi are able to induce growth arrest and apoptosis in transformed cells by accumulation of acetylated histone proteins in nucleosomes [86, 93]. Additionally, HDACi might affect neoplastic growth and suppress angiogenesis by downregulation of the vascular endothelial growth factor (VEGF), basic fibroblast growth factor (bFGF) and hypoxia-inducible factor 1-alpha (HIF1-α) [94]. Furthermore, HDACi sensitize cells, especially tumor cells for other therapeutic agents. Compared to tumor cells, HDACi are well tolerated by non-transformed cells [95]. Nevertheless, the effect of HDACi is unspecific and results in a generally increased transcriptional rate of all genes. Different studies demonstrated that up to 20% of all known genes in transformed cells are affected by HDACi [96].

Because of the impact on tumor cells, HDACi are interesting combination partners for new therapy options. Thus, trying to combine HDACi with drugs, for instance chemotherapeutics, or radiotherapy might be the key to overcome tumor resistance [97-99].

The chosen epigenetic compounds in this dissertation are different HDAC inhibitors. A broad number of HDACi has been isolated from natural sources, for example resveratrol and kaempferol. Others have been synthetically developed, such as SAHA (suberanilide hydroxamic acid) [90].

1.3.6 Resveratrol

Resveratrol (3,5,4'-trihydroxy-trans-stilbene) is a naturally occurring phytoalexin that belongs to the group of polyphenols. It is found in grapes, peanuts, red wine and other berries [100, 101].

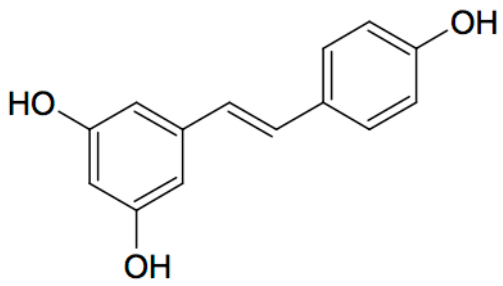

Figure 6. Structural formula of resveratrol.

Plants produce stilbenes as a defense reaction in response to stress like UV-irradiation, bacterial or fungal infection [102]. One of the most discussed effects of resveratrol is the so called "French paradox", which might explain the lower incidence of cardiovascular diseases by low to moderate wine intake, due to the antioxidant activity and the inhibition of platelet aggregation [103-105]. Moreover, anti-inflammatory [106], cardioprotective [107], and anti-proliferative effects as well as cancer chemopreventive activities were shown [108]. Further modulations were identified, for instance the inhibition of phosphodiesterases -1, -3 and -4 [109], activation of protein kinases [110], inhibition of the protea-

some by modulating the NF-κB (nuclear factor kappa-light-chain-enhancer of activated B-cells) pathway and the activation of sirtuin deacetylases [111]. These modulations extend the lifespan in yeast by up to 70% [112].

Since the oral bioavailability of resveratrol is considered to be less than 1%, it is hard to reach suitable levels of resveratrol through oral administration *in vivo* [113]. The development of effective prodrugs of resveratrol to reach higher concentrations *in vivo* remains to be explored [114].

1.3.7 Kaempferol

Kaempferol (3,5,7,4'-Tetrahydroxyflavone) is a natural polyphenol that belongs to the group of flavonoids [115].

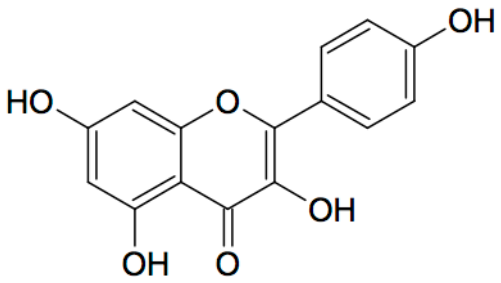

Figure 7. Structural formula of kaempferol.

Kaempferol mainly occurs in vegetables and fruits, predominantly in tomatoes, endive, hops, honey, strawberries and green tea [116-121]. As well as resveratrol, kaempferol also has anti-proliferative and anti-cancer activity resulting in apoptosis in different tumor entities, such as leukemia, prostate cancer, non-small cell lung cancer, oral cavity cancer and colon cancer [122-126].

Plasma concentrations after oral consumption reach up to 0.1 µM, whereas plasma concentrations after intravenous injection reach 4-16 µM [127].

1.3.8 SAHA

SAHA (suberanilide hydroxamic acid) also known as Vorinostat, marketed under the name Zolinza® by Merck, is the first HDACi approved by the US Food and Drug Administration (FDA) for the treatment of advanced cutaneous T cell lymphoma (Zolinza® (vorinostat) Capsules. Full Prescribing Information. Merck & Co., Inc., Whitehouse Station, NJ 08889, USA. Retrieved 1 September 2016). SAHA is a synthetic hydroxamic acid of hybrid polar compounds that induces growth arrest and apoptosis in transformed cells [128].

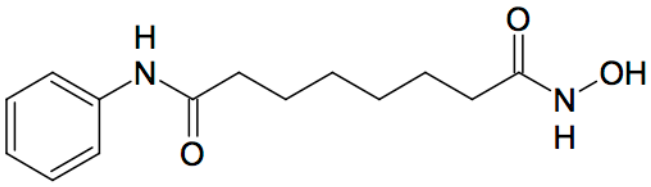

Figure 8. Structural formula of SAHA.

Recent phase I and II trials have shown effects against recurrent glioblastoma multiforme [129], breast cancer [130], leukemia [131] and non-small-cell lung cancer [132]. A further effect is the clearance of latent infection of HIV [133, 134].

Compared to resveratrol and kaempferol, SAHA shows a good oral bio-availability [135]. SAHA selectively modifies the transcription of a few genes, whereby healthy cells are at least 10 times more resistant than transformed tumor cells to SAHA [136].

1.3.9 Advantages and disadvantages

In contrast to synthetically produced SAHA, resveratrol and kaempferol are naturally occurring epigenetic modulating agents, which are present in fruits and vegetables and are therefore less toxic. Nevertheless, with these dietary agents it is hard to reach concentrations under physiological conditions that are high enough to achieve HDACi activity *in vivo*. Thus, these dietary compounds need

higher concentrations for inhibitory capability, compared to SAHA, which is effective even in a low micromolar range [137].

Therefore, SAHA offers an advantage, also because it is applicable in the daily clinic routine and has its approval by the FDA for the treatment of cutaneous T cell lymphoma.

1.4 Combination therapy of Vaccinia Virus GLV-1h68 and epigenetic modulating agents

Combinatorial treatments of different viruses, such as reovirus, vaccinia and HSV with drugs or radiation have been performed so far and showed good response rates [138-141]. Further trials combining HDACi with VACV have been investigated. It is presumed that HDACi decline the response of cancer cells to interferon and hence enhance susceptibility to viral infection [43, 44]. Nevertheless, it is difficult to distinguish whether oncolytic viruses or the combinatorial treatment agent is contributing to these responses. This can be clarified in further investigations by randomized phase 3 trials [40].

1.5 Aim of this dissertation

Besides the improvement of new therapy options for cancer, the prognosis for patients with advanced or relapsing colorectal or renal cancer remains poor.

Oncolytic viruses have emerged as powerful anticancer therapeutics for selectively killing tumor cells with moderate toxicity for healthy non-malignant tissues. However, virus-induced oncolysis is often limited by poor access to tumor sites. Therefore, the administration of combinatorial treatments of oncolytic viruses with histone deacetylase inhibitors (HDACi) with the purpose to overcome both infection barriers and therapy resistance mechanisms, might be a first starting point [142].

The aim of this dissertation was to overcome current high-grade tumor cell resistance to virotherapy by combined application of vaccinia virus GLV-1h68

and distinct HDACi compounds, such as resveratrol, kaempferol or SAHA. A further goal was to determine whether these HDACi compounds can enhance the potency of VACV GLV-1h68 in infection-resistant cancer cell lines and which concentrations are needed to overcome these limitations.

2. Material and methods

2.1 Cell culture

2.1.1 Materials

Cell culture Materials	
Laminar flow work bench	HERAsafe®, Heraeus
Incubator	HERAcell®, Heraeus
Sonifier 450	Branson, Emerson Industrial
Centrifuge	Megafuge 2.0 R, Heraeus
Microscope	CK40, Olympus Corporation
	IX50, Olympus Corporation
75 cm^2 tissue culture flasks	TPP, Techno Plastic Products AG
150 cm^2 tissue culture flasks	Greiner Bio One
24-well microplate	TPP, Techno Plastic Products AG
96-well microplate	Costar, Corning Life Sciences
Dulbecco's modified Eagle medium (DMEM); with stable L-glutamine with 4.5g/l glucose	Sigma-Aldrich Corporation
Dulbecco's phosphate buffered saline (PBS); without Ca^{2+} and Mg^{2+}	Sigma-Aldrich Corporation
Fetal bovine serum (FBS)	PAA Laboratories AG
Ethylendiamintetraacetate-trypsin (EDTA-trypsin)	PAA Laboratories AG
Dimethylesulfoxide (DMSO)	Sigma-Aldrich Corporation
15 ml tubes	Greiner Bio One
50 ml tubes	BD Biosciences

Cryovials	Corning Life Sciences
Isopropanol chamber	“Mr. Frosty” Nalgene® labware
Trypan Blue solution 0.4 %	Sigma-Aldrich Corporation
ddH_2O	Millipore BioPak Polisher, Merck

Table 1. Cell culture materials

DMEM, PBS, FBS and EDTA-trypsin were stored at 4° C, Trypan Blue solution and DMSO were stored at room temperature (RT) during time of use. EDTA-trypsin and FBS were stored at -20° C before use, PBS at RT. FBS was heat-inactivated for 30 minutes at 56° C before used.

2.1.2 Cell lines

Cell line	Origin and histology	Species	Comment
ACHN	Renal cell carcinoma	human	Can Res 42; 4948-4953, 1982
HCT-15	Colon adenocarcinoma	human	Can Res 39; 1020-1025, 1979
HCT-116	Colon carcinoma	human	Can Res 41; 1761-1756, 1981
Colon-26	Colon adenocarcinoma	murine	
CV-1	African green monkey kidney fibroblasts	simian	

Table 2. Cell lines

ACHN, HCT-15 and HCT-116 cells were chosen from the NCI-60 anti-cancer cell line panel from the U.S. National Cancer Institute and purchased from Charles River Laboratories. The murine cancer cell line Colon-26, purchased from Tumorzellbank, DKFZ Heidelberg, was selected to see if results differ to human cell lines and if it might be of use for further experiments in a mouse

model. CV-1 cells were purchased from Genelux Corporation, San Diego, CA, USA.

2.1.3 General cell culture

All cell lines were cultivated in DMEM with 10 % heat-inactivated fetal bovine serum (FBS) (DMEM-10) at 37° C in a humidified incubator in a 5 % CO_2 atmosphere. Cells were kept in 75 cm^2 or 150 cm^2 tissue culture flasks with vented caps as permanent cell cultures and were maintained as adherent monolayer. The media did not contain any antibiotics or fungicides. The cells were treated under a HERAsafe® laminar flow workbench under sterile conditions. The complete media and buffers needed for cell culture were pre-warmed to 37° C. When cell cultures reached a confluent level, cells were passaged (two or three times a week) to avoid overgrowth and lack of nutrients.

To harvest cells, spent cell culture medium was discarded and cells were washed once with pre-warmed PBS (37° C) to eliminate dead cells and remove left over medium, calcium and magnesium, which would inhibit the activity of the ETDA-trypsin. To detach the cell layer, cells were incubated with warmed EDTA-trypsin (0.05 %) at 37° C for a few minutes. When all cells were detached, fresh DMEM-10 was added to inactivate EDTA-trypsin. Cells were resuspended thoroughly, depending on the cell lines between one tenth and one twentieth of the cell solution was transferred into a new flask containing DMEM-10.

2.1.4 Cryopreservation of cells

Cell lines in continuous culture are inclined to genetic drift or microbial contamination. Therefore, cells were preserved for long-term storage and frozen at -180° C in cryovials. Cells were detached from the tissue culture flasks as described in 2.1.3. Cells were resuspended and centrifuged at 1200 revolutions per minute (rpm) for 5 minutes at RT. Supernatant was discarded and the cell pellet was resuspended in DMEM containing 10 % dimethylsulfoxide (DMSO)

and 20 % FBS. DMSO reduces the freezing point of the medium and allows a slower cooling rate, which preserves cells from damage and cell death [143]. Aliquots were dispensed into cryovials and were stored in an isopropanol chamber (Mr. Frosty, Nalgene labware) at -80° C overnight. On the next day, frozen cells were transferred to a -180° C freezer for long-term storage.

2.1.5 Thawing of cells for recultivation

To recultivate cells, the cryovials were thawed in a water bath at 37° C, diluted with pre-warmed DMEM-10, and centrifuged at 1200 rpm for 3 minutes at RT. Supernatant was discarded to remove toxic DMSO. Cell pellet was resuspended in 10 ml DMEM-10 and cells were transferred into a new 75 cm^2 tissue culture flask.

2.1.6 Determination of cell number in solution

Before seeding cells, their exact number had to be counted using an improved Neubauer hemocytometer. Cells were harvested as described in 2.1.3. Then, cells were resuspended in DMEM-10 and 10 µl of the cell suspension was added to 90 µl trypan blue (0.4 % w/v). Trypan blue is taken up only by dead cells, which appear dark blue under the microscope, whereas living cells have a white appearance. 10 µl of the suspension were pipetted between the chamber of the hemocytometer and the cover glass. Cells were counted in the central gridded four large squares under the inverted microscope. One square contains a defined volume of 0.1 µl. The average cell number of the four squares was multiplied with 10.000 resulting in the number of cells per ml. In case of dilution with trypan blue the result had to be multiplied with the dilution factor.

2.2 Virological methods – Virus infection of cells

Cells were seeded in 24-well plates at a density of 4 x 10^4 cells in 500 µl DMEM-10 per well and allowed to adhere over 48 h. After 48 h, cells were

infected with VACV GLV-1h68 at different multiplicities of infection (MOI) or mock-infected to determine the final MOI for further experiments. MOI describes the number of infectious virus particles per cancer cell at the time point of infection. The setting for the treatment is described in Figure 9.

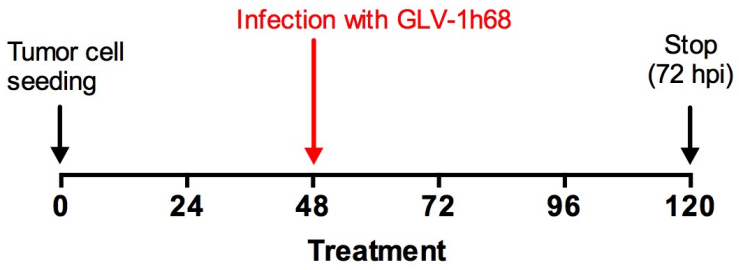

Figure 9. Setting for virotherapy. Application scheme for the determination of suitable MOIs for each cell line. Tumor cells were plated and infected after 48 h with GLV-1h68 or mock-treated. One hour post infection (hpi) medium change was performed. 72 hpi, remnant cell masses were quantified by SRB cytotoxicity assay.

VACV GLV-1h68 was thawed carefully and sonicated for 30 seconds at 4° C in order to disaggregate virus particles. Depending on the needed MOI, the virus was diluted in room-tempered DMEM supplemented with 2 % FBS (DMEM-2). In the first step, medium was removed, and cells were gently washed once with pre-warmed PBS. Infection took place in 250 µl DMEM-2. Virus at different MOIs (0.0001, 0.001. 0.01, 0.1 and 1) was added to the 24-well plate in quadruplicates as described in Figure 10. Four wells were mock-infected, therefore 250 µl DMEM-2 without virus was added to these wells. After infection, the 24-well plates were placed in the incubator at 37° C to allow the virus to adhere to the cells. Every 20 minutes, the plates were gently swayed to ensure an equal virus infection throughout the cell layer. One hour post infection (hpi), the inoculum was removed and 1 ml fresh DMEM-10 was added to each well. At 72 hpi tumor cell viability was analyzed by the sulforhodamine B (SRB) assay (as described in 2.5.1).

VACV GLV-1h68 has been prepared and kindly provided by the Genelux Corporation, San Diego, CA, USA.

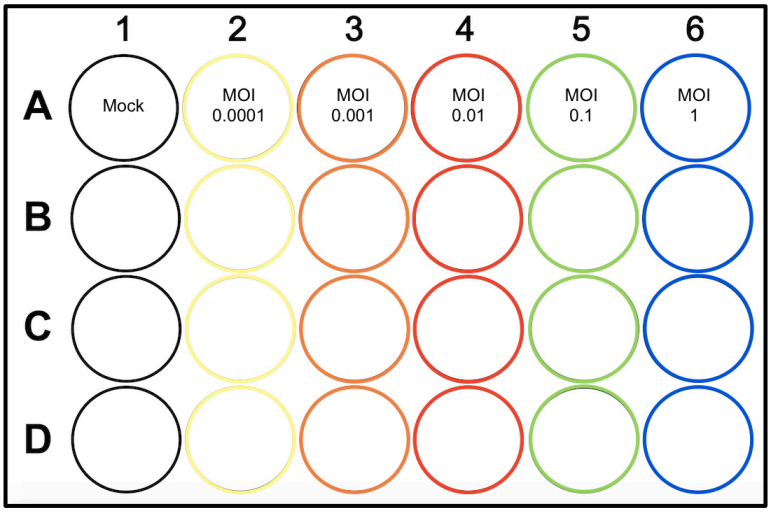

Figure 10. Pipetting scheme for treatment with different VACV GLV-1h68 concentrations. Cells were infected at different MOIs or mock-infected in quadruplicates. Same color indicates same virus concentration. Four wells were mock-treated with DMEM-2 solely (black wells).

2.3 Epigenetic methods – Treatment with the HDAC inhibitors

Cells were treated with different epigenetically modulating agents such as resveratrol, kaempferol and SAHA. The tumor cell lines were treated 24 h after seeding, as shown in the setting (Figure 11).

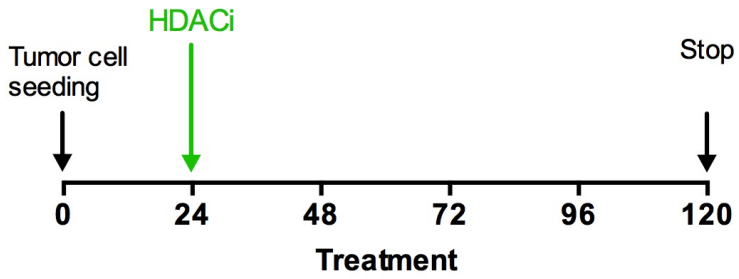

Figure 11. General application scheme for treatment with HDACi. Tumor cells were plated and treated with epigenetic compounds 24 h after seeding. 96 h later, remnant cell masses were quantified by SRB viability assay.

Cells were seeded in 24-well plates at a density of 4 x 10^4 cells in 500 µl DMEM-10 per well and allowed to adhere over 24 h. After 24 h, the epigenetic compound was thawed in the water bath at 37° C. Depending on the needed dilution, resveratrol, kaempferol or SAHA was diluted in pre-warmed DMEM-10.

Medium was removed, and cells were treated in triplicates with 500 µl of the epigenetic compound at different concentrations, as shown in Table 3. Additionally, three wells were treated with 500 µl DMEM-10 solely (control). Thereafter, the 24-well plates were placed in the incubator at 37° C. 96 h later, SRB assay was performed.

HDACi	Concentrations
Resveratrol	1 µM, 2.5 µM, 5 µM, 10 µM, 20 µM, 50 µM, 100 µM
Kaempferol	1 µM, 5 µM, 10 µM, 20 µM, 50 µM, 100 µM
SAHA	0.5 µM, 1 µM, 2.5 µM, 5 µM, 10 µM, 20 µM, 50 µM

Table 3. Concentrations of the epigenetic compounds resveratrol, kaempferol and SAHA that were used in the experiments.

2.4 Combinatorial treatment

Cells were seeded in 24-well plates at a density of 4 x 10^4 cells in 500 µl DMEM-10 per well. After 24 h, supernatant was discarded, and cells were treated with 500 µl of different epigenetic compounds (resveratrol, kaempferol or SAHA). 24 h after treatment, the supernatant containing the epigenetic compound was transferred from each well to the corresponding well of an empty plate and was stored in the incubator. Cells were gently washed with PBS. VACV GLV-1h68 was thawed carefully and sonicated at 4° C for 30 seconds. Depending on the needed MOI, the virus was diluted in room-tempered DMEM-2. Infection took place in 250 µl DMEM-2. Virus was added to the 24-well plate in quadruplicates. Four wells were mock-infected with 250 µl DMEM-2 solely. The application scheme is shown in Figure 12. After infection, the 24-well plates were placed in the incubator for one hour at 37° C. Every 20 minutes, the plates were gently swayed. 1 hpi, the inoculum was removed and replaced by the former medium containing the epigenetics, which had been set aside. 72 hpi different assays were performed as described in the following chapters.

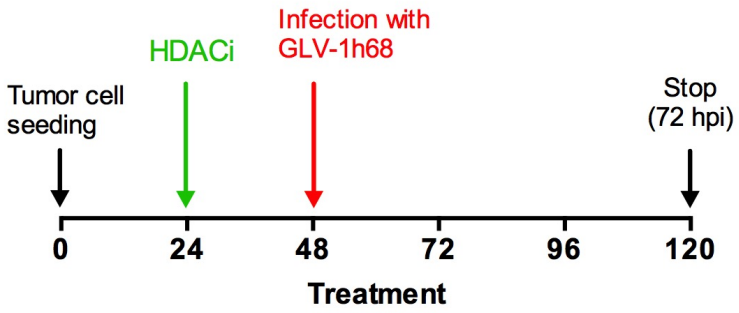

Figure 12. Application scheme for the combinatorial treatment of VACV GLV-1h68 with HDACi. Tumor cells were plated. After 24 h, cells were treated with epigenetic compounds. 24 h later, cells were infected with GLV-1h68 or mock-infected. 72 hpi, remnant tumor cell masses were quantified by different assays, such as SRB cytotoxicity assay.

2.5 Cell viability assays

2.5.1 Suforhodamine B assay (SRB)

Materials	
Tecan GENios Microplate Elisa Reader	MTX lab system, Tecan group Ltd.
Trichloroacetic acid (TCA)	Carl Roth GmbH
Sulforhodamine B	Sigma-Aldrich Corporation
Acetic acid (1 %)	Merck
Tris-base solution (10mM)	Sigma-Aldrich Corporation

Table 4. Materials for SRB assay

To quantify the remaining tumor cell mass after treatment with epigenetically modulating agents and/or VACV GLV-1h68 infection, the **s**ulfo**r**hodamine **B** assay (SRB) was performed [144]. SRB is the standard assay of the US National Cancer Institute (NCI) to measure the drug-induced cytotoxicity in cell cultures. The protein-binding dye sulforhodamine B binds to basic amino acid residues in TCA-fixed cells. The remaining cell mass of the differently treated cells can be quantified by the calculated amount of dye and thus by the

measured optical density (OD). The fewer cells remain, the more effective the virus is killing cells.

Cells were treated and/or infected as described in 2.2, 2.3 and 2.4. After 120h, growth inhibition was evaluated by the SRB assay. First, supernatant was discarded, followed by fixation with 250 µl cold TCA solution (trichloroacetic acid, 10 % w/v, 4° C, 10 g in 100 ml distilled H_2O) per well for 30 minutes at 4° C. After incubation, the TCA solution was discarded, and plates were gently rinsed with tap water for four times. Then, cells were dried overnight in a heating cabinet at 40° C. At this point plates can be stored indefinitely. In the next step, cells were dyed with the SRB staining solution (0.4 % w/v in 1 % acetic acid) for 10 minutes. The dye was removed, and cells were washed with acetic acid (1 % v/v) until all soluble red dye was removed. Plates were dried for at least 3 - 6 h at 40° C and measured within the following 48 hours. Beforehand, photographs of the 24-well plates were taken (Figure 13) for further assays (2.8 Area calculation).

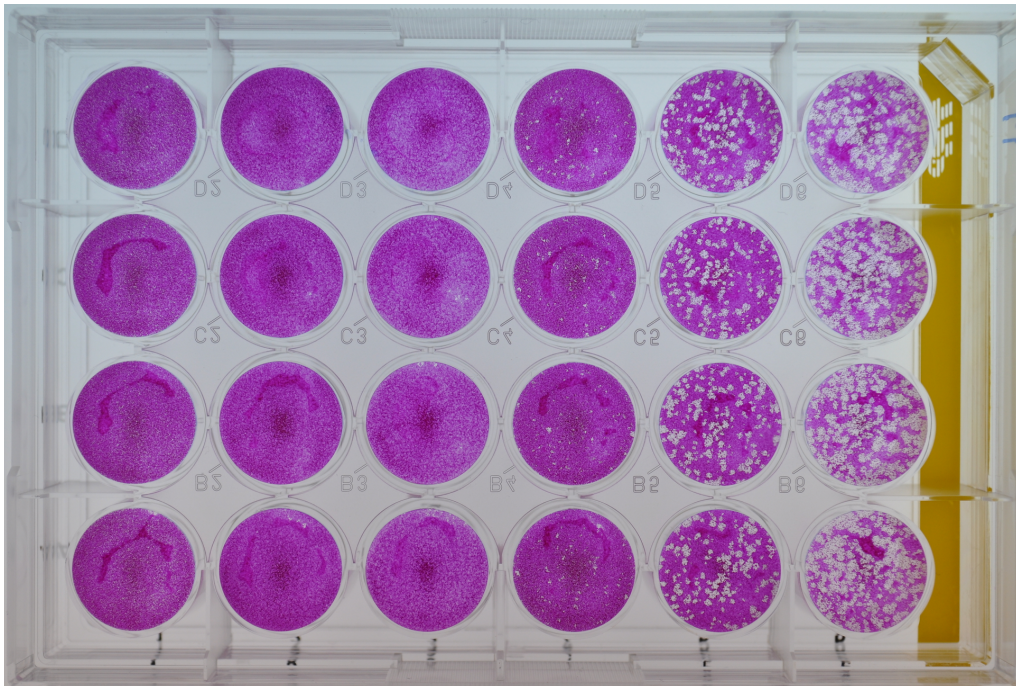

Figure 13. Photograph of a 24-well plate containing ACHN cells after treatment with SAHA and infection with GLV-1h68. The 24-well plate was dyed with sulforhodamin B staining solution and dried overnight. Then, photographs were taken.

Bound dye was solubilized in 1 ml 10 mM Tris base (pH 10.5, 1.211 g in 1000 ml ddH_2O) per well for 10 minutes on a gyratory shaker. 80 µl of the colored solution was transferred to a transparent flat-bottom 96-well plate in duplicates for each sample. The optical density was measured in the Microplate Elisa Reader at 550 nm wavelength using the xFluor 4 software. The values should not exceed 1.8 OD units. If higher values were reached, samples were equally diluted with additional 500 µl Tris.

Results were calculated using GraphPad Prism Software version 6.0 (GraphPad Software, La Jolla, CA, USA). Mean of the duplicates was used for further calculation. Error bars were shown +/- SD.

2.5.2 Resazurin-based viability assay

Also called CellTiter-Blue assay.

Materials	
Tecan GENios Microplate Elisa Reader	MTX lab system, Tecan group Ltd.
CellTiter-Blue© Kit	Promega Corporations

Table 5. Materials for the resazurin-based viability assay

Resazurin-based viability assay is a cell viability assay that monitors cytotoxicity or proliferation of cells. Viable cells are able to reduce a particular dark blue non-fluorescent substrate, called resazurin to the pink product resorufin, which is extremely fluorescent. Resorufin diffuses out of the cell into the medium and thus a color change is visible. Dead cells are not able to reduce resazurin because of the loss of metabolic capacity, therefore no fluorescent signal is measureable at 595 nm wavelength. The increase of the fluorescence is proportional to the amount of viable cells. DMEM-10 is used as a negative control to detect background fluorescence. The CellTiter-Blue© Reagent is nontoxic, which allows further assays after measurement.

Cells were seeded at a density of 4 x 10^4 cells per well and treated and infected as described in 2.4. 120 h after seeding, cell viability was evaluated by CellTiter-Blue Assay© according to the manufacturer's protocol [145, 146].

First, 600 µl supernatant from each well was gently removed so that 400 µl medium was left. 80 µl CellTiter-Blue© Reagent was added to each well in the assay plate and incubated at 37° C for 1 hour. To calculate the percentage of resorufin release, mock-infected wells were used as a 100 % control. Wells containing 400 µl DMEM-10 solely with 80 µl CellTiter-Blue© Reagent were used for background measurement. 100 µl of the colored solution was transferred to a transparent flat-bottom 96-well plate in duplicates for each sample including background measurement and mock control. Measurement was performed in the Microplate Elisa Reader at 595 nm wavelength using xFluor 4 software. In the end, values were compared to the background measurement (blank wells) and to the corresponding mock-treated wells. Mean of the duplicates was used for calculation using GraphPad Prism Software version 6.0 and was given in percent (GraphPad Software, La Jolla, CA, USA). Error bars were shown +/- SD.

2.5.3 MTT assay

Materials	
Synergy HT microplate reader	BioTek Instruments GmbH
MTT staining solution	Sigma-Aldrich Corporation
Hydrogen chloride (HCl)	Merck
Isopropanol	Merck

Table 6. Materials for MTT assay

MTT is a rapid colorimetric assay, which is applicable as another cytotoxicity assay. It is based on the tetrazolium salt MTT (3-(4,5-dimethylthiazol-2-yl)-2,5-diphenyl tetrazolium bromide) that is reduced to formazan when incubated with living cells. The yellow tetrazole MTT is reduced to purple-blue formazan, which

can be quantified by measuring at 570 nm and 650 nm wavelength in a spectrophotometer [147].

Cells were seeded and treated as described before (2.4). Medium was discarded, and cells wells were gently washed with 500 µl PBS. Then, 250 µl MTT staining solution (2.5 mg/ml in DMEM without phenol red) was added to each well and incubated for 2 h at 37° C. After incubation, the staining solution was removed, and the bound dye was resolved in 1 ml MTT solvent (1 ml 10 % HCl in isopropanol) on a gyratory shaker until completely solubilized. 200 µl of the colored solution was transferred from each well to a transparent flat-bottom 96-well plate in duplicates for each sample. Additionally, the background was determined by using the MTT solvent solely. Measurement took place in the Synergy HT microplate reader at 570 nm and 650 nm wavelength using the Gen5 software.

The values were compared to the background measurement and to the corresponding mock-treated wells. The mean of the duplicates was used for further calculation using GraphPad Prism Software version 6.0. Mean values were shown +/- SD and given in percent.

2.6 Cytotoxicity assay

2.6.1 Lactate Dehydrogenase Assay (LDH assay)

Materials	
Tecan GENios Microplate Elisa Reader	MTX lab system, Tecan group Ltd.
LDH-P mono (stored at 4° C)	Analyticon Biotechnologies AG
Triton X-100	Carl Roth GmbH

Table 7. Materials used for Lactate Dehydrogenase Assay

LDH is an enzyme, which is used to evaluate damage and toxicity of cells and tissues. If cells are damaged and lose their membrane integrity, LDH present in the cytosol is released in the surrounding medium. The LDH release can be detected by the LDH-P mono Kit from Analyticon Biotechnologies AG.

The released LDH in damaged cells catalyses the interconversion of lactate and pyruvate under simultaneous production of NAD^+ into NADH in the culture medium. The LDH release is proportional to the amount of the NADH decrease, which can be measured at 340 nm extinction [148].

$$\text{Pyruvate} + \text{NADH} + H^+ \xleftrightarrow{\text{LDH}} \text{Lactate} + NAD^+$$

Cells were seeded and treated as described before (2.4). Additionally, another four wells were seeded, which were treated with Triton X-100 to obtain 100 % cell lysis (Triton control). After 120 h, the LDH solution was prepared according to the manufacturer's protocol. Then, the Microplate Elisa Reader was prepared since the measurement should start immediately after adding the substrate. The mock control shows the basal cell death background. To obtain total LDH release 500 µl PBS/0.1 % Triton X-100 was added to the Triton X-100 control and incubated for 10 min at RT until all cells were lysed. 10 µl of supernatant (including the mock and Triton X-100 control) was transferred to a flat-bottom 96-well plate in duplicates for each sample, after that 200 µl of the reaction solution was added. The well plate was measured at 340 nm wavelength using the Magellan software. The U/l values determined by the Elisa reader were used for the evaluation. The LDH release was calculated, and the mock-treated quadruplicates were set to 100 % LDH release control. The results were calculated using GraphPad Prism Software version 6.0 (GraphPad Software, La Jolla, CA, USA). Mean of the duplicates was used for further calculation. Error bars were shown +/- SD.

2.7 Detection of GFP via fluorescence microscopy

The cells in the 24-well plates were continuously examined under the microscope CK40 from Olympus. Cells were treated and infected as described in 2.2 and 2.4. At 24, 48 and 72 hpi, fluorescence microscopy was performed using the Olympus IX50 microscope including the Olympus U-RFL-T function to visualize the GFP expression. Phase contrast photographs were taken using the PhL ocular at 4x lens magnification. Additionally, fluorescence photographs were taken with the fluorescence light filter from the same spot as the phase contrast photographs. Pictures were taken with F-View Soft Imaging System and analySIS Software. Finally, phase contrast and fluorescence photos were overlaid using Adobe Photoshop 7.

2.8 Area calculation

Additionally, the cell-free area of the wells was identified to evaluate the differences that are clearly visible in the 24-well plates after coloring with SRB dye. Therefore, photographs of the SRB-colored plates (2.5.1, Figure 13) were taken with a Nikon D3000 Camera. The cell-free area was defined and calculated using Paint.NET and Image J respectively.

First, the photographs were processed with Paint.NET (version 4.0.3). A single rectangle was adjusted to cover as much area of the well as possible without overcasting any outside part. For optimal comparison, the same rectangle size was used for every single well of the 24-well plate.

A tonal separation value 2 was chosen, so that each pixel of the photograph was automatically assigned either to the value black or white, depending on its original color shade. The black area shows the cell layer, whereas the white area shows the cell-free area. The photographs were saved in the 32-bit png format. In the next step, the 32-bit png pictures were analyzed with Image J software (version 1.49). Area calculation was performed through histogram values. All values at 255, which represent the white pixels of the photographs, were divided by the complete count of pixels.

$$\frac{pixel\ with\ color\ value\ 255}{total\ pixel\ count} \times 100 = area\ with\ white\ color\ value\ [\%]$$

2.9 Virus growth curves

Materials	
Reaction tubes 1.5 ml, 2 ml	Eppendorf
CV-1 cell line	Genelux Corporation, San Diego, USA
Carboxymethylcellulose sodium salt (CMC)	Sigma Aldrich
Crystal violet	Fluka Chemie AG

Table 8. Materials for virus growth curves

Furthermore, virus growth curves were performed to determine the impact of the epigenetic compounds resveratrol or SAHA on the replication behavior of VACV GLV-1h68.

Preparation

Cells were seeded and treated with virus solely or combinatorial treatment with the epigenetic compound was performed. 24 h after seeding, cells were treated with resveratrol or SAHA. 24 h later, cells were infected with GLV-1h68 as described in 2.4. After infection with GLV-1h68, the rest of the inoculum was directly frozen at -80° C. 1 hpi, the supernatant was removed and replaced by the former medium containing the epigenetic compound, which had been set aside. 1 hpi, 24 hpi, 48 hpi, 72 hpi and 96 hpi cells were scraped off in medium with a sterile cell scraper. The quadruplicates, which were treated the same way, were transferred to one reaction tube. Samples were immediately frozen at -80° C.

Determination of the virus titer

Samples were used to quantify virus replication by titration on CV-1 cells. CV-1 cells were seeded into 24-well plates at a density of 1 x 10^5 per well. On the next day, when cells were confluent, frozen samples were thawed. Next, samples were vortexed and sonicated for 30 seconds. Dilution series at 10 folds from 10^{-1} to 10^{-6} were prepared using 100 µl from the sample and 900 µl DMEM-2. Medium was removed from CV-1 wells and 250 µl of each prepared dilution was transferred to the wells in duplicates. Afterwards, plates were placed in the incubator. Every 20 minutes, plates were gently swayed to ensure an equal virus infection throughout the cell layer. After one hour, 1 ml medium containing 1.5 % carboxymethylcellulose (CMC) sodium salt and 5 % FCS was added, and plates were placed in the incubator for 48 hours at 37° C. To visualize plaques, 250 µl crystal violet staining solution (11.1 % formaldehyde, 5 % ethanol, 0.13 % crystal violet) was added to each well and plates were incubated at RT. After 4 h, supernatant including crystal violet was discarded and wells were washed with H_2O until washing solution was clear. Next, the 24-well plates were dried.

To calculate virus titers in each well, unstained plaques were counted and titers were calculated as described below:

$$viral\ titer = \frac{number\ of\ plaques\ \times\ inverse\ of\ dilution}{volume\ of\ infection\ medium\ (0.25\ ml)}$$

Plaques were counted only in those wells, which contained between 20 and 100 plaques. Less than 20 plaques are imprecise, above 100 plaques calculation will be imprecise as well since plaques conflate. Results were shown in PFU/ml.

Calculation was performed using GraphPad Prism Software version 6.0. Error bars were shown +/- SD.

2.10 Real-time Cellular Impedance measurement

Materials	
xCELLigence	Roche Applied Sciences
E-Plate 96-well microplate	Roche Applied Sciences, Indianapolis, IN, USA
Triton X-100	Carl Roth GmbH

Table 9. Materials used for xCELLigence

The xCELLigence system allows real-time monitoring of cellular impedance. It performs non-invasive continuous monitoring of cell proliferation and viability via electrical impedance readout using interdigitated micro-electrodes located on the bottom of each well of the E-Plate 96 [149]. Cell attachment, spreading, and proliferation were monitored every 30 minutes for 120 h. After every step, the E-Plate 96 was placed back immediately into the SP station in the incubator.

Cells were seeded and treated as described above (2.4). 50 µl DMEM-10 was added to each well of the E-Plate 96 and background was measured in the SP instrument.

Cell lines	HDACi	Concentration
ACHN	Resveratrol	2.5 µM
		5 µM
	SAHA	1 µM
		2.5 µM
HCT-116	Resveratrol	10 µM
		20 µM
	SAHA	0.5 µM
		1 µM

Table 10. HDACi concentrations used for xCELLigence

Cells (ACHN or HCT-116) were added to each well at a density of 2 x 10^3 cells per well in 100 µl DMEM containing 2.5 % FBS. The plate was placed back into the SP instrument, cell monitoring was started, and cell index was continuously monitored for 24 h. After 24 h, 10µl of the HDACi (SAHA or resveratrol) dissolved in DMEM containing 5 % FBS was added in triplicate samples at different concentrations as described in Table 10. 20 µl Triton X-100 was also added to specific wells as Triton X-100 control. Afterwards, the plate was placed back in the SP instrument.

After 23 h, cells were infected with GLV-1h68 at MOI 0.01 in triplicate samples in a volume of 10 µl. As a control, a few wells were mock-infected by adding 10 µl DMEM solely. After one hour, 40 µl DMEM containing 32.5 % FBS was added to each well to inactivate the free virus in the medium. Cell monitoring was stopped after 120 h. The measured impedance from each individual well was converted into cell index values (CI) by the RTCA Software (version 1.2.1.1002, Roche Applied Sciences).

2.11 Flow cytometric (FACS) analysis

Materials	
Flow cytometer	BD LSRII, BD Biosciences
10 mg/ml RNAse, #EN0531	Fermentas, Life Sciences
75 % ethanol (stored at -20 ° C)	Merck
Propidium iodide	Sigma-Aldrich Corporation

Table 11. Materials for FACS

Fluorescence activated cell sorting (FACS assay) analyzes cells according to their size, granularity or fluorescent characteristics by using flow cytometry. Different cell parameters can be distinguished by different fluorescence at the same time.

Flow cytometric analysis of cells stained with propidium iodide (PI) was used to detect the percentage of apoptotic cells. PI is solved in a hypotonic buffer, which is capable to dissolve the cell membranes. Thus, PI is able to reach the cell nucleus, and intercalates into double-stranded nucleic acids. Once PI is bound to the nucleic acids, its fluorescence can be measured. The reduced DNA content of apoptotic nuclei results in an unequivocal hypodiploid DNA peak. The peak can be quantified in the red fluorescence channels using a FACScan flow cytometer BD LSRII with an extinction of 490 nm and emission of 635 nm. The PI staining is able to detect G0/G1-, S, and G2/M-phase cells as well as sub G1 cells (apoptosis) [150].

Preparation of the cells for the staining

Cells were seeded and treated as described in 2.4. After 120 h, supernatant from 2 wells of the quadruplicates was transferred to a 15 ml Falcon-Tube. Subsequently, cells were washed with cold PBS, which was also collected. The remaining cell layer was treated with 200 µl trypsin per well until cells were completely detached. Cells were resuspended in 1 ml DMEM-10 and transferred to the tube. After centrifugation for 5 minutes at 1200 rpm, 4° C, cells were fixed with 1 ml ice-cold 75 % ethanol. Cells can be stored at 4° C for several days when fixed in ethanol.

Cell staining

Approximately 2 ml of cold PBS was added to the fixed cells. The samples were mixed and were centrifuged at 4° C for 10 minutes at 1500 rpm. Supernatant was discarded, and cell pellet was again resuspended in 1 ml cold PBS, centrifuged and PBS was discarded. Then, cells were stained with 200 µl propidium iodide/RNAse solution (50 µg/ml PI + 10 µg/ml RNAse in PBS) per tube and incubated for at least 20 min at 4° C in the dark. Cells were analyzed within 24 h using the flow cytometer BD LSRII and the FACS Diva Software.

2.12 Software

Software	
Adobe Photoshop 7	Adobe Systems
ChemSketch Version 14.0	ACD/Labs
FACSDiva	BD Biosciences
Gen5 Data analysis 1.11	BioTek Instruments GmbH
Graph Pad Prism 6.0	GraphPad Software, La Jolla, CA, USA
Image analysis	Olympus Corporation
Image J (version 1.49)	Wayne Rasband (NIH)
Magellan Data analysis	Tecan group Ltd.
Microsoft Excel for Mac 2011	Microsoft Corporation
Microsoft Word for Mac 2011	Microsoft Corporation
PaintNET (version 4.0.3)	dotPDN LLC
PTCA	Version 1.2.1.1002, Roche Applied Science
xFluor 4	Tecan group Ltd.

Table 12. Software used for the different methods

3. Results

In order to establish an optimized application scheme for the combinatorial treatment of VACV GLV-1h68 and epigenetic compounds, in a first step the different agents were applied in monotherapy to determine suitable concentrations. The subsequent part of this chapter moves on with the combinatorial treatment.

3.1 Identification of optimized concentrations of VACV GLV-1h68 for colorectal and renal adenocarcinoma cell lines

For each tested cell line first a multiplicity of infection (MOI) was determined that was suitable for further experiments.

To this end, all cell lines were infected with VACV GLV-1h68 using ascending viral concentrations: MOI 0.0001, 0.001, 0.01, 0.1 and 1. Four wells were mock-infected. At 72 hpi, the remaining tumor cell mass was determined, using the SRB cytotoxicity assay. Furthermore, to confirm the efficacy of infection and replication of GLV-1h68 in colorectal cancer and renal adenocarcinoma cell lines, the virus-mediated expression of the Renilla Luciferase green fluorescent fusion protein (RUC-GFP) was monitored by fluorescence microscopy (Figure 15).

3.1.1 SRB assay

The 75 % line was charted in the diagrams as the threshold between high-grade resistant and partially resistant tumor cell lines. If remnant tumor cell mass was >75 % after treatment with vaccinia virus at MOI 0.1 and 96 hpi, the cell line was classified as high-grade resistant. Partial resistance is defined as remaining tumor cell masses between 50 - 75 %, and tumor cell masses below 50 % at 96 hpi are classified as tumor cell lines that are susceptible for virus-induced oncolysis (Christian Raff, work in progress).

Since the aim of this study was to investigate whether a combinatorial treatment of VACV GLV-1h68 and epigenetic compounds was superior to the respective mono-treatments, a MOI, which resulted in a remaining tumor cell mass above or around 75 % was chosen for each cell line. The threshold of 75 % was also used for the epigenetic compounds. Furthermore, in this study a different application time was chosen for the epigenetic compounds, compared to infection with GLV-1h68, since both application times were combined in co-treatment setting (compare 3.6).

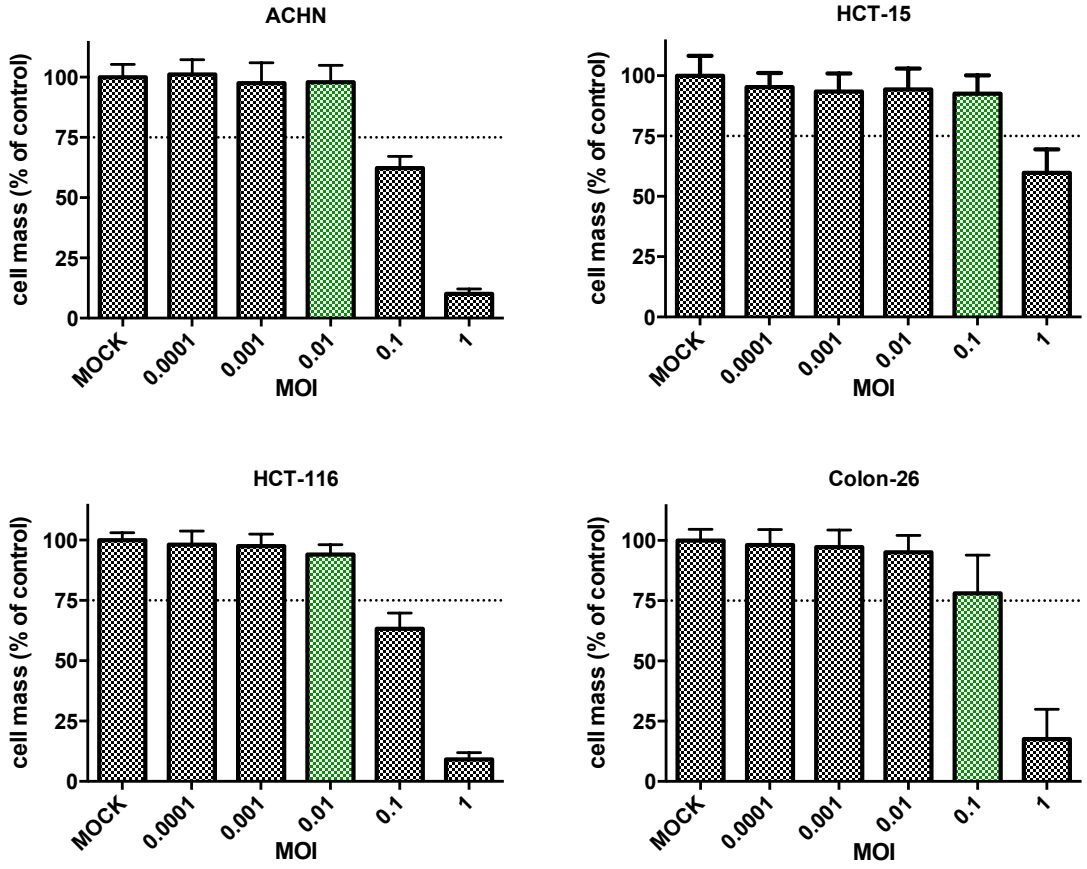

Figure 14. Determination of a suitable MOI of VACV GLV-1h68 for each cell line. 48 h after seeding, cells were mock-treated or infected with VACV GLV-1h68 at different multiplicities of infection (MOI). At 72 hpi, SRB viability assay was performed to quantify remnant tumor cell mass. Error bars indicate +/- SD. Mean of three independent experiments performed in quadruplicates is shown. The mock-treated quadruplicate was set to 100 % cell mass. The green-colored bars show the MOIs, which were chosen for further experiments. As described above, the 75 % line was charted as the threshold between high-grade resistant and partially resistant tumor cell lines.

As seen in Figure 14, the oncolytic effect of VACV GLV-1h68 increased with ascending MOIs in all tumor cell lines. Viral infection with low MOIs showed only a marginal reduction of cell masses compared to the mock-treated controls. The three cell lines ACHN, HCT-116, and Colon-26 were susceptible to viral cytotoxicity with more than 80 % of cells being lysed at 72 hpi at MOI 1. By contrast, cell line HCT-15 was less susceptible with a remaining cell mass of 60 % at MOI 1.

3.1.2 Fluorescence monitoring

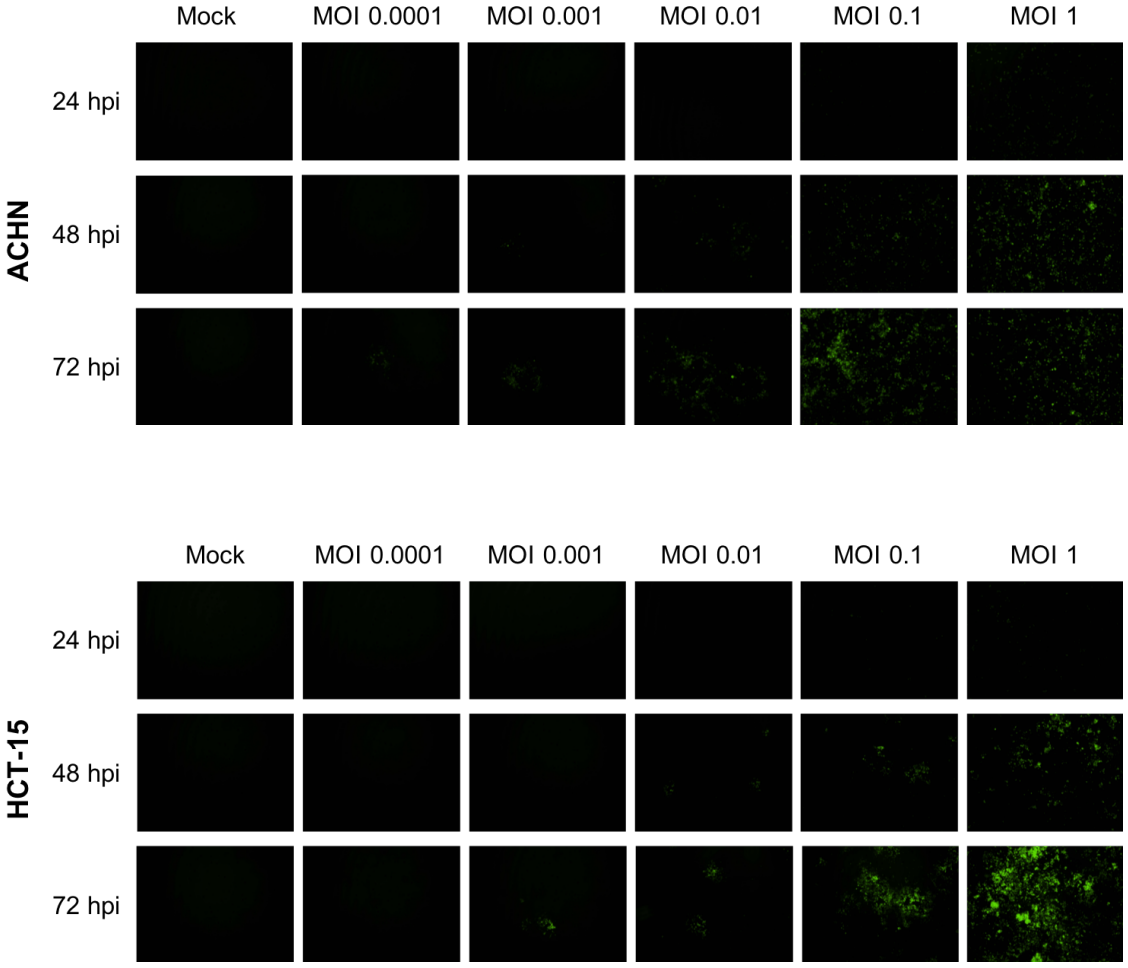

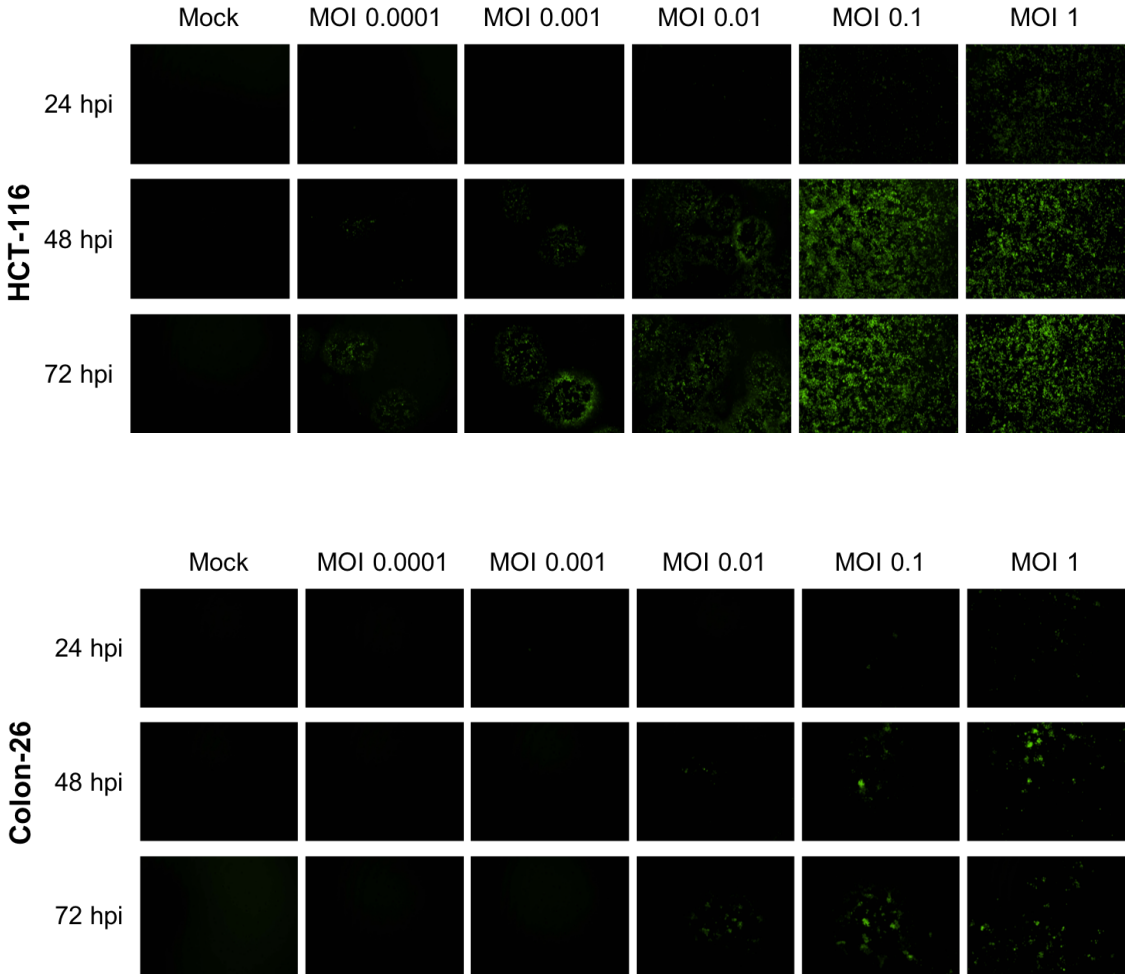

Figure 15. Fluorescence monitoring of VACV GLV-1h68. 48 h after seeding, tumor cells were infected with different concentrations of VACV GLV-1h68 or mock-treated. Fluorescence microscopy photos were taken 24, 48 and 72 hpi. One representative out of three independent experiments performed in quadruplicates is shown. Mock-treated cells did not show any green fluorescence. By contrast, depending on the MOI, virus-infected cells showed an increasing fluorescence intensity.

GLV-1h68 replicated in all four cell lines, but the replication efficacy between the infected cell lines varied (Figure 15). At 24 hpi, only in HCT-116 cells a slight fluorescence signal was visible at MOI 1. In contrast, at 48 hpi at MOI 1 and 0.1, cells emitted higher fluorescence intensities in each cell line. At 72 hpi, the infection at MOI 1 and MOI 0.1 exhibited the strongest GFP expression and the cell layer was already visibly reduced in each cell line. Taken together, in both experiments the efficacy of infection and replication was superior in HCT-116 cells compared to the other cell lines.

For further combinatorial treatment, those MOIs were chosen that might enhance cell death with the different epigenetic compounds. Accordingly, for both ACHN and HCT-116 cells, MOI 0.01 was selected since MOI 1 and 0.1 reduced cell mass already too much (Figure 14). By contrast, MOI 0.1 was selected for HCT-15 and Colon-26 cells.

3.2 Identification of optimized concentrations of resveratrol for the epigenetic treatment of colorectal and renal adenocarcinoma cell lines

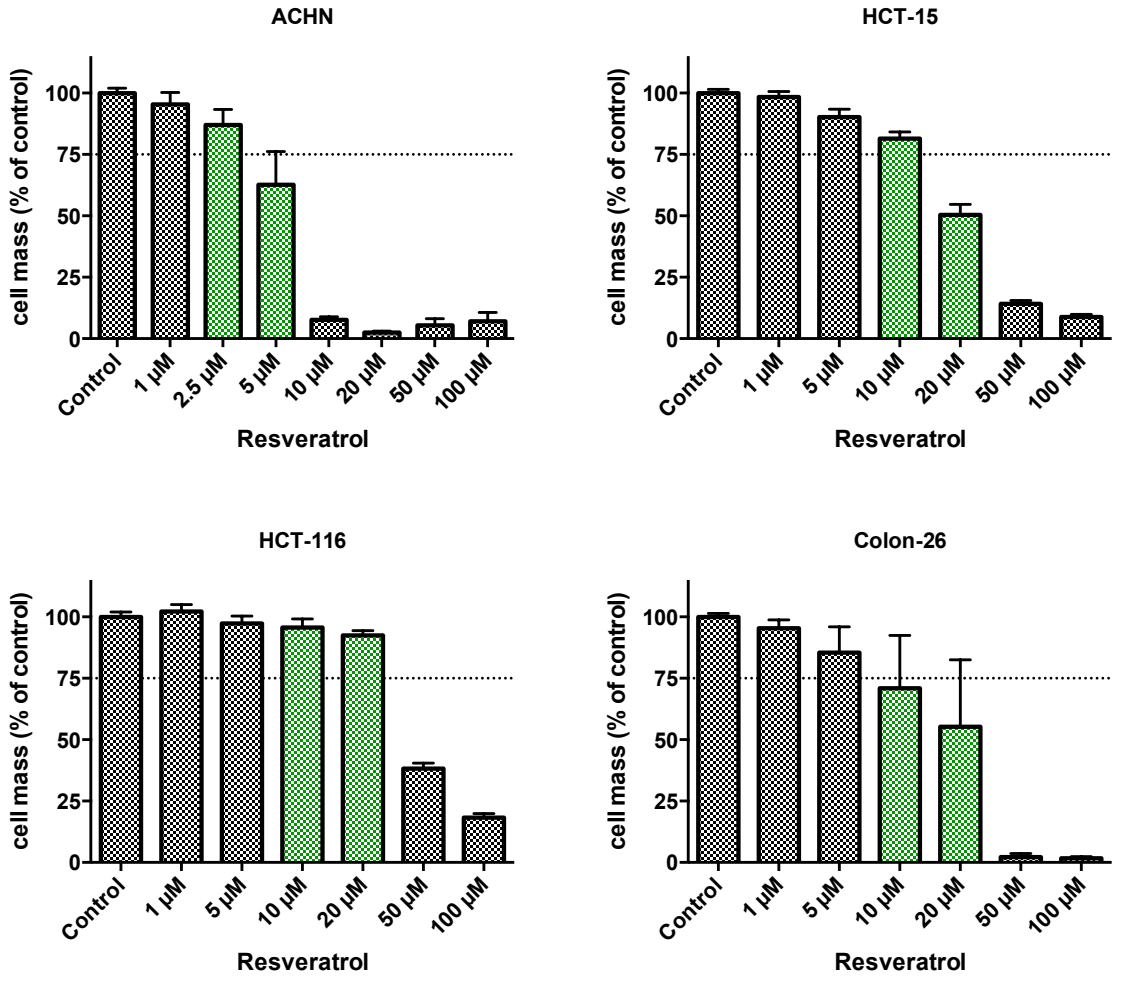

Figure 16. Cytotoxic effect of resveratrol (RV) on colorectal and renal adenocarcinoma cell lines. 24 h after seeding, the cell lines were treated with resveratrol at different concentrations or remained untreated (control). 96 h after treatment, SRB viability assay was performed. Error bars indicate +/- SD. Mean of three independent experiments performed in triplicates is shown. The mock-treated triplicate was set to 100 % cell mass. The green bars indicate the concentrations that were selected for combinatorial treatment.

Initially, cells were treated with different concentrations of resveratrol to evaluate overall HDAC inhibition in a concentration range from 1 µM until 100 µM. 96 h after treatment, SRB assay was performed to evaluate cytotoxic effects.

Most of the cell lines responded only slightly to low resveratrol concentrations and thus only showed small differences to the control. In contrast, ACHN cells showed a reduction of cell mass in the range of 13 – 37 % at 2.5 and 5 µM resveratrol, respectively. While ACHN cells were almost completely eradicated at a concentration of 10 µM, this effect took place at 50 µM for HCT-15 and Colon-26 cells, and at 100 µM for HCT-116 cells (Figure 16). Therefore, resveratrol concentrations of 10 and 20 µM were chosen for all cell lines except for ACHN. For ACHN, concentrations of 2.5 and 5 µM were chosen.

3.3 Identification of optimized concentrations of kaempferol for the epigenetic treatment of colorectal and renal adenocarcinoma cell lines

All cell lines were treated with different concentrations of kaempferol to evaluate overall HDAC inhibition in a concentration range from 1 µM until 100 µM. 96 h after treatment, SRB assay was performed to evaluate cytotoxic effects.

Since kaempferol showed less cytotoxic effects compared to the monotherapy with resveratrol or SAHA (see 3.2 and 3.4), concentrations of 10 µM and 20 µM were selected for each cell line for further combinatorial experiments. Concentrations around 10 µM and 20 µM were between the 75 % threshold and 100 % (Figure 17). Low kaempferol concentrations did not show a reduction of cell mass compared to the control, whereas higher concentrations, e.g. 50 µM reduced cell mass in ACHN, HCT-15, and Colon-26 by more than 60 %. In HCT-116 cells, at a concentration of 50 µM resveratrol, 62 % cell mass was left 96 h after treatment.

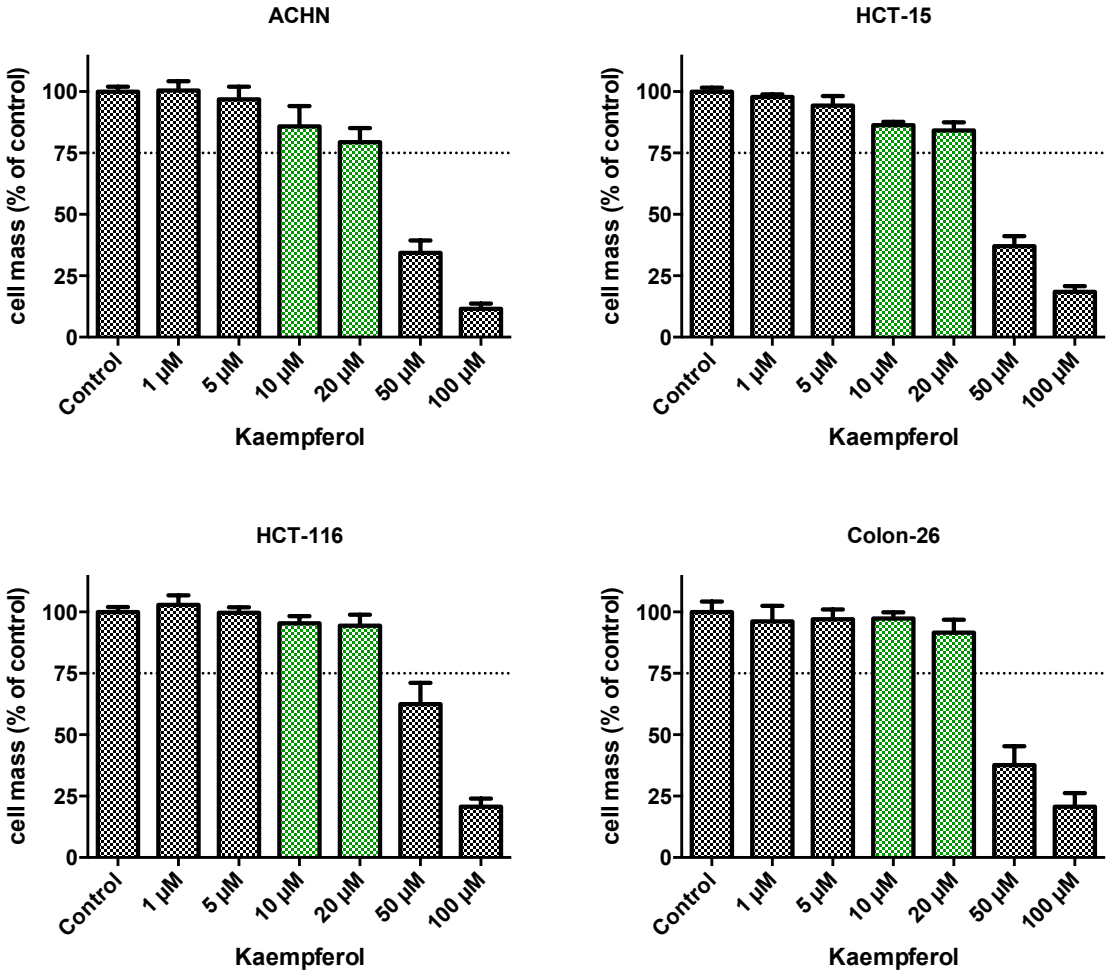

Figure 17. Cytotoxic effect of kaempferol (KMF) on colorectal and renal adenocarcinoma cell lines. 24 h after seeding, cells were treated with kaempferol at different concentrations. 4 wells remained untreated (control). 96 h later, cell mass was quantified via SRB viability assay. Error bars indicate +/- SD. Mean of three independent experiments performed in triplicates is shown. The mock-treated triplicate was set to 100 % cell mass. The green bars indicate the concentrations, which were selected for combination therapy with VACV GLV-1h68.

3.4 Identification of optimized concentrations of SAHA for the epigenetic treatment of colorectal and renal adenocarcinoma cell lines

All cell lines were treated with different concentrations of the potent epigenetic compound SAHA to evaluate overall HDAC inhibition in a concentration range from 1 µM until 50 µM. 96 h after treatment, SRB assay was performed to evaluate cytotoxic effects.

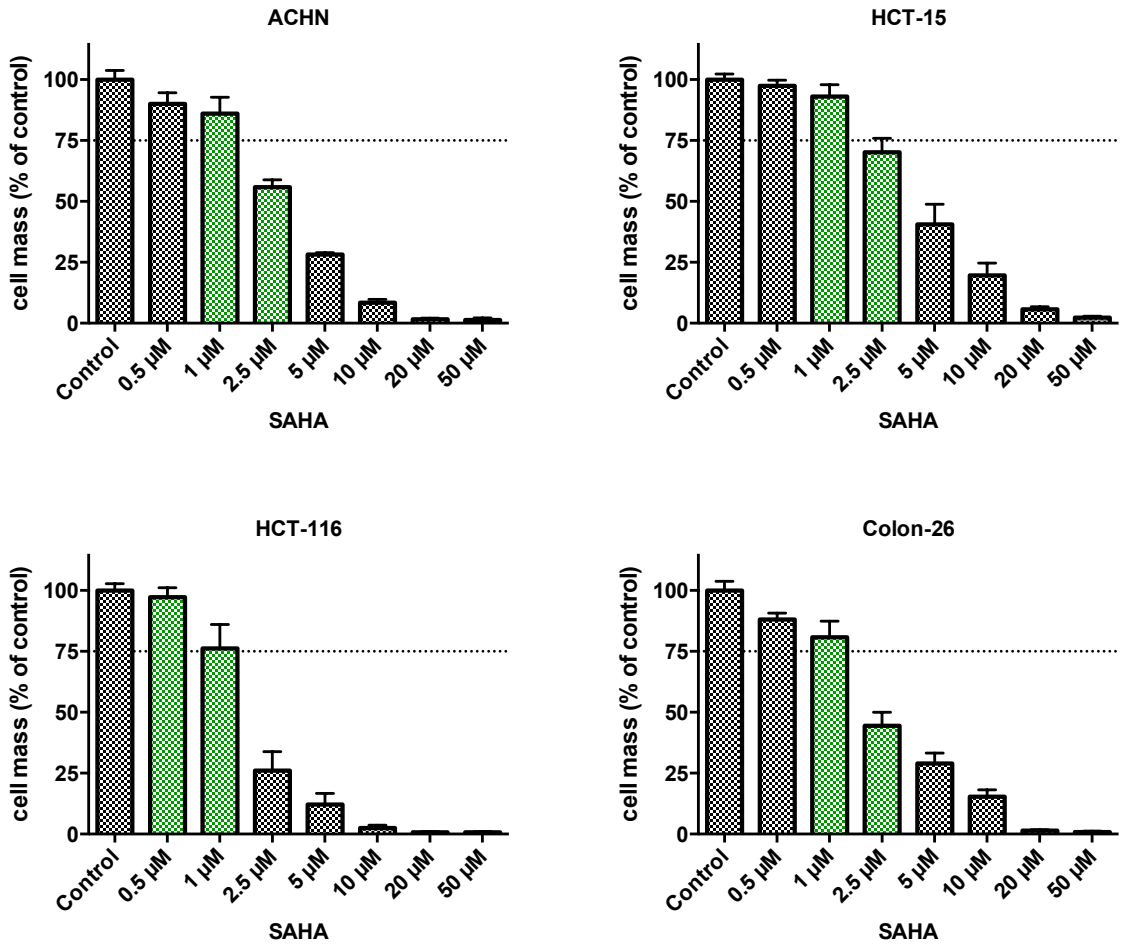

Figure 18. Cytotoxic effect of SAHA on colorectal and renal adenocarcinoma cell lines. Cells were treated with rising SAHA concentrations 24 h after seeding or remained untreated (control). 96 h later, cell mass was quantified via SRB assay. Error bars indicate +/- SD. Mean of three independent experiments performed in triplicates is shown. The mock-treated triplicate was set to 100 % cell mass. The green bars indicate the concentrations, which were selected for combinatorial treatment with VACV GLV-1h68.

Figure 18 illustrates the cytotoxic effect of rising concentrations of SAHA in different tumor cell lines. 96 h after treatment, except for HCT-15, remarkable inhibition values for 5 µM were detected in each cell line, with a reduction of cell mass in the range of 72 - 88 %, depending on the cell line. In HCT-15 cells, 5 µM reduced cell mass to 59 %. Consequently, low concentrations were selected for combinatorial treatment: concentrations of 1 µM and 2.5 µM were chosen for ACHN, HCT-15 and Colon-26, whereas for HCT-116, lower concentrations of 0.5 µM and 1 µM were selected because 2.5 µM already led to a reduction of cell mass by 74 %.

3.5 Summary of the monotherapeutic treatment

The table below shows the MOIs of VACV GLV-1h68 and the concentrations of the different epigenetic compounds, which were chosen for further experiments.

Cell lines	MOI	HDACi	Concentrations
ACHN	0.01	resveratrol	2.5 μM 5 μM
		kaempferol	10 μM 20 μM
		SAHA	1 μM 2.5 μM
HCT-15	0.1	resveratrol	10 μM 20 μM
		kaempferol	10 μM 20 μM
		SAHA	1 μM 2.5 μM
HCT-116	0.01	resveratrol	10 μM 20 μM
		kaempferol	10 μM 20 μM
		SAHA	0.5 μM 1 μM
Colon-26	0.1	resveratrol	10 μM 20 μM
		kaempferol	10 μM 20 μM
		SAHA	1 μM 2.5 μM

Table 13. Summary of the concentrations used for combinatorial treatment.

3.6 Combination therapy of vaccinia virus GLV-1h68 with epigenetic compounds

With the results from the pre-testing above, combinatorial treatment was performed (Figure 19). Tumor cells were plated. After 24 h, cells were treated with one of the epigenetic compounds. 24 h later, cells were infected with GLV-1h68 or mock-infected. 72 hpi, remnant tumor cell masses were quantified in different assays.

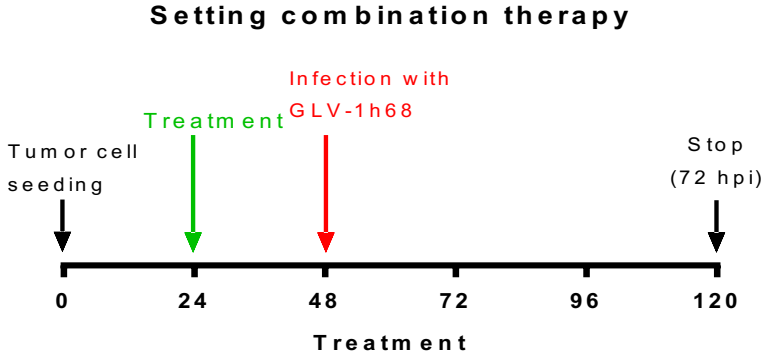

Figure 19. General application scheme for combinatorial treatment of tumor cell lines with the epigenetic compounds and GLV-1h68. 24 hours after cells were plated, treatment with one epigenetic compound, resveratrol, kaempferol, or SAHA, was performed. 24 later, cells were infected with GLV-1h68 or mock-infected. 72 hours post infection (hpi), different assays were performed.

First, SRB viability assay was performed. The results of the SRB viability assay did not measure the expected differences as seen after wells were colored with SRB staining solution. To validate the antiproliferative and cytotoxic potential of the co-treatment, further cell viability assays were performed, such as CellTiter-Blue assay, LDH assay, and area calculation, using the dyed wells from SRB viability assay. Since these differences were also seen in kaempferol and SAHA, same assays were performed as well. For promising co-treatments, mainly with resveratrol or SAHA, further assays were performed, e.g. analysis of the cell cycle profile, viral replication behavior of GLV-1h68, and cell growth over time in the real-time cell monitoring.

For a better distinction, the blue-colored bars in each graph indicate the combinatorial treatments.

3.6.1 Combination therapy of vaccinia virus GLV-1h68 and resveratrol

3.6.1.1 Cell viability and cytotoxicity assays

SRB assay

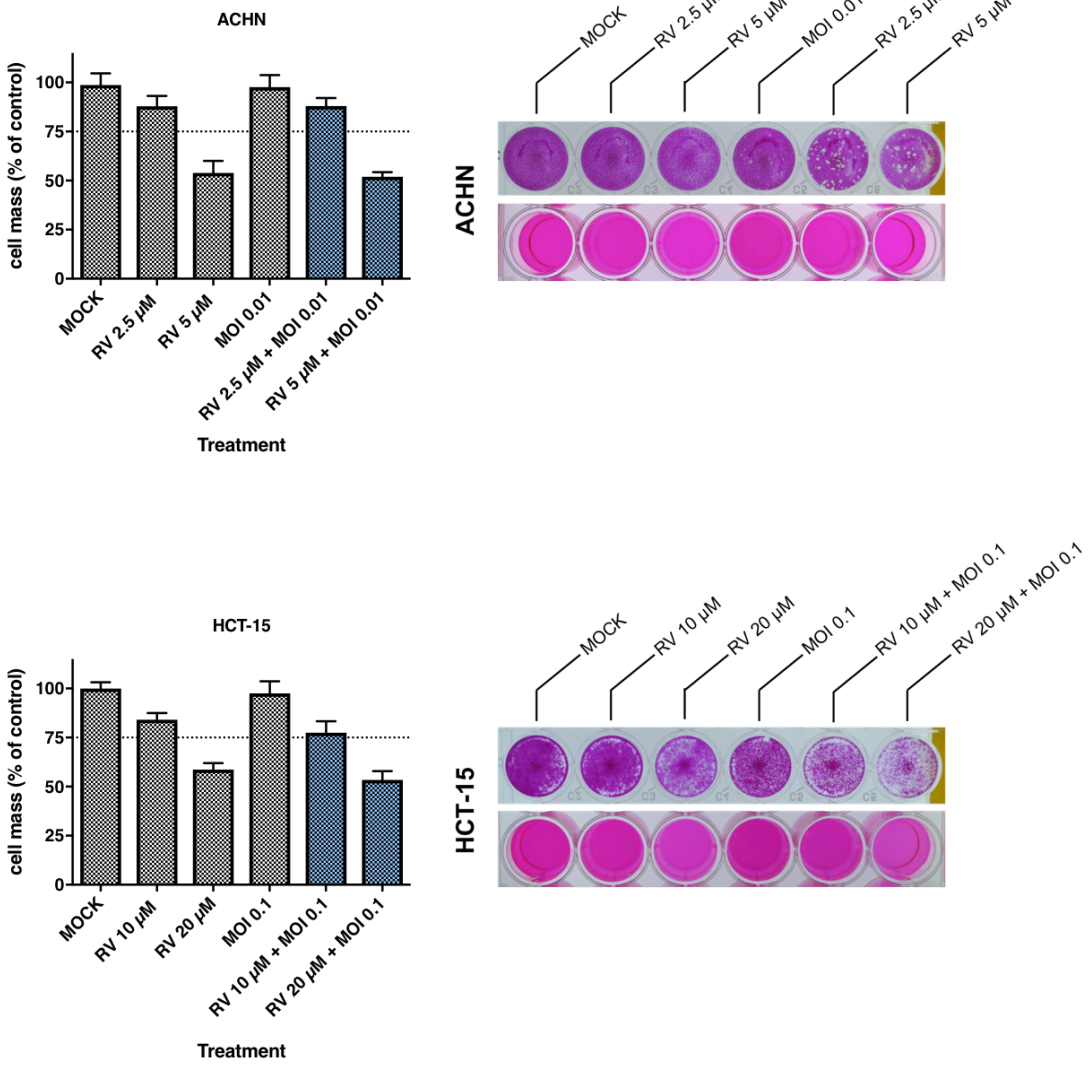

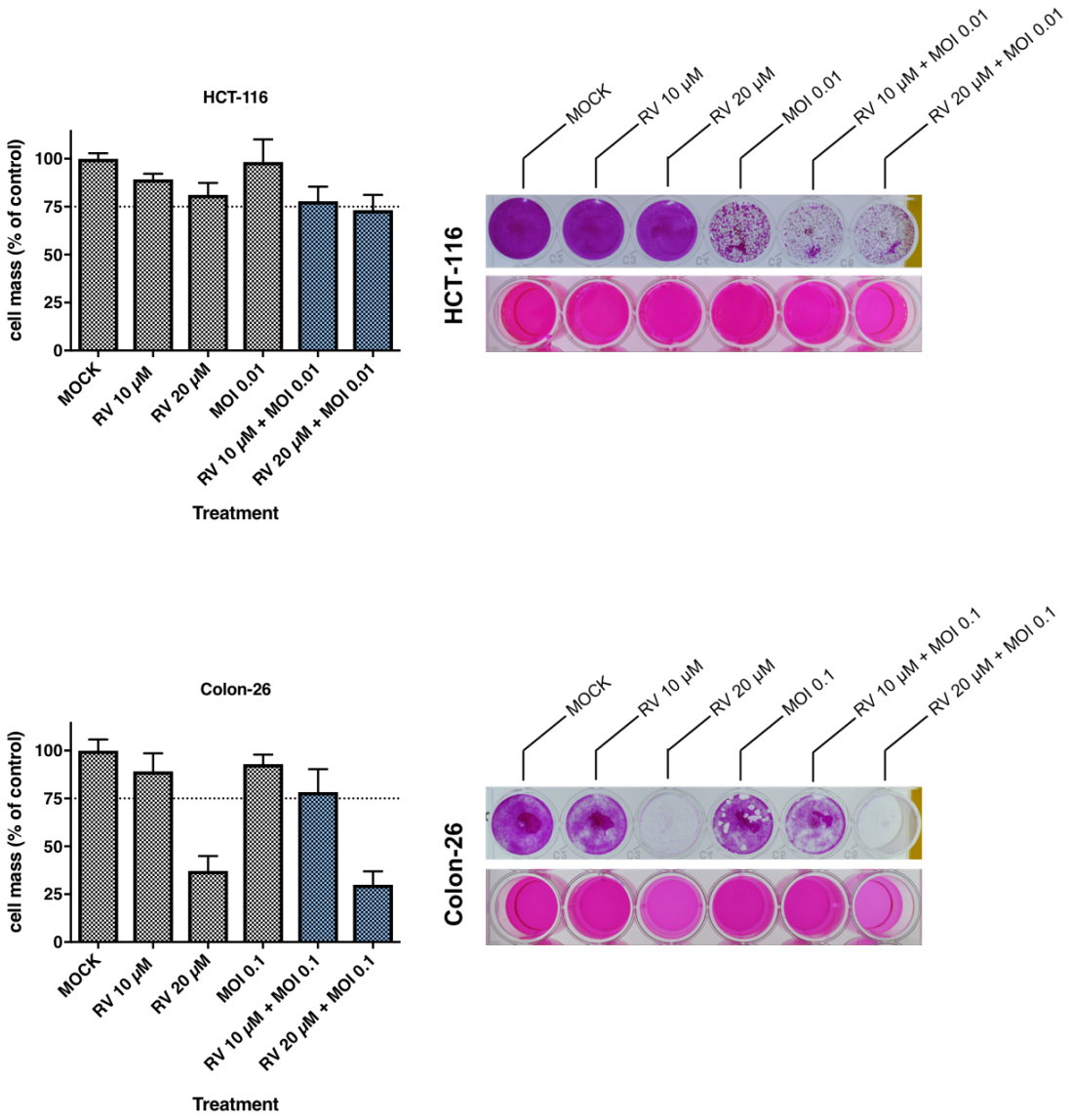

Figure 20. SRB viability assay and pictures of the 24-well plates. Cells were either treated with resveratrol (RV), infected with GLV-1h68 alone or co-treatment was performed. SRB viability assay was performed 72 hpi to quantify the remnant tumor cell masses. On the left-hand side, mean of three independent experiments performed in quadruplicates is shown. Error bars indicate +/- SD. The mock-treated quadruplicate was set to 100 % cell mass. The right-hand side shows the pictures of the 24-well plates after staining with sulforhodamine B dye (above), and after solubilization with Tris base (below). One row of the 24-well plate is exemplarily shown for one of the three experiments.

As seen in the graphs of the SRB assays on the left-hand side in Figure 20, combinatorial treatment only had a marginal or no benefit in ACHN and HCT-15 cells when compared to the respective mono-treatments. By contrast, Colon-26 cell masses were reduced to 78 % in co-treatment with 10 µM resveratrol whereas a reduction to 89 % (RV) and 93% (GLV-1h68) was achieved in

monotherapy. In HCT-116, cell viability in co-treatment with 10 µM resveratrol was reduced to a mean of 78 %, compared to the single treatment 89 % (RV) or 98 % (GLV-1h68).

When looking at the pictures of the stained wells on the right-hand side, combinatorial treatment in ACHN, HCT-15, and HCT-116 showed more and larger plaques than monotherapeutic treatment with GLV-1h68 alone. In Colon-26 cells, combinatorial treatment resulted in fewer plaques in comparison to monotherapy with GLV-1h68 alone, but the cell layer was visibly reduced.

Mainly in HCT-116 and Colon-26, the pictures of the dyed plates and the solubilized dye demonstrated discrepancies. Especially in the last (6^{th}) panel (co-treatment with the higher resveratrol concentration), the cell layer was visibly reduced when color was dried, but when solubilized with Tris, pink color appeared stronger than expected and the measured optical density (OD) didn't show expected outcomes. In contrast, the pictures of the stained wells of ACHN plates were in accordance with the analysis of the solubilized dye. To clear discrepancies, cell-free area of the wells was calculated (see Figure 24).

CellTiter-Blue assay

To further validate the antiproliferative potential of the co-treatment with resveratrol, the cytotoxicity assay CellTiter-Blue (Figure 21) was performed.

In HCT-116 cells, the cell viability decreased in combinatorial treatment and reached values below the indicated 75 % threshold. In HCT-15 and Colon-26 cells, a benefit was detectable between monotherapy with resveratrol concentrations of 10 µM and combinatorial treatment with 10 µM resveratrol at MOI 0.1. In HCT15 cell mass decreased from 85 % in monotherapy (RV alone) to 76 % in co-treatment, whereas in Colon-26 cells cell mass decreased from 80 % (RV alone) to 64 % in co-treatment. At resveratrol concentrations of 20 µM no further reduction of cell viability was observed upon additional infection with GLV-1h68. In ACHN cells, no benefit could be identified in co-treatment compared to single-agent treatment.

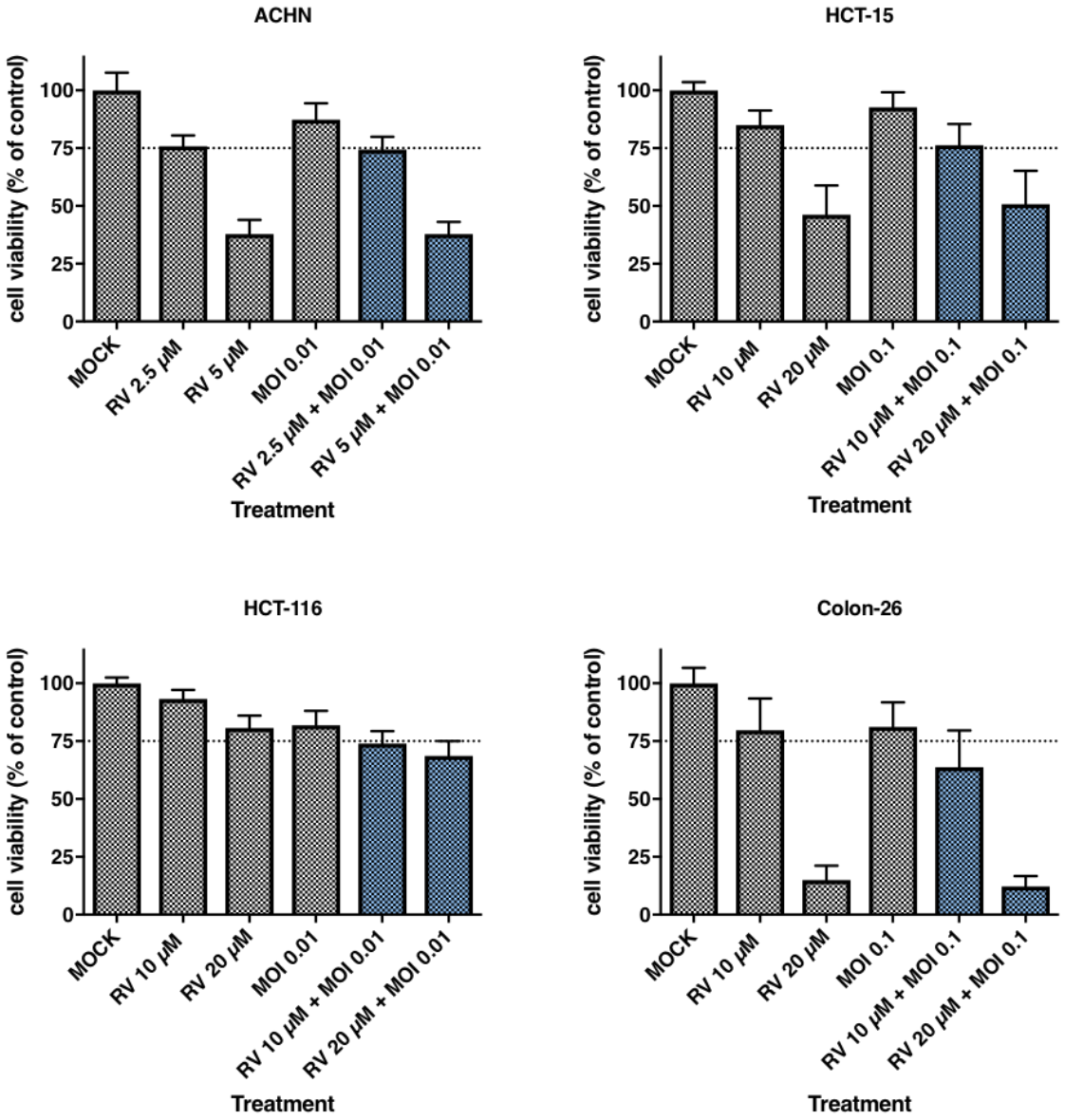

Figure 21. CellTiter-Blue assay. The four cell lines were either treated with resveratrol (RV) alone, infected with GLV-1h68 alone or co-treatment was performed. After 72 hpi, CellTiter-Blue assay was performed. Mean of three independent experiments performed in quadruplicates is shown. Error bars indicate +/- SD. The mock-treated quadruplicate was set to 100 % cell mass.

LDH assay

In the next step, the LDH assay was performed 120 h after cells were plated (Figure 22). It measures the release of LDH into the culture medium after cell death.

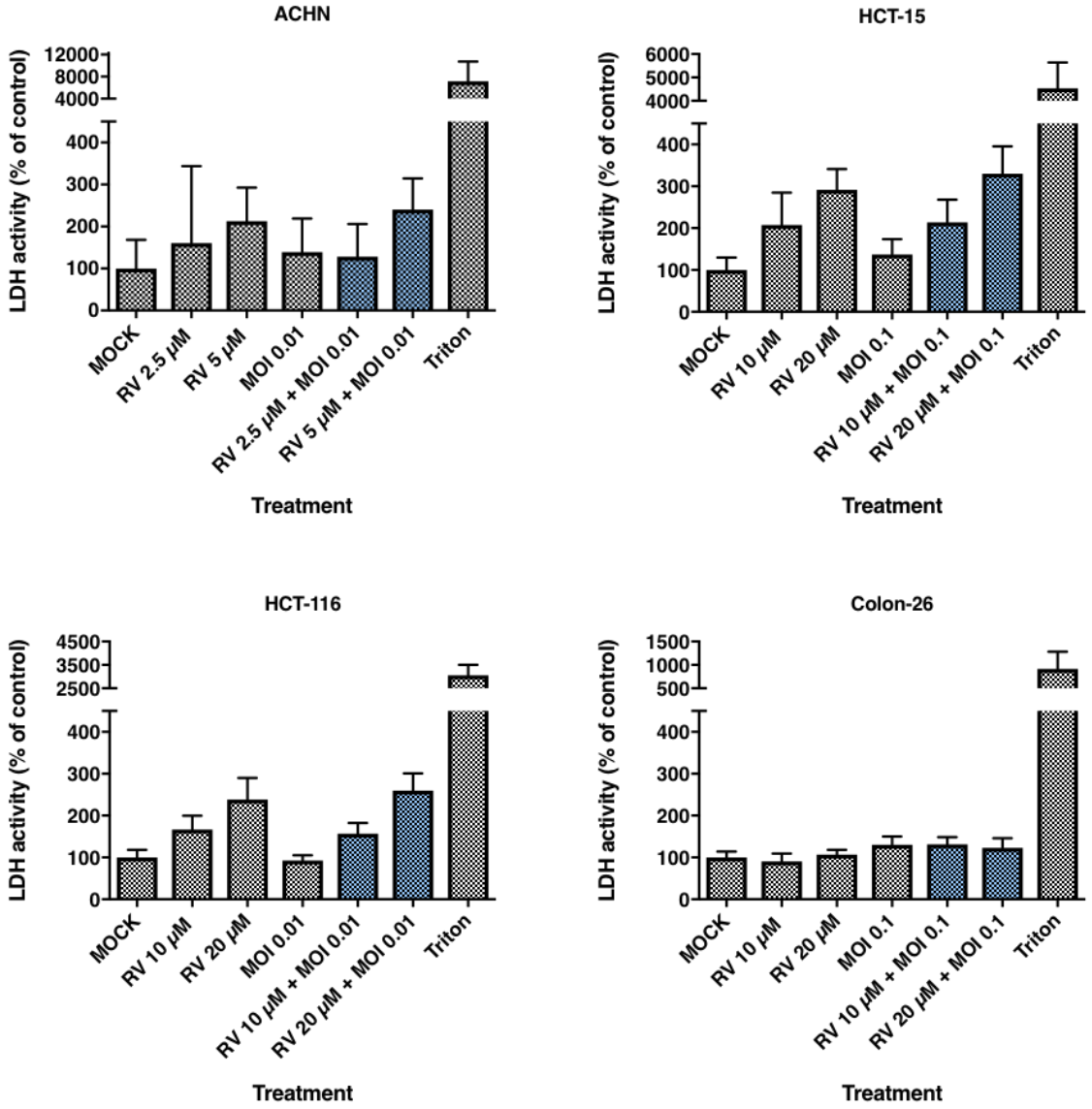

Figure 22. LDH assay. The four cell lines were either treated with resveratrol (RV) alone, infected with GLV-1h68 alone or co-treated. 120 h after seeding, LDH assay was performed. As a control for total LDH release, Triton was added to four wells. Mean of three independent experiments performed in quadruplicates is shown. Error bars indicate +/- SD. The mock-treated quadruplicate was set to 100 % LDH activity.

In all cell lines, combinatorial treatment did not measurably increase LDH activity, when compared to the respective mono-treatments.

3.6.1.2 Fluorescence monitoring

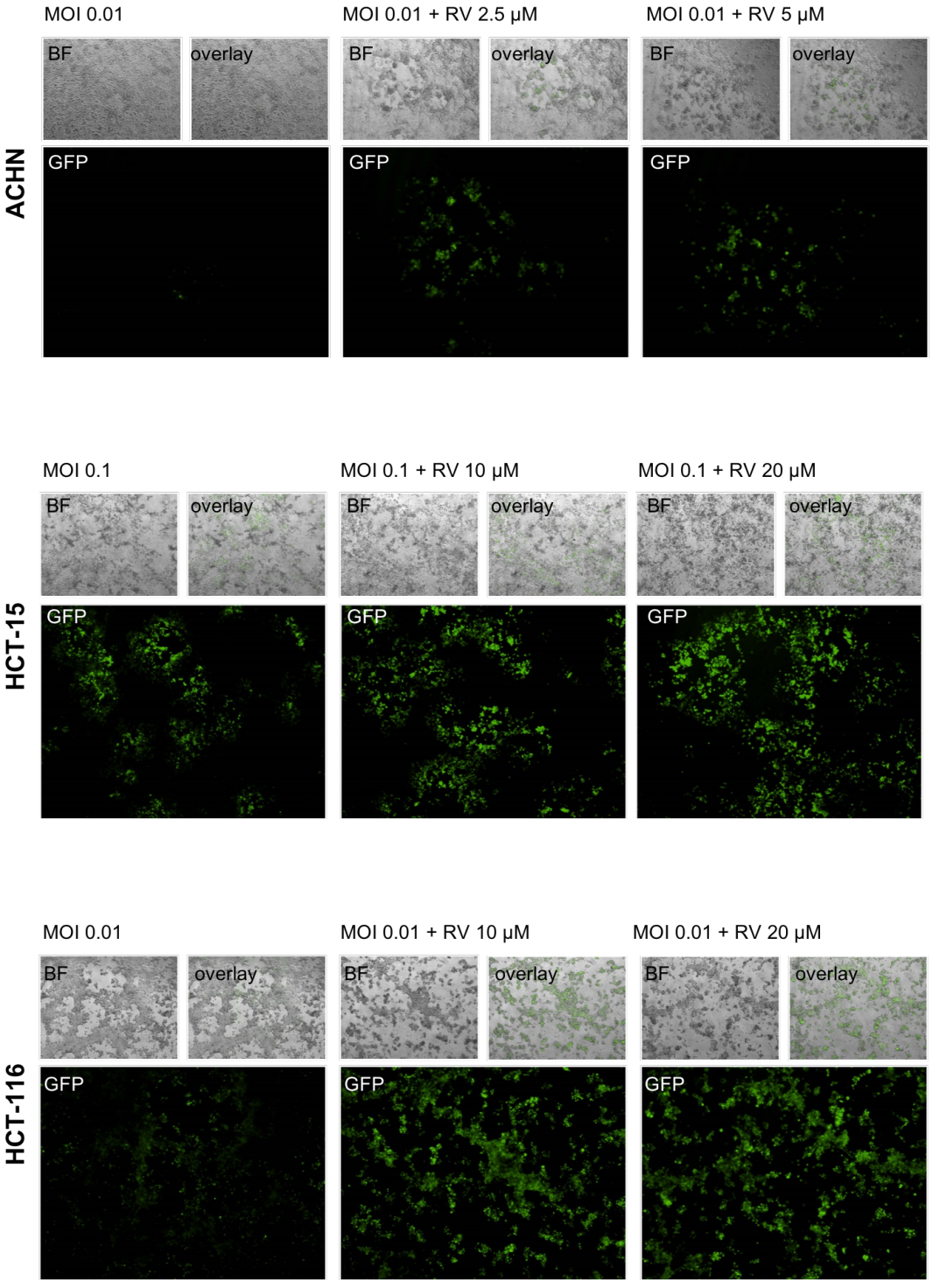

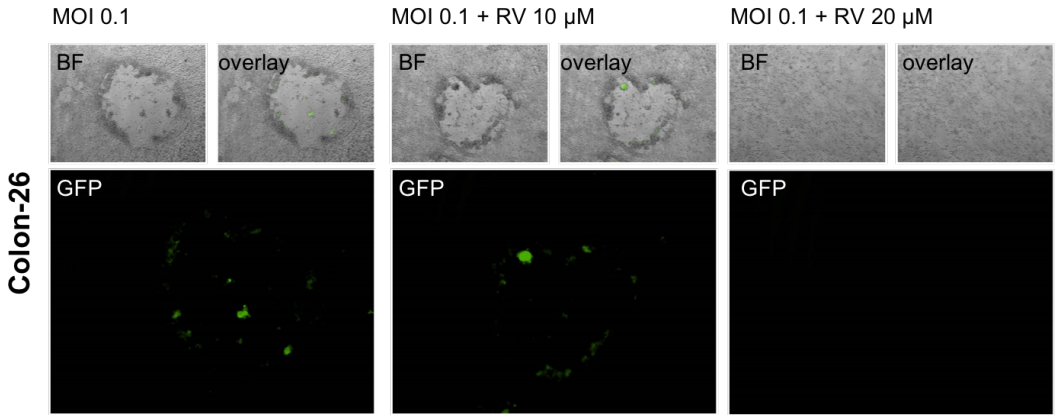

Figure 23. Fluorescence monitoring of the different cell lines in monotherapy with GLV-1h68 compared to combinatorial treatment with resveratrol (RV). The four cell lines were either infected with GLV-1h68 alone or co-treatment with resveratrol was performed. 72 hpi, expression of GFP was analyzed by fluorescence microscopy. Serial phase contrast bright-field microscopy (BF) and corresponding fluorescence photos (GFP) were taken at the same magnification and overlaid. Green fluorescence indicates infection with GLV-1h68.

At 72 hpi, combinatorial treatment with resveratrol resulted in an increased green fluorescence signal when compared to treatment with GLV-1h68 alone in ACHN, HCT-15, and HCT-116 cells. In contrast, murine Colon-26 cells showed an adverse effect in co-treatment with 20 µM resveratrol - the GFP signal was reduced and plaques decreased in number and size. In bright-field (BF) microscopy, the cell mass was visibly reduced in cell lines ACHN and HCT-116, whereas in HCT-15, cell mass appeared constant (Figure 23).

The results of the different viability assays, such as SRB assay, CellTiter-Blue assay and LDH assay did not visualize expected outcomes as seen after detection of GFP in fluorescence microscopy or remaining cells in the wells after colored with SRB staining solution. Therefore, the wells were dyed with SRB staining solution and photographed. Cell-free area was calculated as seen in Figure 24.

3.6.1.3 Area calculation

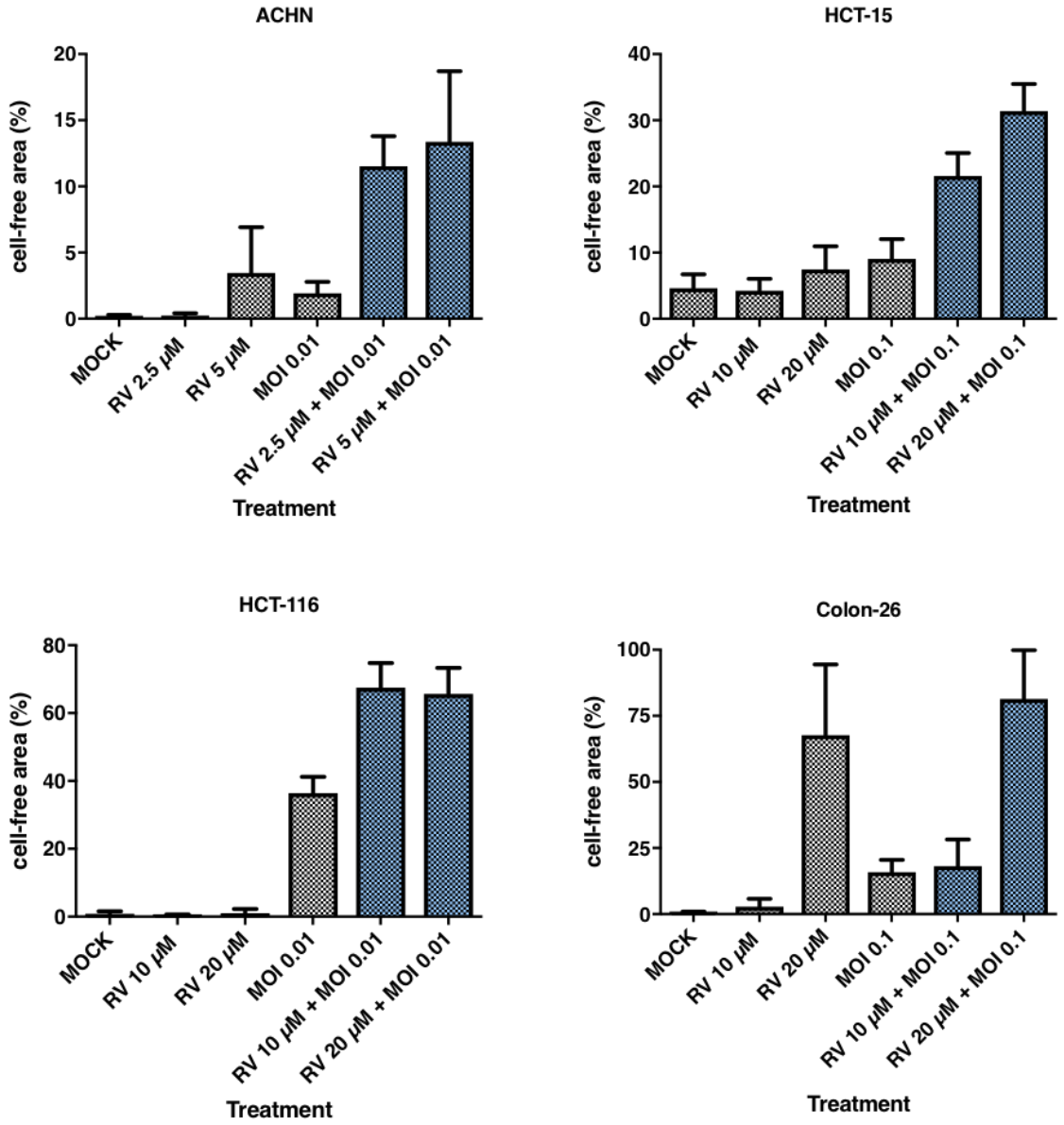

Figure 24. Area calculation. Cells were treated with the chosen concentrations of resveratrol (RV). After 24 h, cells were infected with VACV GLV-1h68. After 72 hpi, SRB assay was performed. After the 24-well plate was dyed with SRB staining solution and dried overnight, area calculation was performed to quantify cell-free area of the wells. The columns of each group show the cell-free area in percent. Mean of three independent experiments performed in quadruplicates is shown. Error bars indicate +/- SD.

Compared to treatment with resveratrol or GLV-1h68 alone, combinatorial treatment leads in all cell lines to increased cell-free areas and thus displayed signs of cell death. Results were promising for co-treatment in HCT-116 cells with GLV-1h68 and resveratrol. Here, a cell-free area in the range of 65 - 67 %

was achieved, whereas monotherapy with GLV-1h68 alone only reached a cell-free area of 36 %. In HCT-15, a cell-free area of 31 % was achieved in co-treatment compared to 7 % (20 µM RV) or 9 % (GLV-1h68 MOI 0.1) in single-agent treatment. ACHN cells showed a cell-free area in the range of 11 - 13 % in co-treatment compared to 3 % in single-agent treatment with 5 µM RV. Combinatorial treatment in Colon-26 cells demonstrated a marginal effect at a resveratrol concentration of 20 µM. In the lower resveratrol concentration, a small benefit could be identified (Figure 24).

Since treatment with ACHN and HCT-116 showed best results with the epigenetic compound resveratrol, further investigations were conducted. The real-time cellular impedance assay was performed with ACHN and HCT-116 solely. Virus growth curves were performed with ACHN cells only.

3.6.1.4 Virus growth curves

ACHN cells were infected with GLV-1h68 at MOI 0.01. Infected cells were harvested and frozen at 1, 24, 48, 72 and 96 hpi. Virus titration was performed using CV-1 cells to quantify the amount of virus plaques. Replication behavior of GLV-1h68 at MOI 0.01 was analyzed via growth curves (chapter 2.9).

Viral replication started post infection in monotherapy and co-treatment. Viral particles increased most strikingly during the first 24 hpi in monotherapy. In the following 24 h, virus production stagnated when looking at GLV-1h68 infection solely (red line). When looking at the complete detection period, resveratrol did not enhance the replication of GLV-1h68 (black line) when compared to infection with GLV-1h68 solely (red line) (Figure 25).

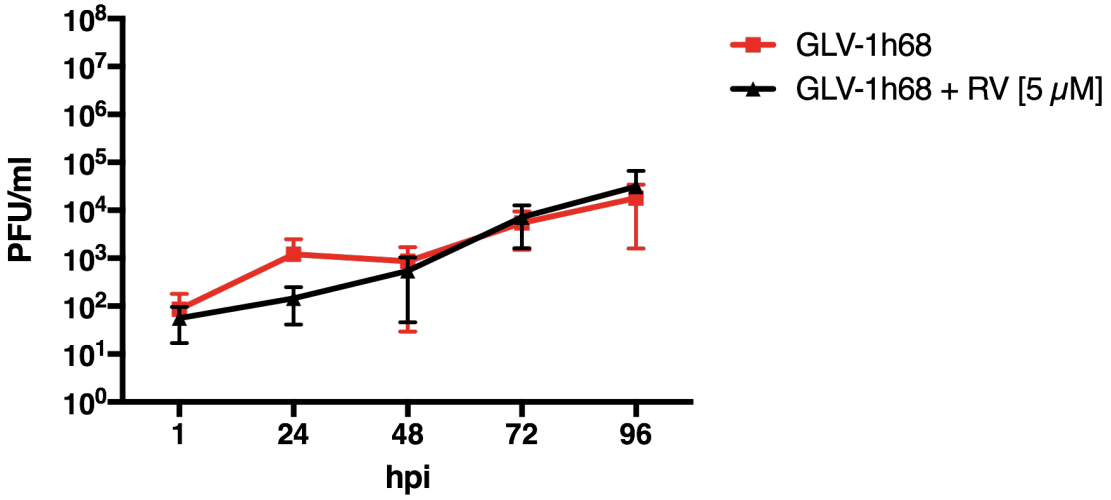

Figure 25. Replication of GLV-1h68 with or without 5 µM resveratrol (RV) in ACHN cells. Cells were treated with resveratrol or mock-treated. After 24 h, cells were infected with GLV-1h68 at MOI 0.01. At 1, 24, 48, 72 and 96 hpi, samples were taken. Titration was performed on CV-1 cells to quantify the amount of virus plaques. The result of solely GLV-1h68-infected cells (red line) is displayed along with GLV-1h68 + resveratrol co-treated cells (black line). Results are shown in PFU/ml. Mean of three independent experiments is shown. Error bars indicate +/- SD.

6.6.1.5 Real-time Cellular Impedance measurement

The techniques above are different kinds of endpoint assays, which do not provide information about the onset of cytopathic effects and kinetics of viral replication. In contrast, the real-time cellular impedance measurement monitors all cell events during the complete detection period, e.g. cell number change and cell viability.

Based on the dynamic monitoring of cell proliferation, 24 hours after seeding, ACHN and HCT-116 cells were treated using different resveratrol concentrations and 24 h later infected with GLV-1h68 at MOI 0.01 alone or combinatorial treatment was performed.

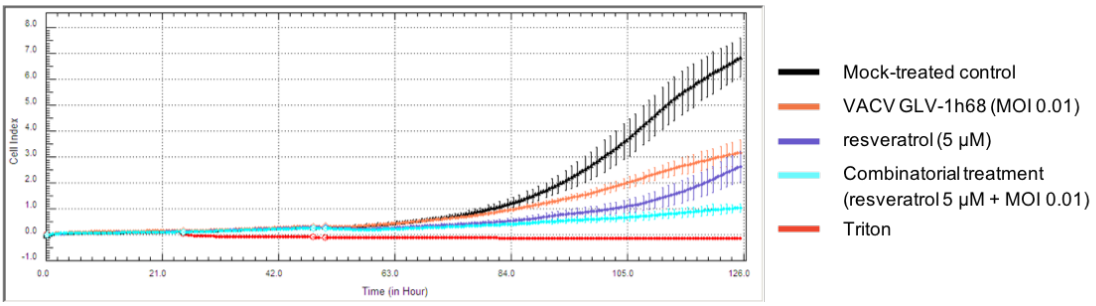

Figure 26. Real-time monitoring of proliferation of ACHN tumor cells after treatment with 5 µM resveratrol (RV) and infection with GLV-1h68. The colored lines indicate the different treatments. Cells were measured every 30 minutes using the RCTA SP instrument. Measured electrode impedance is expressed as Cell Index and graphically represented.

Combinatorial treatment with GLV-1h68 and 5 µM resveratrol (Figure 26, light blue line) showed an increased oncolytic cell death in ACHN tumor cells over 120 h in comparison to mock treatment or monotherapy alone.

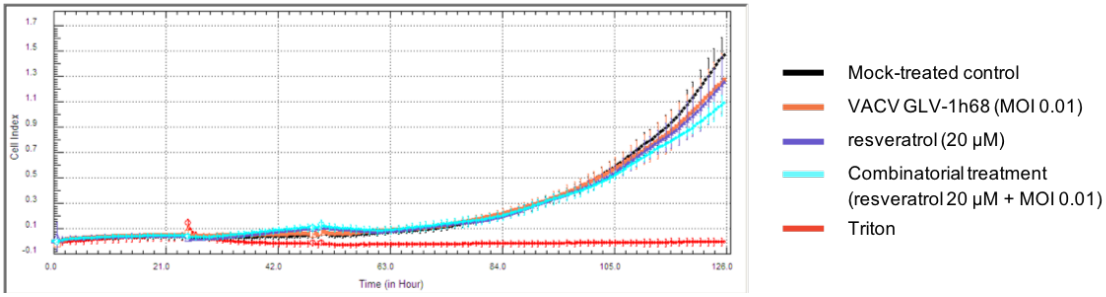

Figure 27. Real-time monitoring of proliferation of HCT-116 tumor cells after treatment with 20 µM resveratrol (RV) and infection with GLV-1h68. The colored lines indicate the different treatments. Cells were measured every 30 minutes using the RCTA SP instrument. Measured electrode impedance is expressed as Cell Index and graphically represented.

Experiments with the tumor cell line HCT-116 showed in co-treatment a marginal benefit with 20 µM resveratrol (Figure 27, light blue line).

3.6.2 Combination therapy of vaccinia virus GLV-1h68 and kaempferol

3.6.2.1 Cell viability assays

SRB assay

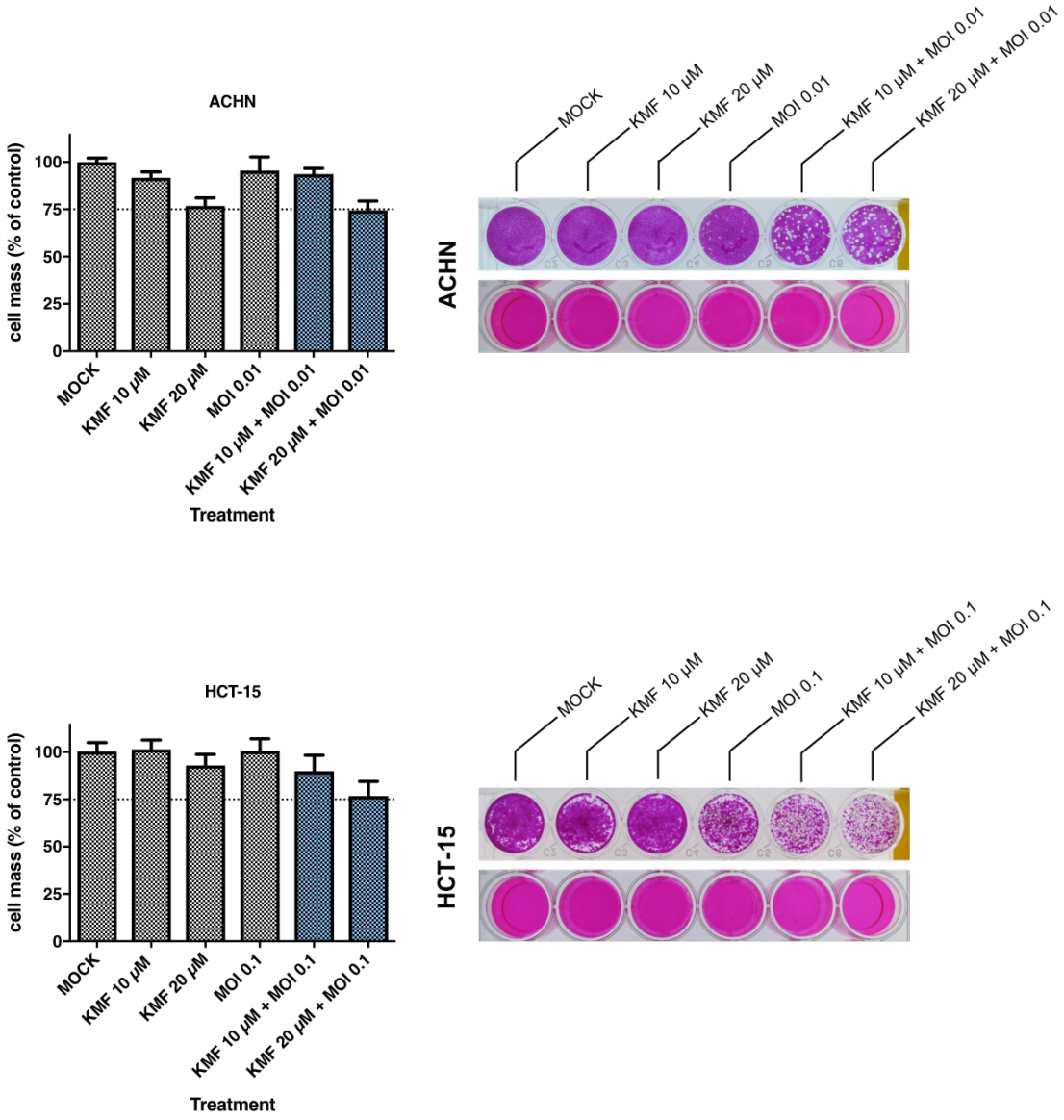

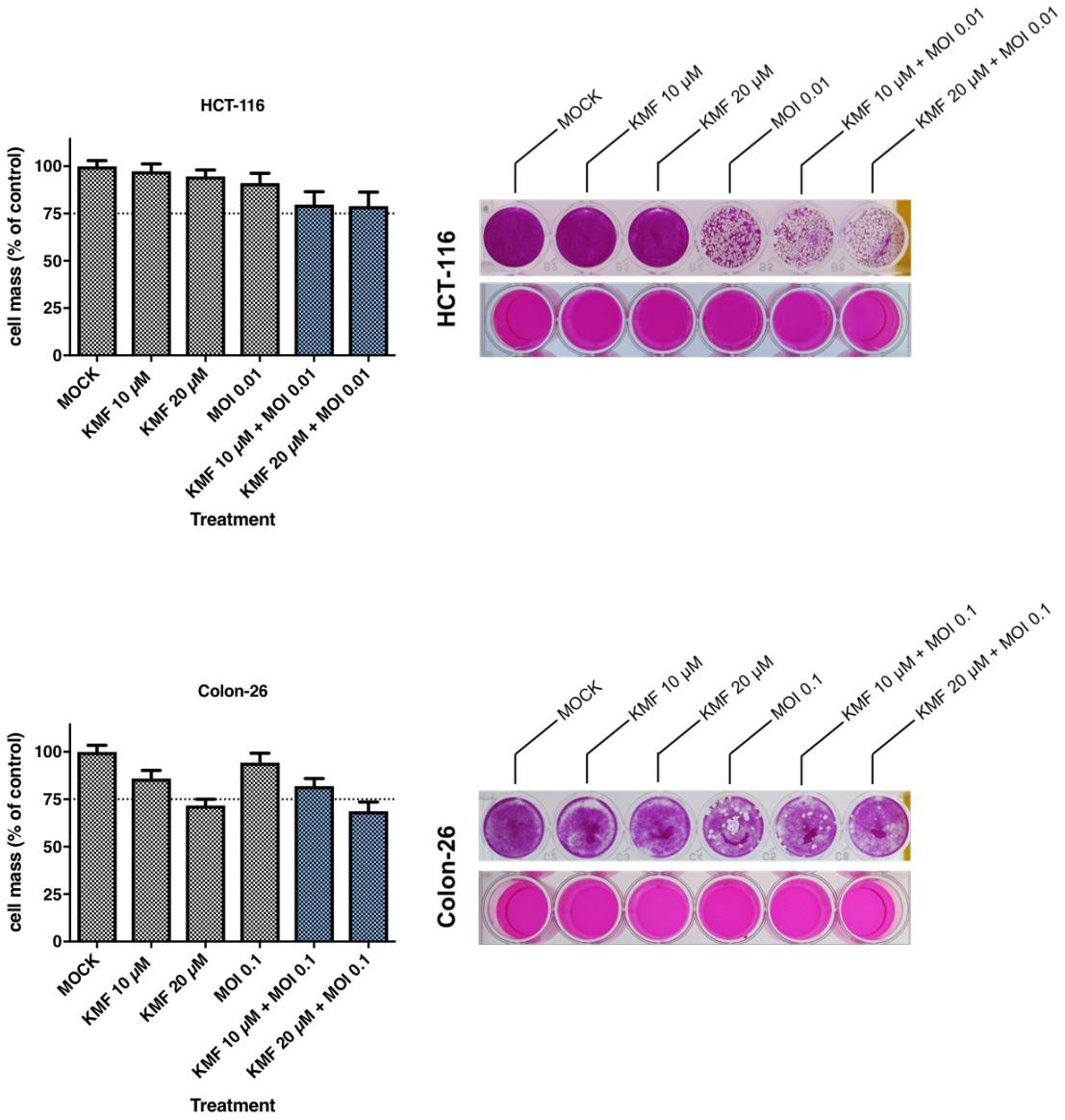

Figure 28. SRB viability assay and pictures of the 24-well plates. Cells were treated with the chosen concentrations of kaempferol (KMF). After 24 h, cells were infected with VACV GLV-1h68. At 72 hpi, SRB assay was performed. On the left-hand side, mean of three independent experiments performed in quadruplicates is shown. Error bars indicate +/- SD. The mock-treated quadruplicate was set to 100 % cell mass. The right-hand side shows the pictures of the 24-well plates after staining with sulforhodamine B dye (above), and after solubilization with Tris base (below). One row of the 24-well plate is exemplarily shown for one of the three experiments.

As seen in the graphs on the left-hand side in Figure 28, combinatorial treatment of HCT-15 and HCT-116 tumor cells leads to a slight increased cell death compared to monotherapies. Co-treatment with 20 µM kaempferol was found to reduce cell mass in HCT-15 cells to 76 % compared to 93 % kaempferol (KMF) or 100% (GLV-1h68) in the corresponding monotherapies.

Combinatorial treatment in HCT-116 cells led to a reduction of cell mass to 79 %, whereas the respective mono-treatments reduced cell mass only to a range of 91 - 97 %. By contrast, combination therapy had little or no benefit in ACHN and Colon-26 cells. As a result, in none of the four analyzed cell lines combinatorial treatment could reduce cell mass to significantly less than 70 %.

When looking at the images on the right-hand side, in panel 1, the mock-treated cells showed no cell-free area except for HCT-15 and Colon-26, similar to panel two and three with the two different concentrations of kaempferol.

Plaques were visible in panel four in all cell lines. Combinatorial treatment in ACHN, HCT-15, and HCT-116 showed more and larger plaques. In Colon-26 cells, combinatorial treatment displayed fewer plaques when compared with monotherapy GLV-1h68 alone.

Nevertheless, in all cell lines, dried dye and solubilized dye demonstrated discrepancies. Especially for HCT-15 and HCT-116 cells, cell layers were visibly reduced in combinatorial treatment; however, when the dye was solved, the optical density (OD) was higher than expected. Therefore, cell-free areas of the wells were calculated to graphically display the visible increased cell death in ACHN, HCT-15, and HCT-116 cells (see Figure 32).

CellTiter-Blue assay

A slight benefit was observed in combination therapy in Colon-26, HCT-15 and HCT-116 cells (see Figure 29). When GLV-1h68 was added to 10 µM kaempferol, co-treatment reduced the cell mass from 84 % to 73 % in Colon-26 cells. Co-treatment with 10 µM kaempferol was found to reduce cell mass in HCT-116 cells to 80 % compared to 94 % (KMF) or 81 % (GLV-1h68) in the corresponding monotherapies. The cell line ACHN hardly responded to combinatorial treatment.

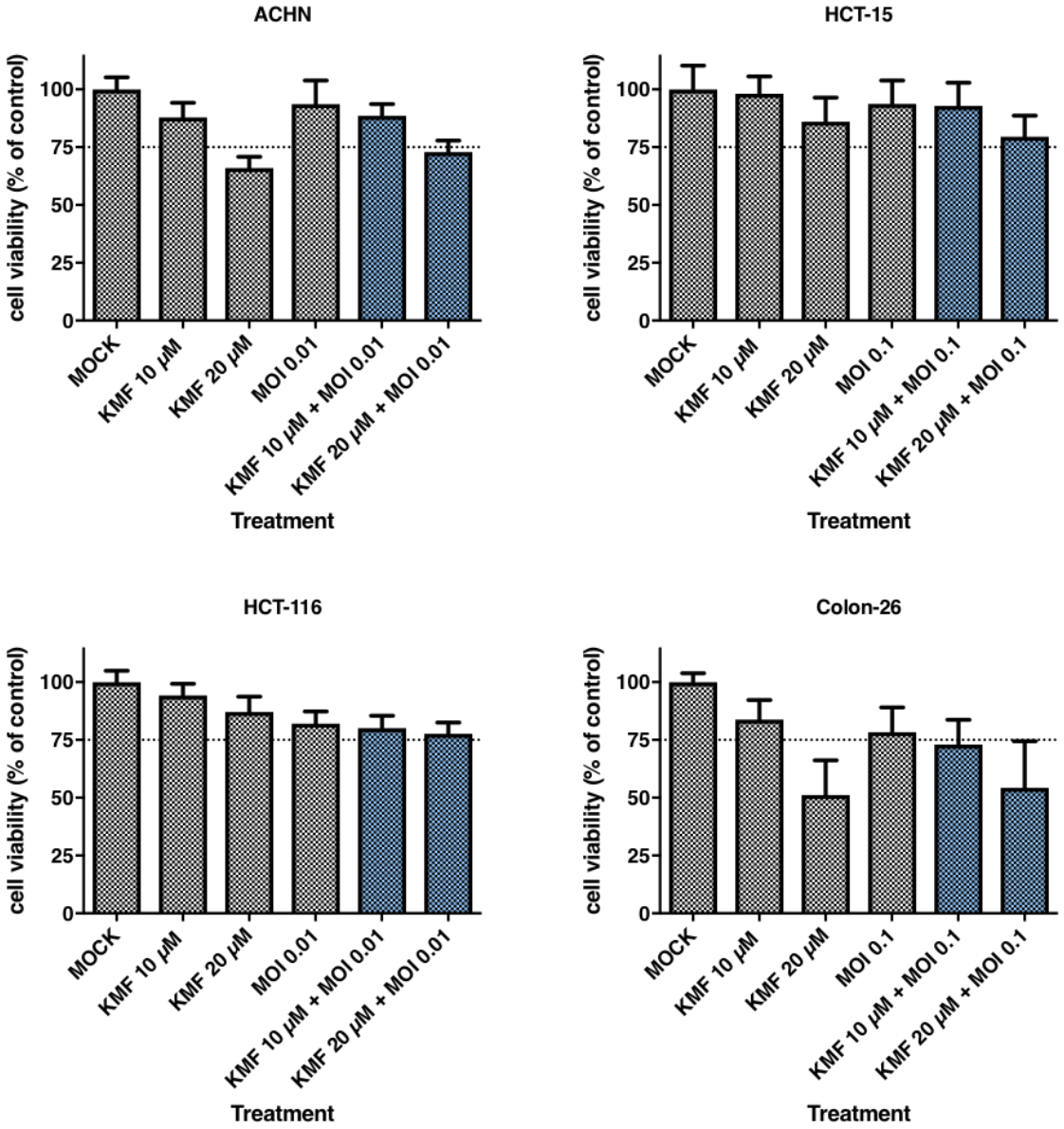

Figure 29. CellTiter-Blue assay. The graphs represent the four cell lines, which were either treated with kaempferol (KMF) alone, infected with GLV-1h68 alone or co-treatment was performed. After 72 hpi, CellTiter-Blue assay was performed to quantify cell viability. Mean of three independent experiments performed in quadruplicates is shown. Error bars indicate +/- SD.

LDH assay

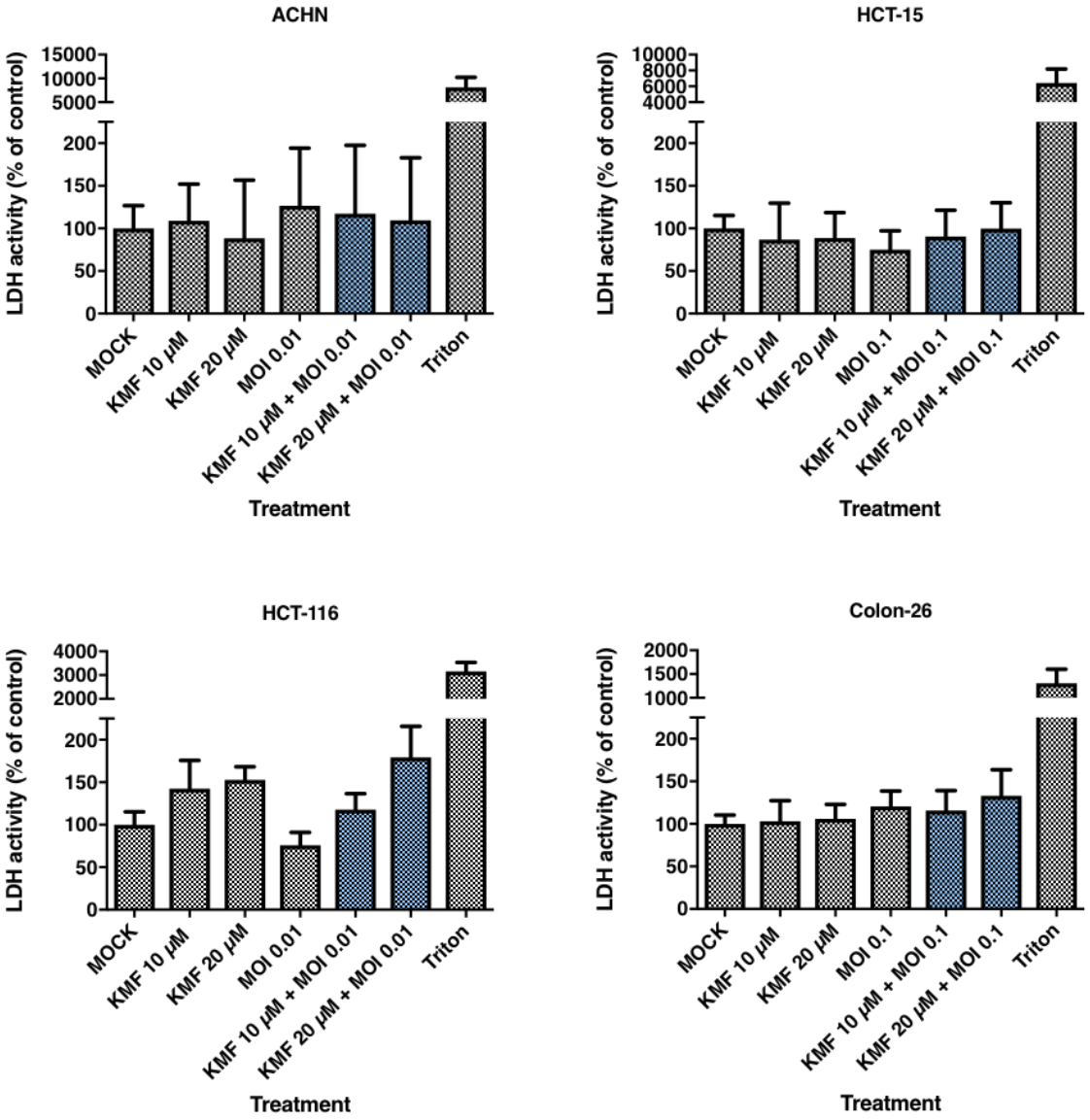

Figure 30. LDH assay. The graphs represent the four cell lines, which were either treated with kaempferol (KMF) alone, infected with GLV-1h68 alone or co-treatment was performed. Thereafter, LDH assay was performed. As a control for total LDH release, cells were completely lysed with Triton. Mean of three independent experiments performed in quadruplicates is shown. Error bars indicate +/- SD. The mock-treated quadruplicates were set to 100 % LDH activity.

In ACHN, Colon-26, HCT-15, and HCT-116 cells, combinatorial treatment did not measurably increase LDH activity when compared to the respective mono-treatments. A slight increased LDH activity could be seen in co-treatment in HCT-116 cells at a concentration of 20 µM KMF compared to the respective mono-treatments (Figure 30).

3.6.2.2 Fluorescence monitoring

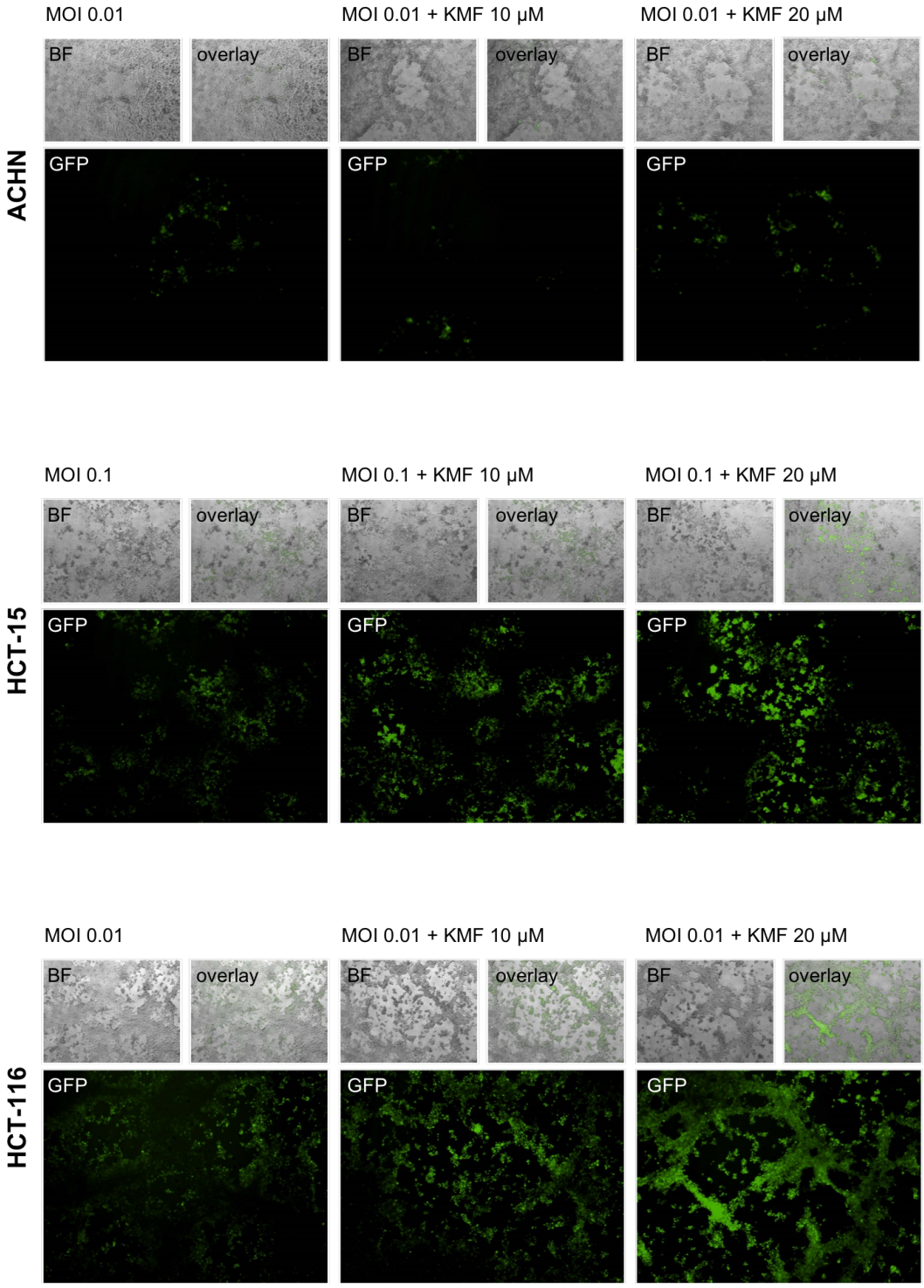

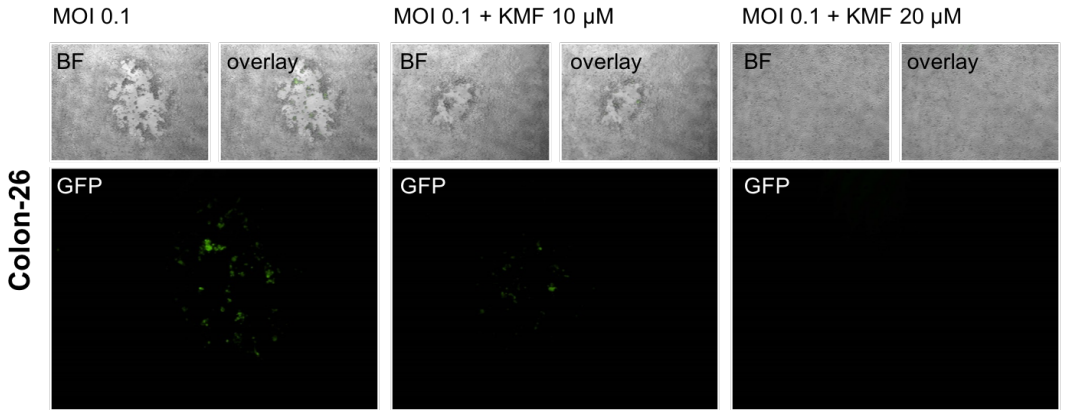

Figure 31. Fluorescence monitoring of the four cell lines in monotherapy with GLV-1h68 compared to combinatorial treatment with kaempferol (KMF). The four cell lines were either infected with GLV-1h68 alone or co-treatment with KMF was performed. After 72 hpi, the expression of GFP was analyzed by fluorescence microscopy. Green fluorescence indicated the infection of tumor cells. Phase contrast and fluorescence photos were taken and overlaid.

In ACHN cells, the presence of kaempferol resulted in more and larger plaques. Additionally, slightly more green fluorescence was emitted. In HCT-15 and HCT-116 cells, combinatorial treatment led to an increased virus-associated GFP expression. In HCT-116 cells, at MOI 0.01 and 20 µM kaempferol almost every cell was infected. In contrast, murine Colon-26 cells displayed an adverse effect in combination therapy when compared to the other cell lines. Less green fluorescence as well as fewer plaques were visible in combinatorial treatment with kaempferol in comparison to monotherapy. Nevertheless, the cell layer was visibly reduced at a concentration of 10 µM kaempferol (Figure 31).

3.6.2.3 Area calculation

Except for Colon-26, each cell line showed an increased cell-free area in combinatorial treatment and thus displayed signs of increased cell death (see Figure 32). Co-treatment in ACHN cells achieved a cell-free area in the range of 13 - 15 % compared to 2 % (GLV-1h68 single-treatment alone). In HCT-15 cells, cell-free area was found to be further increased to a mean of 40 % in co-treatment with 20 µM kaempferol compared to 12 % (GLV-1h68) or 6 % (kaempferol) in the monotherapeutic approaches. In HCT-116 cells, the combination therapy reduced the cell layer further to a range of 59 - 62 %

compared to 43 % in single-agent treatment with GLV-1h68. Only Colon-26 cells showed a decreased cell-free area in combinatorial treatment.

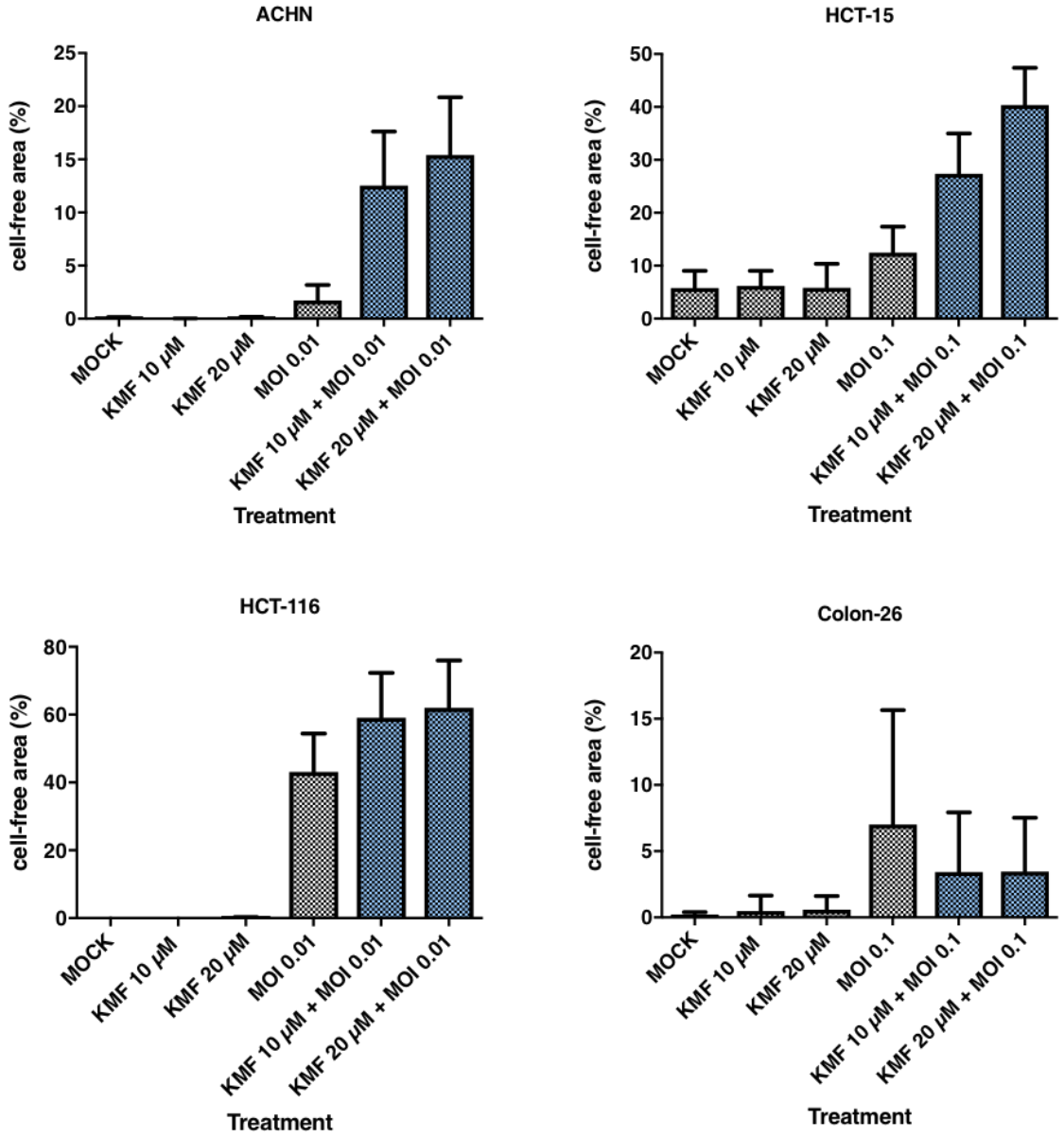

Figure 32. Area calculation. Cells were treated with the chosen concentrations of kaempferol (KMF). After 24 h, cells were infected with VACV GLV-1h68. After 72 hpi, the cell-free area was determined to quantify remnant tumor cell mass. The columns of each group show the cell-free area in percent. Mean of three independent experiments performed in quadruplicates is shown. Error bars indicate +/- SD.

3.6.3 Combination therapy of vaccinia virus GLV-1h68 and SAHA

3.6.3.1 Cell viability and cytotoxicity assays

SRB assay

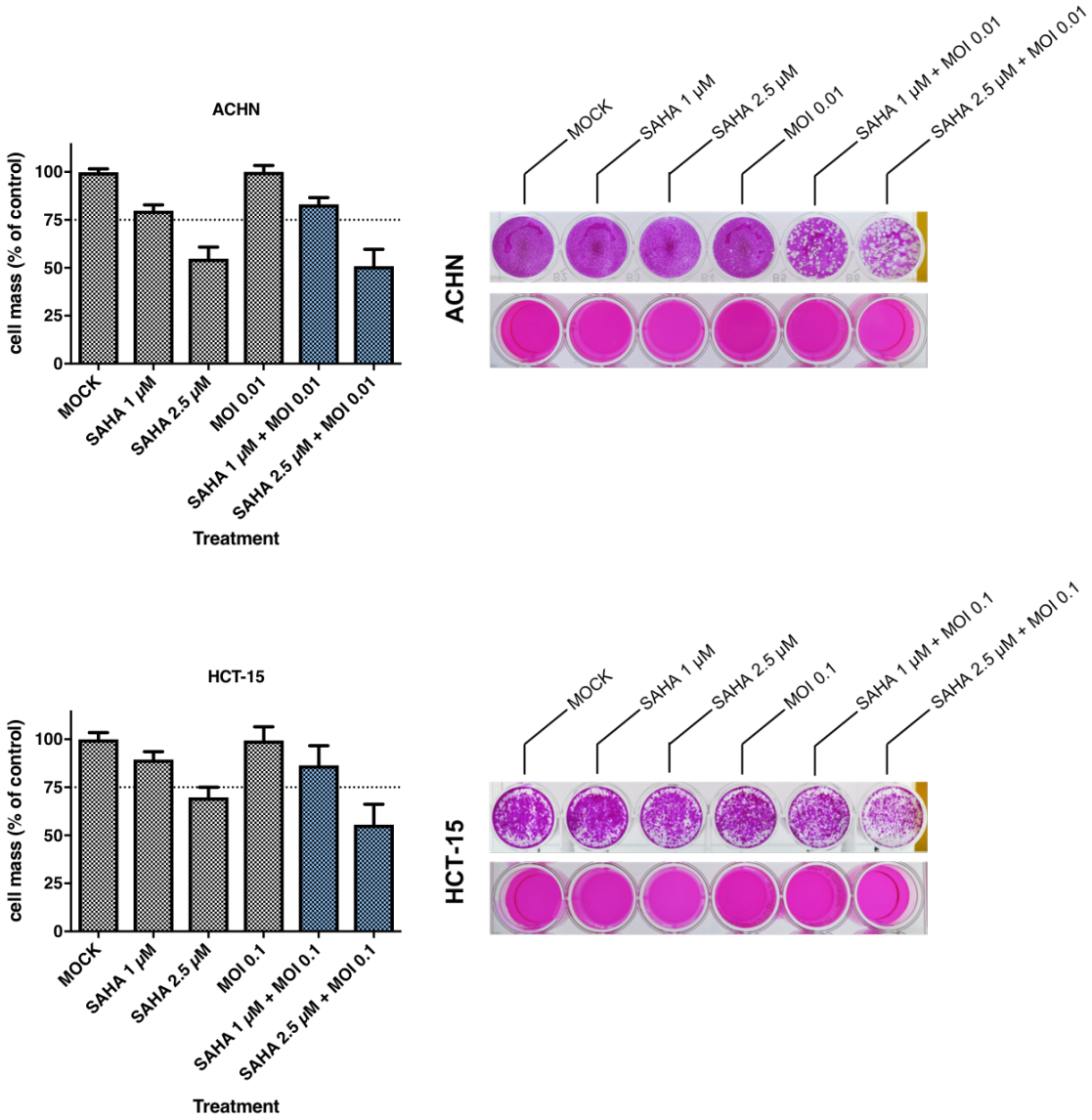

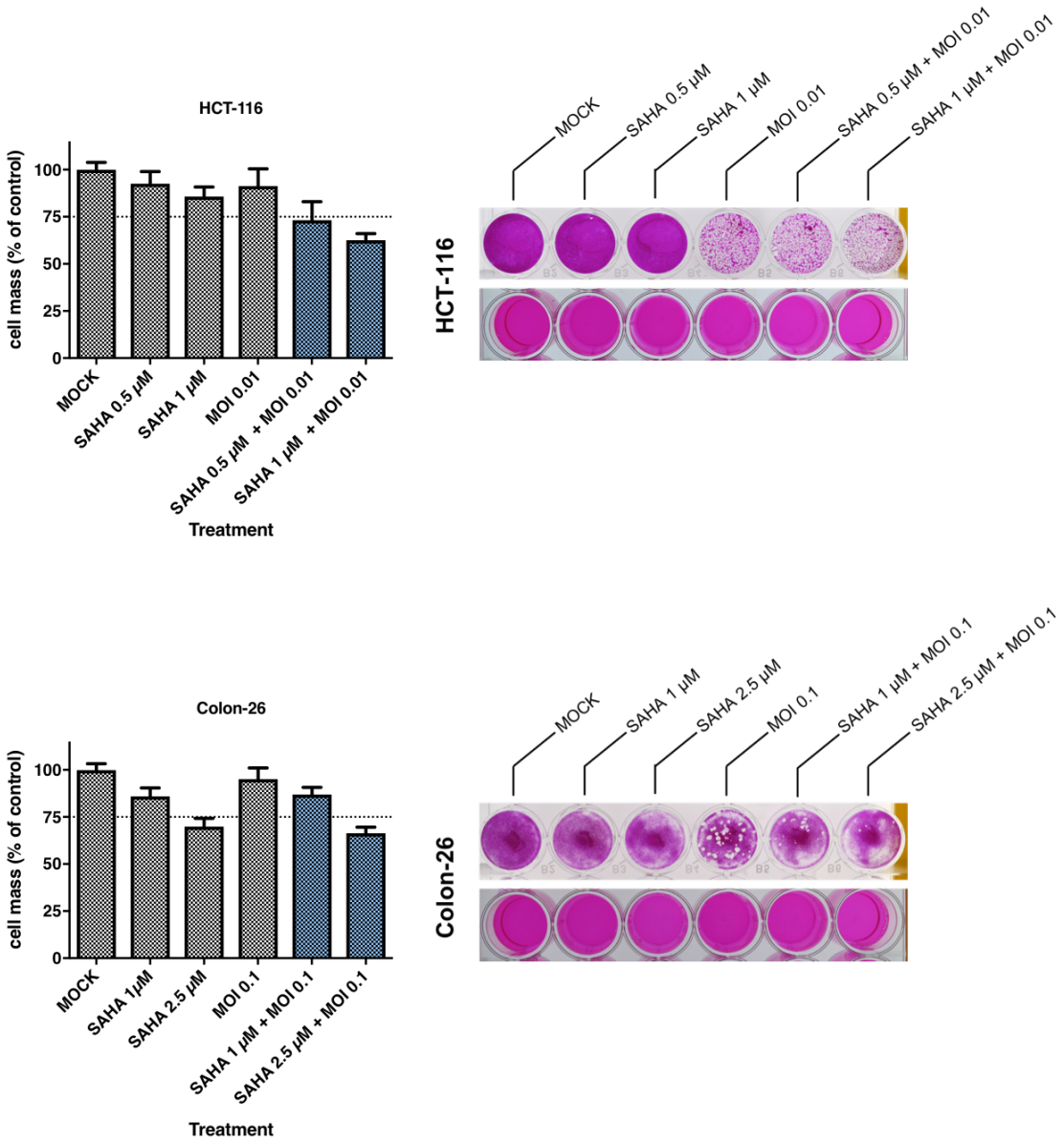

Figure 33. SRB viability assay and pictures of the 24-well plates. Cells were treated with SAHA alone, infected with GLV-1h68 alone or co-treatment was performed. After 72 hpi, SRB assay was performed. On the left-hand side, mean of three independent experiments performed in quadruplicates is shown. Error bars indicate +/- SD. The mock-treated quadruplicate was set to 100 % cell mass. The right-hand side shows the pictures of the 24-well plates after staining with sulforhodamine B dye (above) and after solubilization with Tris base (below). One row of the 24-well plate is exemplarily shown for one of the three experiments.

As seen in the graphs on the left-hand side in Figure 33, combinatorial treatment of HCT-116 leads to increased tumor cell killing compared to the respective mono-treatments. In detail, HCT-116 cell masses were reduced to 62 % in co-treatment (with 1 µM SAHA) whereas a reduction to only 86 % (1 µM SAHA) or 91 % (GLV-1h68) could be achieved in monotherapies. The lower

SAHA concentration reduced the cell mass to 72 % in co-treatment compared to the respective single-agent treatment with 0.5 µM SAHA alone. In HCT-15 cells, co-treatment with 2.5 µM SAHA showed also an increased tumor cell killing. Cell mass was reduced from 69 % in monotherapy (2.5 µM SAHA) to 56 % in co-treatment (2.5 µM SAHA with GLV-1h68). In contrast, in ACHN and Colon-26 cell lines combination therapy was not superior to monotherapy.

When looking at the images on the right-hand side in Figure 33, except for HCT-15, in panel 1, the mock-treated cells showed no cell-free area, similar to panel two and three with the two different concentrations of SAHA. In panel four in ACHN, HCT-116, and Colon-26, plaques were visible. Combinatorial treatment in ACHN, HCT-15, and HCT-116 showed more and larger plaques. In Colon-26 cells, combination therapy displayed fewer plaques than in monotherapy with GLV-1h68 alone.

Nevertheless, when dyed wells were solubilized, previous differences could not be displayed. Particularly, in combinatorial treatment in ACHN, HCT-15, and HCT-116 cells, cell layer were visibly reduced, but after solubilization of the dye the OD was higher. To clear these discrepancies, cell-free areas of the wells were calculated (see Figure 38).

CellTiter-Blue assay

As seen in Figure 34, a reduced cancer cell viability was achieved for HCT-116 cells in combinational treatment (53 %), compared to 1 µM SAHA (71 %) and GLV-1h68 (84 %) single-agent treatment. ACHN, HCT-15, and Colon-26 did not respond to combinatorial treatment compared to monotherapy.

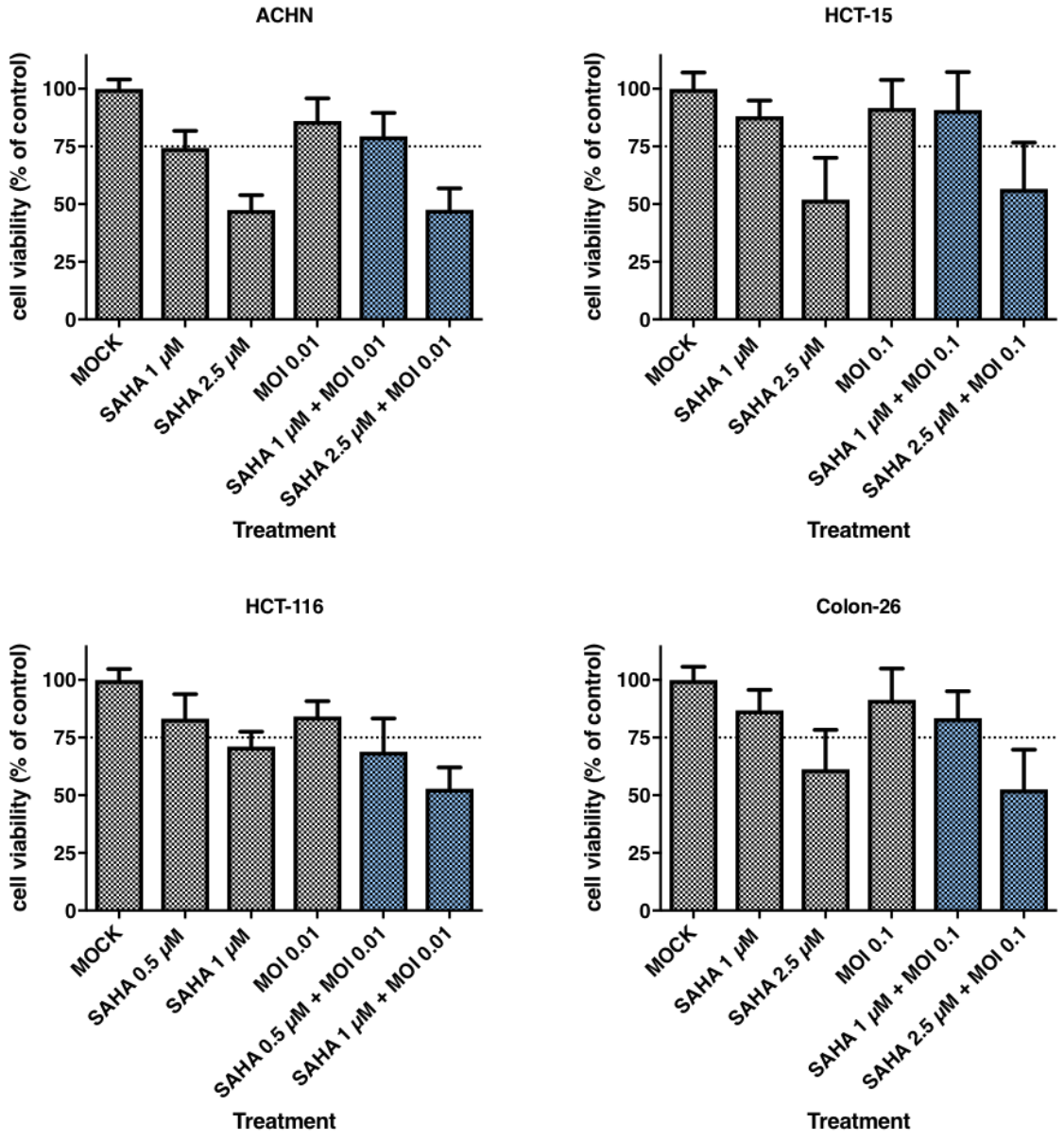

Figure 34. CellTiter-Blue assay. The graphs represent the four cell lines, which were either treated with SAHA alone, infected with GLV-1h68 alone or co-treatment was performed. After 72 hpi, CellTiter-Blue assay was performed. Mean of three independent experiments performed in quadruplicates is shown. Error bars indicate +/- SD.

LDH assay

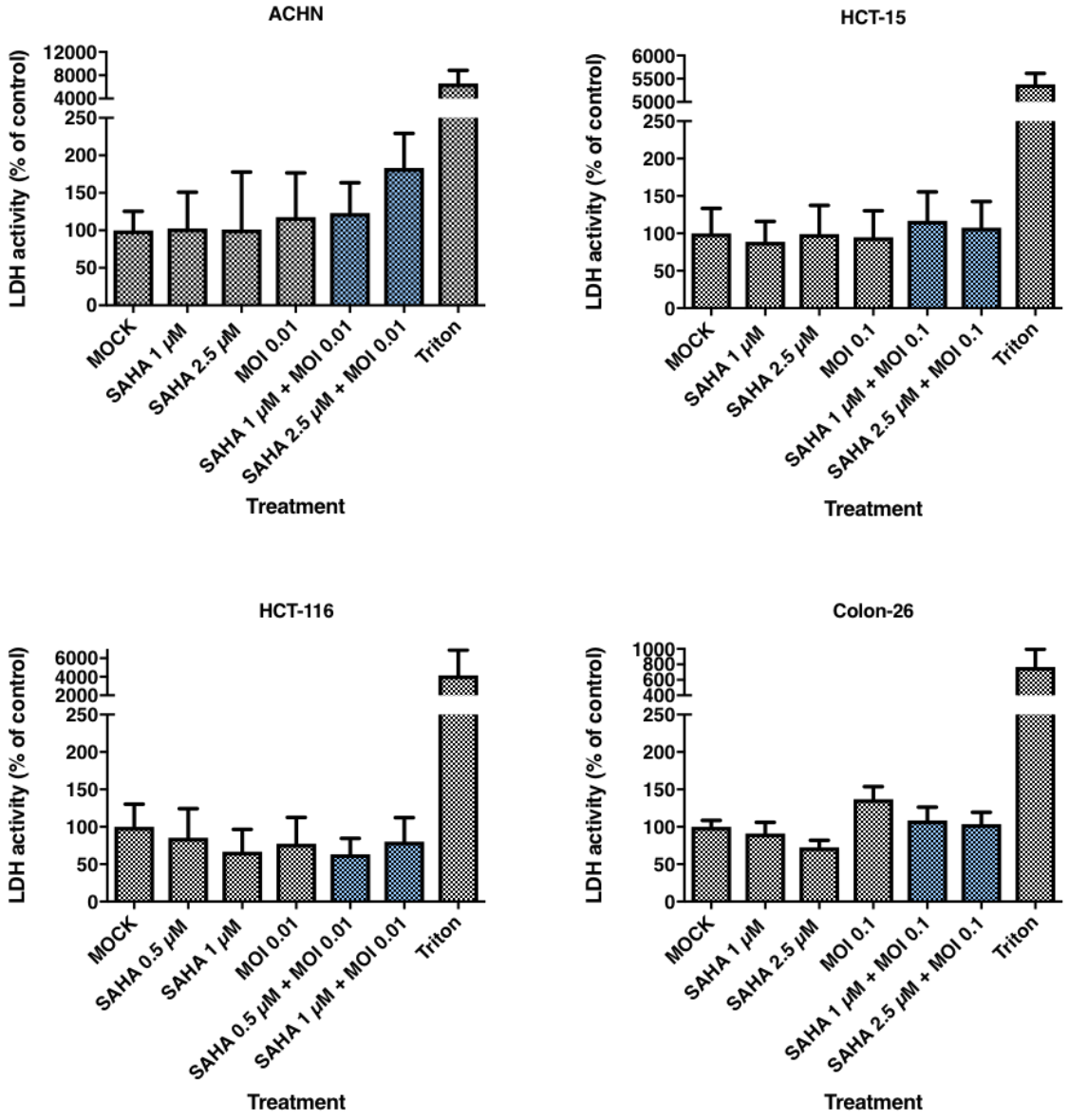

Figure 35. LDH assay. The graphs represent the four cell lines, which were either treated with SAHA alone, infected with GLV-1h68 alone or co-treatment was performed. Afterwards, LDH assay was performed. As a control for total LDH release, cells were completely lysed with Triton. Mean of three independent experiments performed in quadruplicates is shown. Error bars indicate +/- SD. The mock-treated quadruplicates were set to 100 % LDH activity.

In ACHN cells, co-treatment with 2.5 µM SAHA led to an increased LDH activity (183 %) compared to single-agent treatment with GLV-1h68 alone (118 %). In HCT-15, HCT-116, and Colon-26, combination therapy displayed less LDH activity in contrast to monotherapy with GLV-1h68 or mock-treatment solely (see Figure 35).

MTT assay

Since treatment of ACHN and HCT-116 showed best results with the epigenetic compound SAHA, further investigations were conducted. MTT assay, flow cytometry and real-time cellular impedance assay were performed solely with ACHN and HCT-116 cells. Virus growth curves were performed with ACHN cells only.

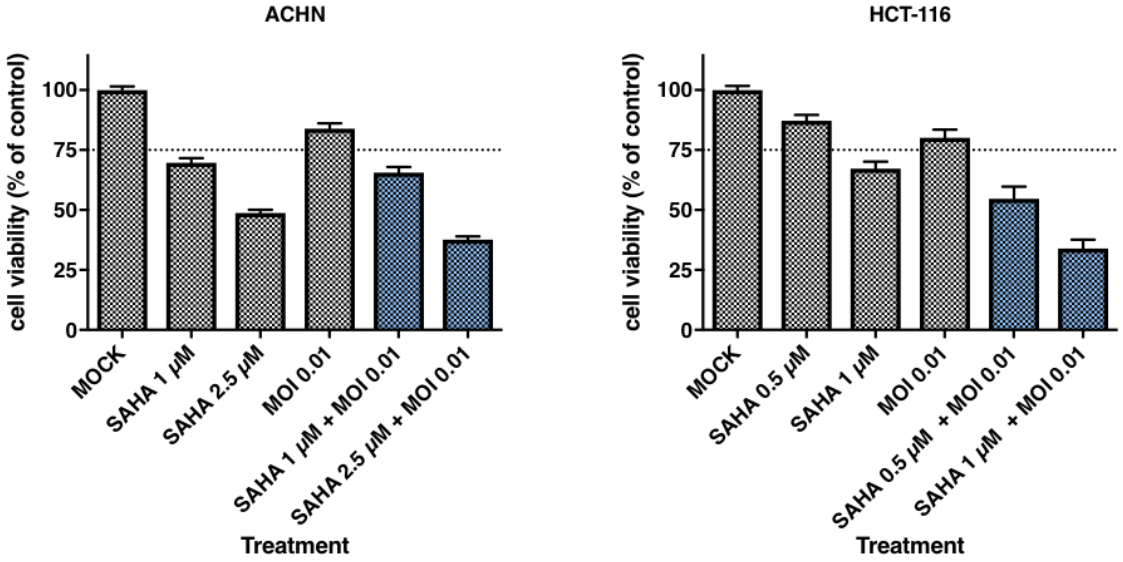

Figure 36. MTT assay. ACHN and HCT-116 cells were either treated with SAHA alone, infected with GLV-1h68 alone or co-treatment was performed. After 72 hpi, MTT assay was performed. Mean of three independent experiments performed in quadruplicates is shown. Error bars indicate +/-SD. The mock-treated quadruplicates were set to 100 % viability.

Combinatorial treatment showed an improved tumor cell killing in ACHN and HCT-116 cells. Especially the higher SAHA concentration in each cell line (ACHN 2.5 µM, HCT-116 1 µM) reduced cell viability to 38 % in ACHN cells and 34 % in HCT-116 cells (Figure 36).

3.6.3.2 Fluorescence monitoring

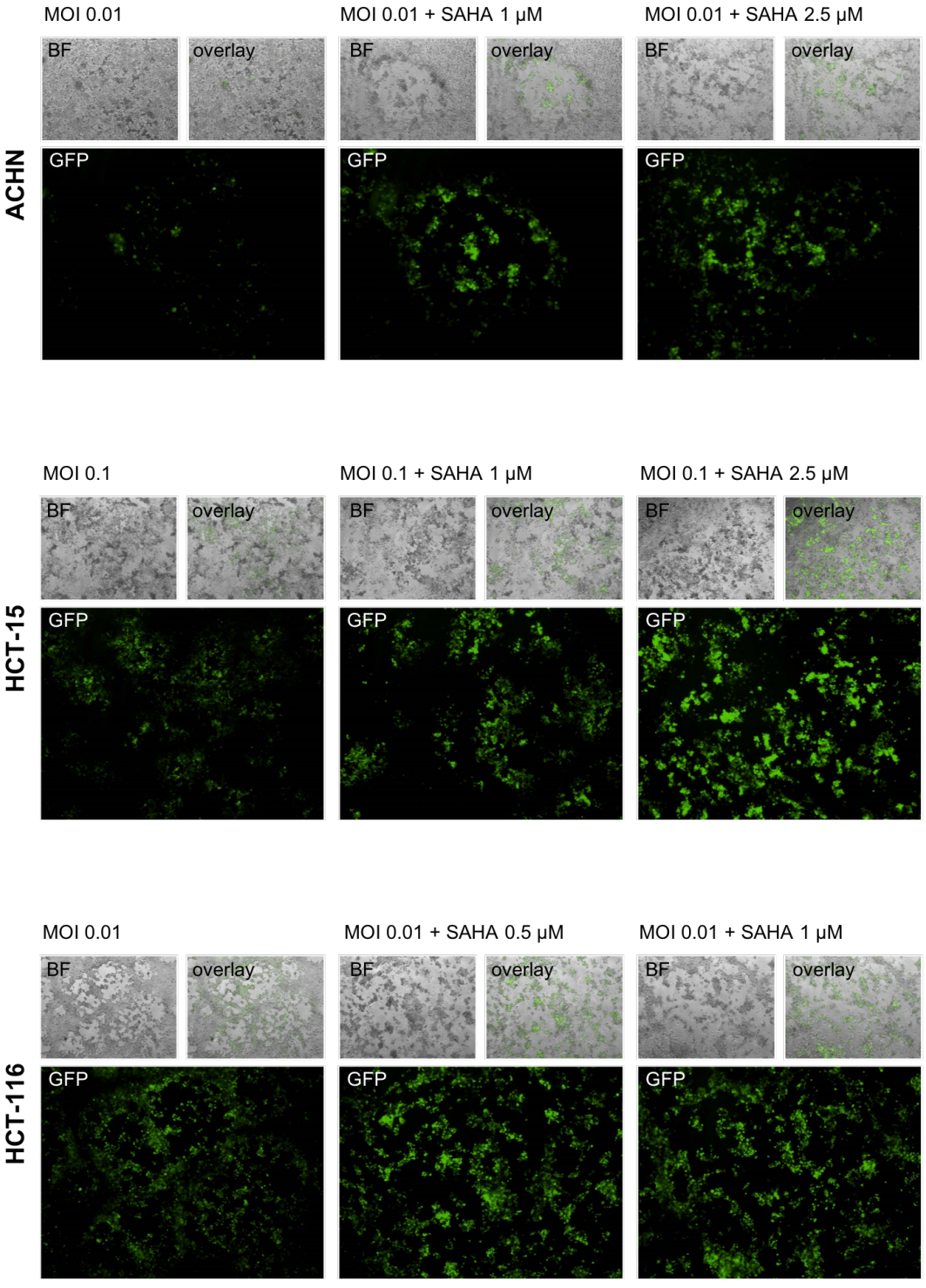

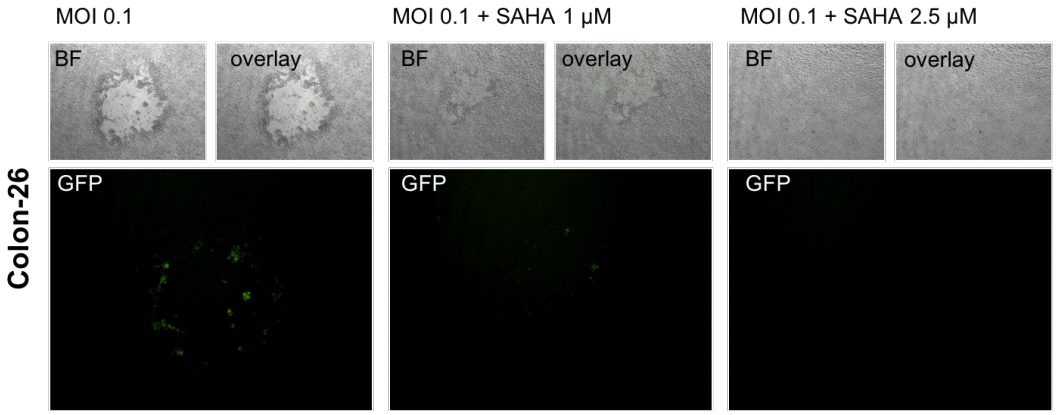

Figure 37. Fluorescence monitoring of the four different cell lines either in monotherapy with GLV-1h68 alone or in combinatorial treatment with SAHA. The four cell lines were either infected with GLV-1h68 alone or co-treatment with SAHA was performed. After 72 hpi, expression of GFP was analyzed by fluorescence microscopy. Green fluorescence indicated the infection of tumor cells. Phase contrast and fluorescence photos were taken and overlaid.

At 72 hpi, combinatorial treatment with SAHA resulted in an increased virus-associated expression of GFP in ACHN, HCT-15, and HCT-116 cells. In Colon-26 cells, a reduced GPF signal was seen in combinatorial treatment in comparison to monotherapy with GLV-1h68 at MOI 0.1.

3.6.3.3 Area calculation

At 72 hpi, combinatorial treatment with SAHA caused a significant cell mass reduction in ACHN, HCT-15, and HCT-116 cells. Using the higher concentration of SAHA, ACHN reached almost 40 % cell-free area, in comparison to mono-therapy with a cell-free area of 2 % (GLV-1h68 alone). Similar results were achieved in HCT-15 cells with SAHA 2.5 µM in combinatorial treatment. The cell-free area increased from 15 % with 2.5 µM SAHA alone to 43 % in co-treatment with GLV-1h68. A benefit in combinatorial treatment was visible in HCT-116 cells as well. Co-treatment enhanced the cell-free area to 60 – 67 % compared to the respective mono-treatment with GLV-1h68 alone (45 %). In Colon-26, combinatorial treatment reduced cell mass less than monotherapy with GLV-1h68 (Figure 38).

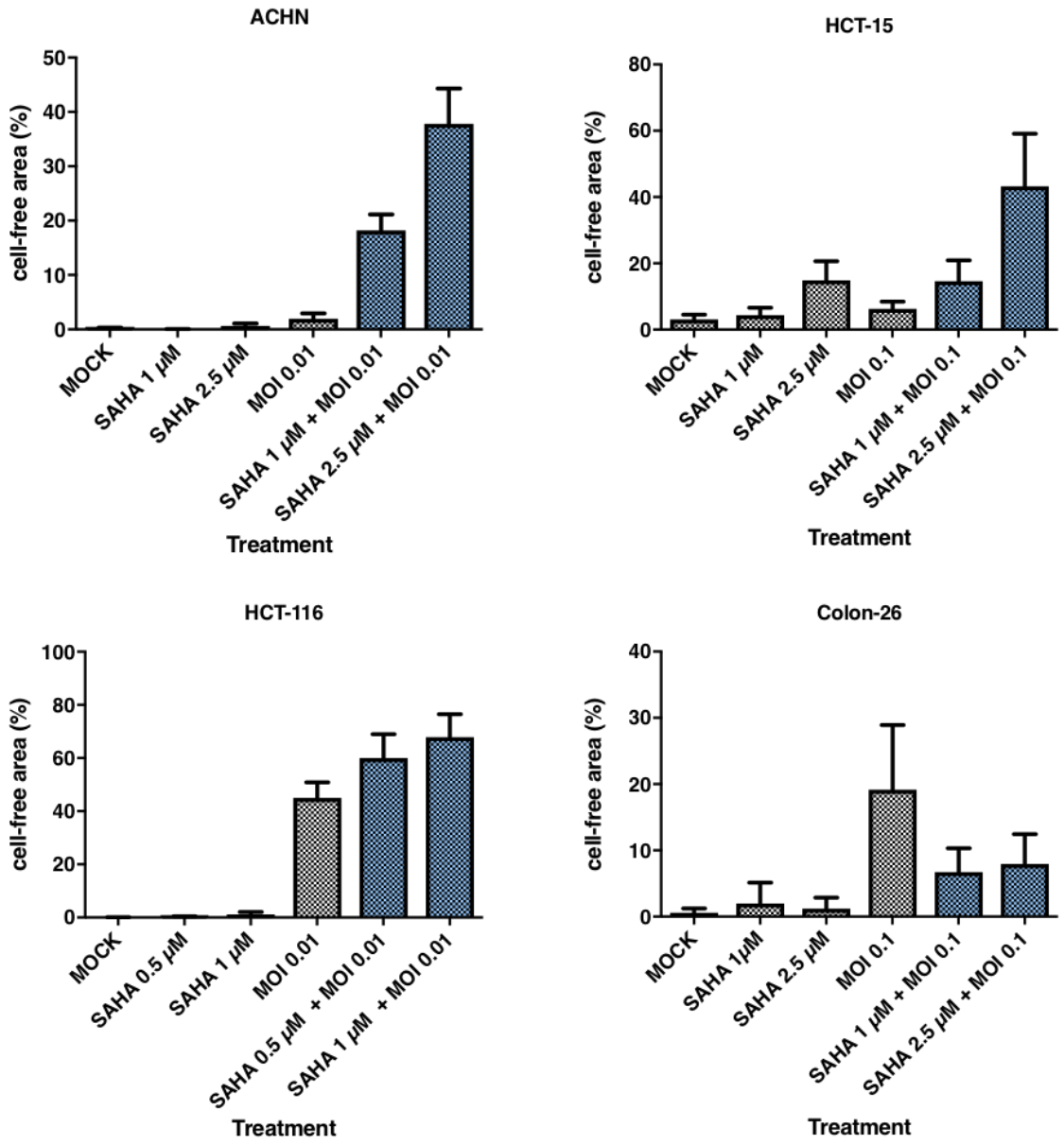

Figure 38. Area calculation. 72 hpi after treatment, the cell-free area was determined to quantify remnant tumor cell mass. The columns of each group show the cell-free area in percent. Mean of three independent experiments performed in quadruplicates is shown. Error bars indicate +/- SD.

3.6.3.4 Virus growth curves

In a next step, the replication behavior of GLV-1h68 at MOI 0.01 in combination with SAHA at a concentration of 2.5 µM in ACHN cells was analyzed via growth curves.

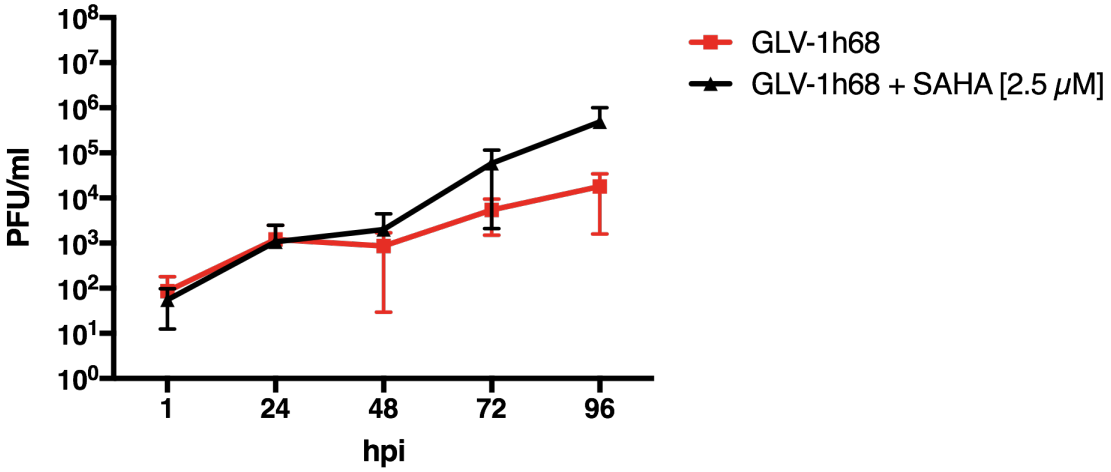

Figure 39. Replication of VACV GLV-1h68 with or without SAHA (2.5 µM) in ACHN cells. Cells were treated with SAHA or mock-treated. After 24 h, cells were infected with VACV GLV-1h68 at MOI 0.01. At 1, 24, 48, 72 and 96 hpi, samples were taken. Titration was performed using CV-1 cells to quantify the amount of virus plaques. The result of GLV-1h68 mono-infected cells (red line) is displayed along with GLV-1h68 + SAHA co-treated cells (black line). The results are shown in PFU/ml. Mean of three independent experiments is shown. Error bars indicate +/- SD.

Replication behavior of GLV-1h68 at MOI 0.01 was analyzed via growth curves. Viral replication started post infection in monotherapy and co-treatment. After 24 hours, virus production stagnated when looking at GLV-1h68 monotherapy (red line), whereas virus production slightly increased in co-treatment. Starting at 48 hpi, SAHA enhanced the replication of GLV-1h68 (black line) compared to infection with GLV-1h68 alone (red line).

3.6.3.5 Flow cytometry

When compared to resveratrol and kaempferol, SAHA seemed to be the most promising epigenetic compound. Thus, flow cytometry was performed to analyze the cell cycle of ACHN and HCT-116 cells in detail for better understanding of growth behavior in co-treatment (Figure 40).

In ACHN, combinatorial treatment with GLV-1h68 and 2.5 µM SAHA enhanced the population of apoptotic cells (black sub2N bar) greatly (37 %) compared to combinatorial treatment with 1 µM SAHA (9 %), monotherapy (SAHA or GLV-1h68, 11 % each) or mock-treated tumor cells only (11 %).

In HCT-116, diminishing fractions of apoptotic cells (sub2N) in combinatorial treatment or monotherapy with GLV-1h68 were observed (4 - 8 %), alongside an enhanced fraction of proliferating cells (characterized by S and G2 phases).

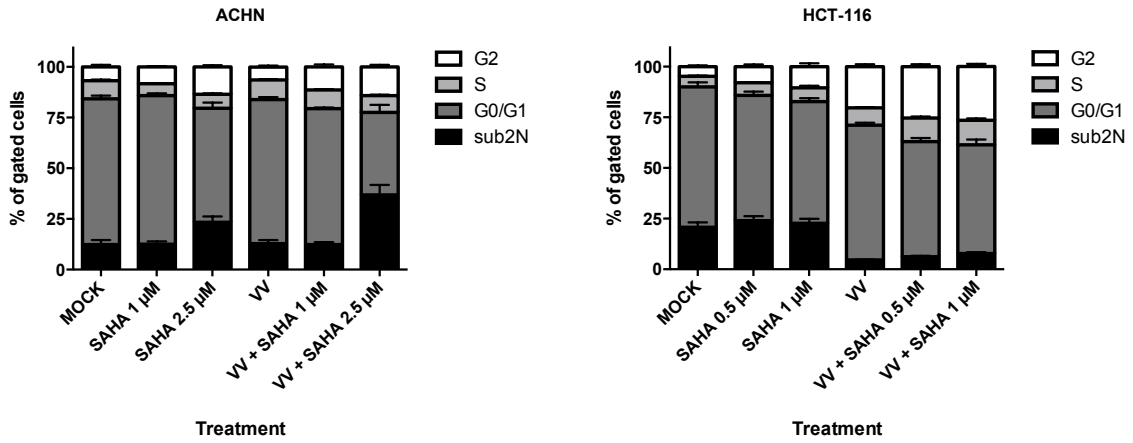

Figure 40. Cell cycle profile of treated ACHN and HCT-116 cells at 72 hpi. Cell lines were either mock-treated, or monotherapy with SAHA or GLV-1h68 or co-treatment was performed. DNA was stained with propidium iodide (PI) and cells were analyzed by flow cytometry. Mean of three independent experiments performed in quadruplicates is shown. Error bars indicate +/- SD.

3.6.3.6 Real-time Cellular Impedance measurement

Based on the dynamic monitoring of cell proliferation, 24 hours after seeding, ACHN and HCT-116 cells were treated using different SAHA concentrations and 24 h later infected with GLV-1h68 at MOI 0.01 or combinatorial treatment was performed.

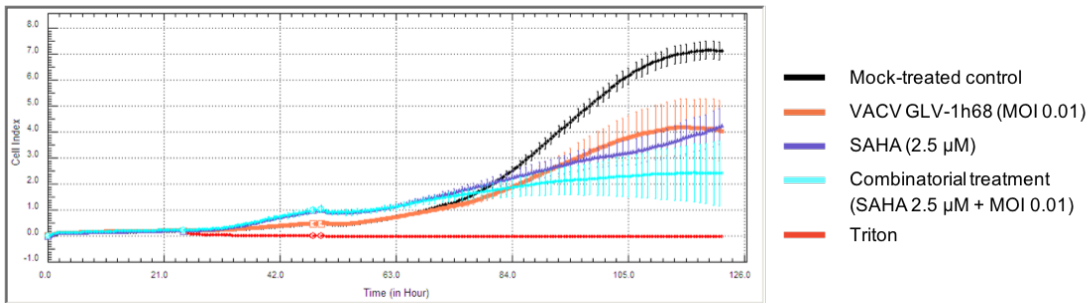

Figure 41. Real-time monitoring of ACHN tumor cell proliferation after treatment with SAHA (2.5 µM) and infection with GLV-1h68. The colored lines indicate the different treatments in the E-Plate. Cells were measured every 30 minutes using the RCTA SP instrument. Measured electrode impedance is expressed as a Cell Index and graphically represented.

Combinatorial treatment of the epigenetic compound SAHA with GLV-1h68 (cyan blue line) showed increased oncolytic cell death when compared to the respective mono-treatments (Figure 41).

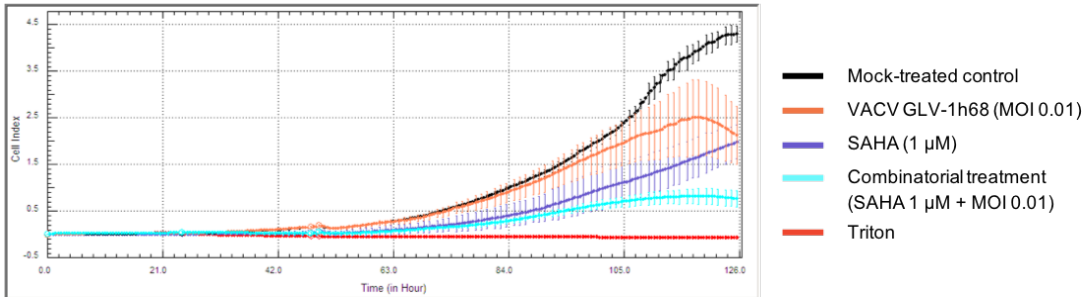

Figure 42. Real-time monitoring of HCT-116 tumor cell proliferation after treatment with SAHA (1 µM) and infection with GLV-1h68. Cells were measured every 30 minutes using the RCTA SP instrument. Measured electrode impedance is expressed as a Cell Index and graphically represented.

Combinatorial treatment (cyan blue line) showed increased oncolytic cell death in HCT-116 tumor cells over 120 h when compared to the respective mono-treatments.

4. Discussion

Cancer is one of the leading causes of death worldwide. In order to improve current cancer treatment modalities, novel therapy options are needed beyond the standard approaches such as surgery, chemotherapy and radiotherapy.

Immunovirotherapy is one of these new alternatives. Because several tumor entities show resistances towards virotherapy, combining virotherapy with different other agents such as epigenetic modulating compounds, chemotherapy or immune checkpoint inhibitors is necessary. Previous studies have shown promising results concerning virotherapeutics as well as epigenetic compounds, both independently and in combinatorial treatment [43, 44, 151].

In this study, a panel of 4 different cell lines, three colorectal cancer cell lines and one renal adenocarcinoma cell line, were tested regarding their susceptibility to vaccinia virus (VACV) GLV-1h68 infection and to different epigenetic compounds, such as resveratrol (RV), kaempferol (KMF) and SAHA, both in monotherapy and in co-treatment.

Depending on dose and length of exposure, monotherapy with GLV-1h68 and also the epigenetic compounds killed tumor cells in all 4 cell lines. For combinatorial treatment, a low multiplicity of infection (MOI) of GLV-1h68 as well as low concentrations for RV, KMF and SAHA were chosen, which reduced cell mass by purpose ”only” in the range of 25 %.

Combinatorial treatment showed a beneficial cytotoxic effect in all cell lines, although this effect was minimal in some experiments. The murine cell line Colon-26 behaved differently regarding the cytotoxic effects as shown in different experiments, e.g., area calculation and fluorescence monitoring (3.6.1.2 Fluorescence monitoring and 3.6.1.3 Area calculation). Nevertheless, cytotoxic effects varied in all examined cell lines depending on the performed method. Further limitations were observable and are mentioned in the subsequent parts.

Monotherapy with VACV

Infection with VACV GLV-1h68 was monitored through fluorescence microscopy and SRB assay. HCT-15 and Colon-26 were classified as highly resistant and therefore a MOI of 0.1 was chosen for further experiments. HCT-116 and ACHN were classified as susceptible to GLV-1h68; therefore, a MOI of 0.01 was used for combinatorial treatment. The aim was to overcome these resistance profiles in co-treatment.

Depending on the MOI, the different cell lines reacted in various degrees of cytotoxicity, virus replication and intensity of GFP marker gene expression, which correlate with the reports by Ascierto et al. [152].

According to Ehrig et al., HCT-116 cells were highly susceptible to GLV-1h68 at MOI 0.1 *in vitro* as well as in xenograft mouse models. GLV-1h68 efficiently infected, replicated in and lysed the human colorectal cancer cell line. Treatment with VACV GLV-1h68 was less effective in HCT-15 cells both *in vitro* and in an *in vivo* mouse model [153]. Of note, these findings correlate with our results and the results from C. Raff (MD thesis work also performed in Prof. Lauer´s laboratory; submitted for publication) that HCT-116 cells were more susceptible to VACV compared to HCT-15. HCT-15, on the other hand was classified as a tumor cell line being resistant to VACV GLV-1h68.

The impact of resveratrol on viral replication

In several previous *in vitro* and murine *in vivo* studies, inhibitory effects were shown in monotherapy with different resveratrol concentrations starting at 10 µM. Resveratrol suppresses the growth in multiple tumor entities, and also in the tumor cell lines used in this study [154-159]. Nevertheless, results of proliferation inhibition as well as induction of apoptosis were strongly dependent on the resveratrol concentrations [160].

In this study, resveratrol concentrations for co-treatment were reduced to 2.5 - 20 µM compared to the above-mentioned studies, which used concentrations up to 100 µM. In this project, which rather aimed at overcoming resistances and

inducing apoptosis in low resveratrol concentrations, inhibitory effects were diminished. As a general rule, synergistic effects could only be achieved when inhibitory effects in monotherapy were subtherapeutic. Additionally, low concentrations seemed to be a useful aspect, since high blood levels could not be reached *in vivo* so far due to its fast metabolism [113]. However, in further investigations it might be reasonable to use higher resveratrol concentrations since Tsunoda et al. observed that 10 µM resveratrol were insufficient for inducing apoptosis of HCT-116 cells in monotherapy *in vitro* [161].

New forms of administration include on the one hand a combination with nano-particles due to an increased stability of resveratrol [162], or on the other hand through micronized resveratrol, small particles, which increase the orally administered resveratrol into the organism significantly [163]. Alternative methods of administration need to be performed and validated to improve the bioavailability of resveratrol [164].

In previous studies, resveratrol has been shown to inhibit replication of many viruses such as influenza or herpes simplex [165, 166]. Last year, Cao et al. demonstrated that resveratrol strongly suppresses the replication of a Western Reserve VACV strain in various cell types, such as HeLa cells. Therefore, it was difficult to predict the impact of resveratrol not only on GLV-1h68 but also on the used tumor cell lines in this study.

Our results demonstrate that co-treatment with resveratrol and GLV-1h68 did not lead to significant benefits, which could possibly also be explained by a resveratrol-mediated inhibition. Further comparative experiments are necessary in order to form a better understanding of the cellular function and molecular way of action of VACV [167].

Nevertheless, fluorescence microscopy analysis showed in all cell lines, except for Colon-26 that combinatorial treatment led to an enhanced GFP signal indicating a stronger virus replication compared to VACV monotherapy. As seen in Colon-26, less GFP signal as well as less cell-free area in co-treatment could be detected when compared to single-agent treatment (3.6.1.2 Fluorescence monitoring and 3.6.1.3 Area calculation).

When looking directly at virus growth curves, co-treatment in ACHN cells was not beneficial, whereas a synergistic effect could be determined in further experiments including the real-time cell monitoring xCELLigence and area-calculation. Consequently, cell mass reduction could not exclusively be dependent on virus replication in cells, but also on resveratrol.

In contrast, the cell line HCT-116 showed promising results in almost every experiment; however, no synergistic effect of co-treatment could be detected in xCELLigence analysis. This could possibly be explained by the complicated methodology of the real-time impedance measurement and the resulting assay variations. For example, cells in the peripheral wells of the 96-well plates did not reach confluency and cell growth was visibly reduced compared to the centered wells. Temperature difference in the instrument reader could be one reason for the weaker growth. For more reliable results, a different application scheme would be useful.

Furthermore, minor synergistic effects can be due to low resveratrol concentrations and/ or low MOIs, which were chosen for monotherapy. Therefore, one possible improvement would be to focus on higher concentrations in co-treatment in further investigations to see if these adjustments can overcome existing resistances.

According to Ascierto et al., who screened the NCI-60 panel for the susceptibility to VACV GLV-1h68, ACHN and HCT-15 cells express low levels of GFP compared to HCT-116. This study confirmed these results. In the study of Ascierto, MOIs of 0.3 and 0.6 were chosen, which are higher than the MOIs used in this study [152].

The impact of kaempferol on virus replication

Jamillo-Carmona et al. and Kalyani et al. showed cytotoxic potential and induction of apoptosis of kaempferol in colon cancer cell lines, such as HCT-15 and HCT-116 cells [168, 169]. Song et al. demonstrated many resistances of kaempferol towards renal adenocarcinoma cell lines. Nevertheless, they demonstrated inhibition of cell growth and induction of cell death in the renal

adenocarcinoma cell lines 786-O and 769-P with kaempferol at a concentration of 100 µM [170].

In this study, kaempferol in monotherapy showed less cytotoxic effects when compared to resveratrol or SAHA. When compared to the concentrations used by Song et al., in this study low kaempferol concentrations were used with the aim of overcoming resistances in tumor cells by co-treatment. Furthermore, the required plasma concentration levels of kaempferol could not be reached yet because of its poor bioavailability [117]. Zhou et al. illustrated that co-administration of kaempferol and ethanol by oral gavage enhanced the bio-availability of kaempferol [171].

Co-treatment with kaempferol showed similar results as seen in experiments with resveratrol. In different viability assays with HCT-15, HCT-116 and Colon-26 cells, marginal benefits in co-treatment were visible. In contrast, ACHN cells were not susceptible to co-treatment. However, GFP signal intensity increased in combinatorial treatment in each cell line except for Colon-26. As already described for resveratrol, Colon-26 showed adverse effects in co-treatment with a reduced GFP signal. These results were concordant with the cell-free area in the wells. Here, Colon-26 had less cell-free area compared to the other cell lines. Regarding the antiviral activity of kaempferol, it was shown that kaempferol inhibits the replication of various viruses, such as influenza, polio, herpes simplex, coronavirus and vaccinia virus [172-176]. In particular, Dave et al. and Kumar et al. described that the leaves of cassia tora, which contain kaempferol, have an antiviral activity against both Newcastle and vaccinia virus (Dave 2010, Kumar 2017). Whether the anti-viral function of kaempferol plays a role in this study could not be clarified in detail and has to be investigated in further studies.

The impact of SAHA on virus replication

Compared to the other epigenetic compounds used in this study, SAHA seemed to be the most potent epigenetic modulating agent. Already low SAHA concentrations strongly reduced cell mass in monotherapy.

According to Bressan et al., the colorectal carcinoma cell line HCT-116 seemed to be very sensitive to SAHA [177]. Additionally, SAHA was less cytotoxic towards healthy colorectal cells [178], and thus might have a therapeutic potential for the treatment of colorectal cancer *in vivo*. Furthermore, SAHA has an impact on renal cell carcinoma cell lines *in vitro* [179] as well as in murine *in vivo* models [180].

In this thesis, SAHA concentrations of 2.5 and 5 µM were used. Virus growth curves and real-time cell monitoring in ACHN cells with a SAHA concentration of 2.5 µM showed a successful replication in co-treatment over 96 hpi. Cell cycle analysis showed that 2.5 µM SAHA increased the population of apoptotic cells (sub-2N fraction) in ACHN cells compared to co-treatment with 1 µM SAHA. In HCT-116, after 120 h an increased fraction of S and G2 phase cells was observed, indicating a growth arrest at the S/G2 phase transition. Accordingly, co-treatment with SAHA has a different effect on colorectal and renal carcinoma cell lines. Furthermore, in the different cell viability assays and in real-time cell monitoring, HCT-116 cells were susceptible to SAHA and resulted in a synergistic benefit. Again, the Colon-26 cell line showed different effects when looking at the GFP signal intensity in fluorescence monitoring. Thus, the murine cell line seemed to behave differently in all co-treatments with the different epigenetic modulating agents (compare RV and KMF). These results were confirmed by area calculation. Here, co-treatment had less cell-free area. In the other cell lines, co-treatment resulted in a higher cell-free area.

Limitations in this study

Methodic issues occurred leading to a limitation of validity of the results, such as the observation of an incipient therapeutic effect on the end-point of certain assays, variations in results depending on cell passage numbers or limited half-life of LDH assay.

The cell numbers were determined for cell survival of 120 h in a 24 well plate. In a few experiments, such as real-time cell monitoring xCELLigence and growth curves, progression beyond 120 h would be an interesting approach due to its

great synergistic effect. The initiation of the synergistic effect was detected the later the end-point of the experiment the higher. Unfortunately, in the chosen setting (Figure 19), progression beyond 120 h was difficult to accomplish, because mock-treated cells were already confluent at this time point and thus cell growth was inhibited (compare Figure 20, Figure 28, Figure 33). Furthermore, the medium was depleted after 120 h of incubation, which might influence the results.

Passage numbers of the used cell lines also played an important role in this study. Low cell passage numbers present the biology of the original tumor. The growth behavior changed with increasing cell passages [181]. Thus, passage numbers had to be kept low to obtain consistent results. Nevertheless, results varied with different passage numbers. After a specific time, different characteristics, such as alterations in morphology, genomic abnormalities, alterations in proliferation rates, transfection efficiency and changes in protein expression can occur. Consequently, reliability and reproducibility of results might vary [182]. Norden et al. demonstrated that Colon-26 cells changed their behavior *in vitro* in protein secretion and IL-6 mRNA depending on the storage conditions and passage numbers [183]. Therefore, in further investigations it would be important to monitor if different cell passages show variances in drug efficiencies, which would explain varying results.

A further problem, which is frequently ignored by the research community is the assessment of reliability and accuracy of the used cells and the question if they represent their tumor tissues of origin. Often, the reference strain is not known, or multiple unknown passage numbers have been performed, which lead to the result that cells have little in common with the original reference strain [184, 185]. At these conditions, in this study, we tried to stay as close as possible to the origin passage number and thus decided to keep the cell passage numbers below 20.

Further limitations could be identified in viability assays, such as the LDH assay. The LDH assay measures the activity of marker enzymes that leak out of dead cells into the culture medium. LDH, which is released from cells into the medium, has a half-life of approximately 9 h. Thus, the assay mostly reflects the

last 9 hours of the experiment instead of the total amount of LDH release of the whole experiment. It might therefore underestimate the quantity of the absolute level of cytotoxicity [186]. In this thesis, the enzyme release varied in the three experiments, which were independently performed. In further investigations, LDH enzyme activity should be measured at different time points for more reliable results.

Current preclinical and clinical studies with VACV, HDACi and different co-treatment options

Lately, oncolytic virotherapy has resulted in promising treatment options for various cancer entities. First clinical trials in Phase I/II for the anticancer vaccine GL-ONC1 (proprietary name of GMP-derived material of GLV-1h68) are currently under investigation to treat solid tumors. Results from first clinical trials showed that GL-ONC1 was well-tolerated with low cytotoxicity and successfully entered the tumor sites when applied intraperitoneally in patients with peritoneal carcinomatosis [187]. Further ongoing clinical trials for ovarian cancer (NCT02759588) and malignant pleura effusion (NCT01766739) are in progress [188]. When looking at the current progress in epigenetic cancer therapy, SAHA (Zolinza®) is already approved by U.S. FDA for the treatment of cutaneous T-cell lymphoma. Furthermore, multiple studies have been performed for the treatment of glioblastoma multiforme, myelodysplastic syndromes and NSCLC [129, 132, 189].

Regarding co-treatment with VACV and HDACi it was shown that several HDACi enhance the susceptibility of tumor cells to VACV killing and thus increase OV therapy by suppressing the IFN-mediated pathway. Consequently, the tumor selectivity for the oncolytic virotherapy is increased. Furthermore, the efficiency of viral replication is enhanced, and the negative effect of the innate immunity is lessened [190]. So far, different *in vitro* experiments of co-treatment with oncolytic viruses and HDACi have been performed [44]. MacTavish et al. addressed the impact of the oncolytic vaccinia virus JX-594 (Pexa-Vec®) and Trichostatin A (TSA) co-treatment in various tumor cell lines. TSA was found to enhance the replication of VACV in several cancer cell lines *in vivo* in nude

mice, such as the human colon carcinoma cell line HCT-116, as well as murine breast cancer and melanoma cells. Furthermore, significantly fewer lung metastases were found after TSA and VACV co-treatment in murine *in vivo* models [43].

A literature research of different co-treatment options with HDACi and other virus types revealed that VSV and HDACi (TSA) co-treatment resulted in increased susceptibility of VSV *in vitro* and *in vivo* in nude mice in breast cancer [191], in VSV-infected hepatocellular carcinomas [192], as well as in prostate cancer [193].

Otsuki et al. showed the impact of HSV and HDACi (TSA, VPA) co-treatment in human glioblastoma cell lines [194, 195]. Cody et al. demonstrated that HSV and HDACi co-treatment led to increased HSV replication in breast cancer cells [196].

According to Ruf et al., co-treatment with oncolytic measles vaccine virus and resminostat resulted in enhanced efficacy in hepatocellular carcinoma cell lines compared to monotherapy [151].

Different co-treatment options with VACV

The co-treatment of oncolytic viruses with chemotherapy is an alternative combination scheme to eliminate cancer cells [42]. Multiple oncolytic viruses have been combined with different chemotherapy medications and have shown to be a more efficient way to improve cancer treatment [197]. Tumor regression was seen in co-treatment with the vaccinia virus strain Western Reserve (WR) with 5-FC/CD system (suicide gene therapy of the cytosine deaminase (*CD*) gene and 5-fluorocytosine (5-FC)) in an *in vivo* mouse model [41]. Foloppe et al. demonstrated the effective potentiation of oncolytic efficiency by co-treatment of VACV with fluorouracil (5-FU) in human colon cancer cell lines *in vitro* and *in vivo* in a murine model [198]. Yu et al. showed in a mouse model that co-treatment of VACV GLV-1h68 with cisplatin/gemcitabine enhanced therapeutic results in pancreatic cancer compared to single-agent use [199].

In addition, oncolytic viruses enhance the effect of immune check point inhibitors on tumor cells. The effectiveness of immune checkpoint inhibitors might be enhanced by oncolytic viruses, which initiate an immune system attack on cancer cells. Two animal studies have been performed so far [200, 201]. T cells recognize cancer cells by altered surface properties (antigens). Infection with oncolytic viruses can further increase the number of these antigens. Virotherapy destroys cancer cells and multiple antigens are released, which on their part increase the immune activity. Bourgeois-Daigneault et al. addressed the impact of OV to immune checkpoint blockade in refractory triple-negative breast cancer. After intravenous infusion, the virus was able to reach all metastases and the tumor was eliminated in 20-30% by the OV Maraba MG1 solely. Combinatorial treatment with the immune check-point-inhibitor PD-1 increased the remission rate to 60-90% [200]. Thus, combinatorial treatment seems to be a promising therapy option for advanced cancer.

Further investigations

Different application schemes were performed with other co-treatments such as HSV and VPA. Results depended on the timing of the epigenetic treatment [202]: Whereas the onset of epigenetic treatment before viral infection led to improved tumor cell killing, simultaneous treatment decreased viral susceptibility [194]. Pretreatment with HDACi arrested the cell cycle in G1 and increased HSV-1 replication. In contrast, co-administration weakened the virus replication [203].

The application scheme used in this study is based on the above-mentioned studies. In further investigations, different application schemes such as pulsed application of epigenetic compounds could help to improve co-treatment and support further decreases of tumor cell growth. Since resveratrol and kaempferol are naturally occurring compounds, a daily application could be performed to keep bioavailability at a constant level.

HDACi impair the transcriptional activation of the interferon-mediated pathway and thus interfere with the antiviral response in tumor cell lines [190]. This

induction of immunostimulatory effects being triggered by the epigenetic compound could lead to further improved cytotoxic effects in cancer patients. Consequently, it provides a perfect combinatorial treatment to overcome resistances in OV therapy in different cancer entities. These findings may have an enormous translational potential for treatment of human colorectal and/or renal carcinomas as well as other solid tumors and has to be tested in forthcoming virotherapeutic clinical trials.

5. Summary

Cancer is one of the leading causes of death worldwide. In order to improve current cancer treatment modalities, the development of new therapy options for cancer is an important and necessary task of current medical research. Oncolytic viruses represent a promising strategy for cancer treatment (so-called virotherapy). Oncolytic viruses are capable of selectively infecting, replicating within and killing tumor cells with moderate toxicity for healthy non-malignant tissues. However, primary resistances of tumor cells against all the available virotherapeutics, which are mainly used in monotherapy, limit the efficiency of virus-induced oncolysis. Thus, there is a clinical need to accurately characterize these viral resistance phenomena and to find ways to efficiently overcome them. Because of the impact on inducing cancer cell death and inhibition of tumor proliferation, histone deacetylase inhibitors (HDACi) are interesting combination partners for new therapy options and might be a key to overcome current high-grade tumor cell resistance to virotherapy. Previous studies have shown promising results concerning virotherapeutics as well as epigenetic compounds, both independently and in combinatorial treatment.

The aim of this thesis was to establish a combined application scheme of vaccinia virus GLV-1h68 and distinct HDACi compounds, such as resveratrol, kaempferol (both natural compounds) or SAHA (suberylanilide hydroxamic acid, an FDA approved non-natural/chemical HDACi agent) on a panel of four different human cell lines, i.e., three colorectal cancer cell lines and one renal adenocarcinoma cell line. A further aim was to determine whether the above mentioned HDACi compounds can enhance the potency of VACV GLV-1h68 in infection-resistant cancer cell lines.

After having determined suitable concentrations of each agent in a pre-testing phase, next cell viability, tumor cell proliferation and oncolytic effects were analyzed in co-treatment by viability assays (sulforhodamin B, CellTiter-Blue), quantification of lactate dehydrogenase (LDH) release, as well as by real time monitoring of tumor cell growth. To further evaluate possible effects on viral replication, virus growth curves were performed. Finally, also cell cycle analysis,

area calculation of the cell coverage of the surface of the culture wells and a comprehensive fluorescence microscopy analysis were determined.

Our results indicate that co-treatment of HDACi compounds with vaccinia virus GLV-1h68 causes a moderate increase of cytotoxic effects compared to the respective single-agent treatments in all cell lines. In addition, co-treatment resulted in an increased virus-associated expression of GFP in ACHN, HCT-15 and HCT-116 cells when compared to the treatment with GLV-1h68 alone. Nevertheless, cytotoxic effects varied in all examined cell lines depending on the performed method.

The murine cell line Colon-26 behaved adverse regarding the virus-associated expression/cytotoxic effects as presented in different experiments, e.g., area calculation and fluorescence monitoring. Here, further investigations need to be performed to identify reasons for the above-mentioned effects. Furthermore, SAHA seemed to be the most potent epigenetic compound when compared to the other epigenetic compounds used in this study.

In conclusion, our data show that epigenetic compounds, such as resveratrol, kaempferol and SAHA are able to further enhance the potency of VACV GLV1-h68 in partially or highly resistant tumor cell lines when compared to either of the monotherapeutic approaches. Induction of immunostimulatory effects being triggered by the epigenetic compound could lead to further improved cytotoxic effects in cancer patients. These findings may have an enormous translational potential for treatment of human colorectal and/or renal carcinomas as well as other solid tumors and have to be tested in forthcoming virotherapeutic clinical trials [142].

Zusammenfassung

Krebs ist eine der häufigsten Todesursachen weltweit. Um die derzeitigen Möglichkeiten der Krebsbehandlung zu verbessern, ist die Entwicklung neuer Therapieoptionen für Krebs eine wichtige und notwendige Aufgabe der aktuellen Forschung. Der Einsatz von onkolytischen Viren stellt eine vielversprechende Strategie zur Krebsbehandlung dar (sog. Virotherapie). Bei gleichzeitig mäßiger Toxizität gegenüber gesundem, nicht-malignem Gewebe sind onkolytische Viren in der Lage, Tumorzellen selektiv zu infizieren, sich darin zu replizieren und schließlich diese abzutöten. Primäre Resistenzen von Tumorzellen gegen die verfügbaren Virotherapeutika, die hauptsächlich in der Monotherapie eingesetzt werden, begrenzen jedoch die Effizienz der virusinduzierten Onkolyse. Daher besteht ein hoher klinischer Bedarf, diese virotherapeutischen Resistenzphänomene genauer zu charakterisieren und somit Wege zu finden, diese in effizienter Weise zu überwinden. Wegen des Einflusses auf die Induktion von Krebszelltod und Hemmung der Tumorproliferation sind Histon Deacetylase-Inhibitoren (HDACi) interessante Kombinationspartner für neue Therapieoptionen und könnten ein Schlüssel zur Überwindung der gegenwärtigen hochgradigen Tumorzellresistenzen gegen die derzeit verfügbaren Virotherapeutika sein. Frühere Studien haben vielversprechende Ergebnisse in Bezug auf Virotherapeutika als auch auf epigenetische Wirkstoffe gezeigt, sowohl in Mono- als auch in Kombinationstherapie.

Das Ziel dieser Arbeit war es, ein kombiniertes Anwendungsschema von Vaccinia Virus GLV-1h68 und verschiedenen HDACi-Wirkstoffen wie Resveratrol, Kaempferol (beides Naturstoffe) oder SAHA (Suberylanilid Hydroxamsäure, ein von der FDA zugelassener HDACi-Wirkstoff) an vier verschiedenen Karzinomzelllinien, drei kolorektalen und einer Nierenadenokarzinomzelllinie, zu erarbeiten. Ein weiteres Ziel bestand darin, zu bestimmen, ob die oben genannten HDACi-Verbindungen die Wirksamkeit von VACV GLV-1h68 in infektionsresistenten Krebszelllinien erhöhen können. Geeignete Konzentrationen jedes Wirkstoffs wurden nun in einem Vortest

bestimmt. Anschließend wurden die Viabilität der Zellen, die Tumorzellproliferation und die onkolytischen Effekte in einer Kombinationsbehandlung durch Viabilitäts-Assays (Sulforhodamin B und CellTiter-Blue), Quantifizierung der Freisetzung von Lactatdehydrogenase (LDH) sowie durch Echtzeitüberwachung des Tumorzellwachstums analysiert. Um mögliche Auswirkungen auf die Virusreplikation genauer zu untersuchen, wurden Viruswachstumskurven durchgeführt. Schließlich wurden auch die Zellzyklusanalyse, die Flächenberechnung der Wells und eine umfassende Fluoreszenzmikroskopie durchgeführt.

Unsere Ergebnisse zeigen, dass die gleichzeitige Behandlung von HDACi-Wirkstoffen mit dem Impfvirus GLV-1h68 einen moderaten Anstieg der zytotoxischen Wirkungen im Vergleich zu den jeweiligen Monotherapie-Behandlungen in allen untersuchten Zelllinien bewirkte. Verglichen mit der alleinigen Behandlung mit GLV-1h68, führte die Kombinationstherapie zu einer erhöhten Virus-assoziierten Expression von GFP in ACHN-, HCT-15- und HCT-116-Zellen. Dennoch variierten die zytotoxischen Effekte in allen untersuchten Zelllinien in Abhängigkeit von der durchgeführten Methode.

Die murine Zelllinie Colon-26 verhielt sich in Bezug auf die Virus-assoziierte Expression / cytotoxische Wirkung, wie sie in verschiedenen Experimenten, z. B. Flächenberechnung und Fluoreszenzüberwachung, dargestellt wurde, entgegengesetzt. Hier sollten weitere Untersuchungen durchgeführt werden, um die Ursache für die oben genannten Effekte zu identifizieren. Darüber hinaus zeigte sich in dieser Studie der Wirkstoff SAHA im Vergleich zu den anderen epigenetischen Wirkstoffen als am effektivsten.

Zusammenfassend zeigen unsere Daten, dass epigenetische Wirkstoffe wie Resveratrol, Kaempferol und SAHA in der Lage sind, die Wirksamkeit von VACV GLV1-h68 in teilweise oder hochgradig resistenten Tumorzelllinien im Vergleich zu jedem der monotherapeutischen Ansätze weiter zu erhöhen. Die Induktion immunstimulierender Effekte durch die epigenetischen Wirkstoffe könnte zu einer weiteren Verbesserung der zytotoxischen Wirkung bei

Krebspatienten führen. Diese Befunde können ein enormes klinisches Potential für die Behandlung von humanen Kolorektal- und / oder Nierenzellkarzinomen sowie anderen soliden Tumoren haben und sollten in zukünftigen klinischen Studien weiter getestet werden.

6. Index of Abbreviations

ACHN	Renal Cell Carcinoma cell line
BF	Bright-field microscopy
BFGF	Basic fibroblast growth factor
CD8+ T cells	Cytotoxic T lymphocyte
CI	Cell index
CMC	Carboxymethyl cellulose
CO_2	Carbon dioxide
Colon-26	Colon adenocarcinoma cell line
CpG	Cytosine-guanosine dinucleotide sites
CRC	Colorectal cancer
CV-1	African green monkey kidney fibroblast cell line
ddH_2O	Double-destilled water
DMEM	Dulbecco's modified Eagle medium
DMEM-10	DMEM supplemented with 10 % FBS
DMEM-2	DMEM supplemented with 2 % FBS
DMSO	Dimethylesulfoxide
DNA	Deoxyribonucleic acid
DNMT	DNA methyltransferases
EDTA-trypsin	Ethylendiamintetraacetatic acid-trypsin
EEV	Extracellular enveloped virus
EGFR	Epidermal growth factor receptor
FACS	Fluorescence Activated Cell Sorting
FBS	Fetal bovine serum

FDA	US Food and Drug Administration (FDA)
g	gram
GFP	Green fluorescent protein
GLV-1h68	Vaccinia vaccine virus
GL-ONC1	proprietary name of GMP-derived material of GLV-1h68
h	Hour(s)
H_2O	Water
HAT	Histone acetyltransferases
HCl	Hydrogen chloride
HCT-116	Colon carcinoma cell line
HCT-15	Colon adenocarcinoma cell line
HDAC	Histone deacetylases
HDACi	Histone deacetylase inhibitor(s)
HIF1-α	Hypoxia-inducible factor 1-alpha
HIV	Human immunodeficiency virus
hpi	Hours post infection
HSV	Herpes simplex virus
IFN	Interferon
IL-6	Interleukin 6
KMF	Kaempferol
kbp	Kilo-base pair
lacZ	Gene that encodes for β-galactosidase
LDH	Lactate dehydrogenase
LIVP	Lister strain from the Institute for Research on Viral Preparations

MDR-1	Multidrug resistance protein-1
mg	Milligram
ml	Milliliter
mM	Millimolar
MOI	Multiplicity of infection
MTT	3-(4,5-dimethylthiazol-2-yl)-2,5-diphenyl tetrazolium bromide
NAD^+	Nicotinamide adenine dinucleotide $_{ox}$
NADH	Nicotinamide adenine dinucleotide $_{red}$
NCI	US National Cancer Institute
NF-κB	Nuclear factor 'kappa-light-chain-enhancer' of activated B-cells
NK cells	Natural killer cells
nm	nanometer
NSCLC	Non-small-cell lung carcinoma
OD	Optical density
OV	Oncolytic virotherapy
PBS	Dulbecco's phosphate buffered saline
PD-1	Programmed cell death protein 1
PFU	Plaque forming units
PI	Propidium iodide
png	Portable network graphics
RCC	Renal cell carcinoma
RV	Resveratrol
RNA	Ribonucleic acid
RNAse	Ribonuclease
rpm	Rounds per minute

RT	Room temperature
RUC-GFP	Renilla Luciferase green fluorescent protein fusion gene
SAHA	Suberanilide hydroxamic acid
SD	Standard deviation
Sir2	Silent information regulator 2
SRB	Sulforhodamine B
TCA	Trichloroacetic acid
tk	thymidine kinase
TRIS	Trishydroxymethylaminomethane
Triton X-100	Nonionic detergent
TSA	Trichostatin A
U/l	Units/liter
UV	Ultra violet
v/v	Volume per volume
VACV	Vaccinia virus
VEGF	Vascular endothelial growth factor
VPA	Valproic acid
VSV	Vesicular stomatitis Indiana virus
w/v	Weight per volume
WHO	World Health Organization
WR	Western Reserve
° C	Degree Celsius
µM	micromolar
5-FU	fluorouracil

7. List of figures

8. List of tables

9. References

1. Stewart, B.W., et al., *World cancer report 2014*. 2014, Lyon, France. Geneva, Switzerland: International Agency for Research on Cancer. WHO Press. xiv, 630 pages.
2. Hanahan, D. and R.A. Weinberg, *The hallmarks of cancer.* Cell, 2000. **100**(1): p. 57-70.
3. Jones, P.A. and S.B. Baylin, *The epigenomics of cancer.* Cell, 2007. **128**(4): p. 683-92.
4. Chen, N.G., et al., *Oncolytic viruses.* Adv Virol, 2012. **2012**: p. 320206.
5. Siegel, R.L., K.D. Miller, and A. Jemal, *Cancer statistics, 2016.* CA Cancer J Clin, 2016. **66**(1): p. 7-30.
6. Chan, A.T. and E.L. Giovannucci, *Primary prevention of colorectal cancer.* Gastroenterology, 2010. **138**(6): p. 2029-2043 e10.
7. Johnson, C.M., et al., *Meta-analyses of colorectal cancer risk factors.* Cancer Causes Control, 2013. **24**(6): p. 1207-22.
8. Kufe, D.W., et al., *Cancer medicine 6*. 6th ed. 2003, Hamilton, Ont. ; Lewiston, NY: BC Decker.
9. Wolpin, B.M. and R.J. Mayer, *Systemic treatment of colorectal cancer.* Gastroenterology, 2008. **134**(5): p. 1296-310.
10. Klatte, T., et al., *Tumor size does not predict risk of metastatic disease or prognosis of small renal cell carcinomas.* J Urol, 2008. **179**(5): p. 1719-26.
11. B. Ljungberg, C., L. Albiges, K. Bensalah, A. Bex (Vice-chair), R.H. Giles (Patient Advocate), M. Hora, M.A. Kuczyk, T. Lam, L.Marconi, A.S. Merseburger, T. Powles, M. Staehler, A. VolpeGuidelines Associates: S. Dabestani, S. Fernandez-Pello Montes,F. Hofmann, R. Tahbaz *2017 Renal Cell Cancer EAU Guidelines*. 2017.
12. Leibovich, B.C., et al., *Histological subtype is an independent predictor of outcome for patients with renal cell carcinoma.* J Urol, 2010. **183**(4): p. 1309-15.
13. Rojas, J.J. and S.H. Thorne, *Theranostic potential of oncolytic vaccinia virus.* Theranostics, 2012. **2**(4): p. 363-73.
14. Bluming, A.Z. and J.L. Ziegler, *Regression of Burkitt's lymphoma in association with measles infection.* Lancet, 1971. **2**(7715): p. 105-6.
15. Dock, G., L. Brothers, and Company, *The Influence of Complicating Diseases Upon Leukaemia*. 1904: Lea Brothers & Company.
16. Hansen, R.M. and J.A. Libnoch, *Remission of chronic lymphocytic leukemia after smallpox vaccination.* Arch Intern Med, 1978. **138**(7): p. 1137-8.
17. Greentree, L.B., *Hodgkin's disease: therapeutic role of measles vaccine.* Am J Med, 1983. **75**(6): p. 928.
18. Yap, T.A., et al., *Reovirus therapy in cancer: has the orphan virus found a home?* Expert Opin Investig Drugs, 2008. **17**(12): p. 1925-35.
19. Schirrmacher, V., et al., *Immunization with virus-modified tumor cells.* Semin Oncol, 1998. **25**(6): p. 677-96.
20. Diaz, R.M., et al., *Oncolytic immunovirotherapy for melanoma using vesicular stomatitis virus.* Cancer Res, 2007. **67**(6): p. 2840-8.

21. Roberts, M.S., et al., *Naturally oncolytic viruses.* Curr Opin Mol Ther, 2006. **8**(4): p. 314-21.
22. Grote, D., et al., *Live attenuated measles virus induces regression of human lymphoma xenografts in immunodeficient mice.* Blood, 2001. **97**(12): p. 3746-54.
23. Liu, T.C., E. Galanis, and D. Kirn, *Clinical trial results with oncolytic virotherapy: a century of promise, a decade of progress.* Nat Clin Pract Oncol, 2007. **4**(2): p. 101-17.
24. Ferguson, M.S., N.R. Lemoine, and Y. Wang, *Systemic delivery of oncolytic viruses: hopes and hurdles.* Adv Virol, 2012. **2012**: p. 805629.
25. Naik, S. and S.J. Russell, *Engineering oncolytic viruses to exploit tumor specific defects in innate immune signaling pathways.* Expert Opin Biol Ther, 2009. **9**(9): p. 1163-76.
26. Clemens, M.J. and M.A. McNurlan, *Regulation of cell proliferation and differentiation by interferons.* Biochem J, 1985. **226**(2): p. 345-60.
27. Colamonici, O.R., et al., *Correlation between interferon (IFN) alpha resistance and deletion of the IFN alpha/beta genes in acute leukemia cell lines suggests selection against the IFN system.* Blood, 1992. **80**(3): p. 744-9.
28. Haralambieva, I., et al., *Engineering oncolytic measles virus to circumvent the intracellular innate immune response.* Mol Ther, 2007. **15**(3): p. 588-97.
29. Stojdl, D.F., et al., *Exploiting tumor-specific defects in the interferon pathway with a previously unknown oncolytic virus.* Nat Med, 2000. **6**(7): p. 821-5.
30. Errington, F., et al., *Reovirus activates human dendritic cells to promote innate antitumor immunity.* J Immunol, 2008. **180**(9): p. 6018-26.
31. Prestwich, R.J., et al., *Oncolytic viruses: a novel form of immunotherapy.* Expert Rev Anticancer Ther, 2008. **8**(10): p. 1581-8.
32. Cattaneo, R., et al., *Reprogrammed viruses as cancer therapeutics: targeted, armed and shielded.* Nat Rev Microbiol, 2008. **6**(7): p. 529-40.
33. Coukos, G., et al., *Oncolytic herpes simplex virus-1 lacking ICP34.5 induces p53-independent death and is efficacious against chemotherapy-resistant ovarian cancer.* Clin Cancer Res, 2000. **6**(8): p. 3342-53.
34. Cripe, T.P., et al., *Targeting cancer-initiating cells with oncolytic viruses.* Mol Ther, 2009. **17**(10): p. 1677-82.
35. Mahller, Y.Y., et al., *Neuroblastoma cell lines contain pluripotent tumor initiating cells that are susceptible to a targeted oncolytic virus.* PLoS One, 2009. **4**(1): p. e4235.
36. Kirn, D.H. and S.H. Thorne, *Targeted and armed oncolytic poxviruses: a novel multi-mechanistic therapeutic class for cancer.* Nat Rev Cancer, 2009. **9**(1): p. 64-71.
37. Reid, T., et al., *Hepatic arterial infusion of a replication-selective oncolytic adenovirus (dl1520): phase II viral, immunologic, and clinical endpoints.* Cancer Res, 2002. **62**(21): p. 6070-9.

38. Ong, H.T., et al., *Evaluation of T cells as carriers for systemic measles virotherapy in the presence of antiviral antibodies.* Gene Ther, 2007. **14**(4): p. 324-33.
39. White, C.L., et al., *Characterization of the adaptive and innate immune response to intravenous oncolytic reovirus (Dearing type 3) during a phase I clinical trial.* Gene Ther, 2008. **15**(12): p. 911-20.
40. Russell, S.J., K.W. Peng, and J.C. Bell, *Oncolytic virotherapy.* Nat Biotechnol, 2012. **30**(7): p. 658-70.
41. Gnant, M.F., et al., *Systemic administration of a recombinant vaccinia virus expressing the cytosine deaminase gene and subsequent treatment with 5-fluorocytosine leads to tumor-specific gene expression and prolongation of survival in mice.* Cancer Res, 1999. **59**(14): p. 3396-403.
42. Ottolino-Perry, K., et al., *Intelligent design: combination therapy with oncolytic viruses.* Mol Ther, 2010. **18**(2): p. 251-63.
43. MacTavish, H., et al., *Enhancement of vaccinia virus based oncolysis with histone deacetylase inhibitors.* PLoS One, 2010. **5**(12): p. e14462.
44. Nguyen, T.L., et al., *Chemical targeting of the innate antiviral response by histone deacetylase inhibitors renders refractory cancers sensitive to viral oncolysis.* Proc Natl Acad Sci U S A, 2008. **105**(39): p. 14981-6.
45. Meyers, D.E., et al., *Current Immunotherapeutic Strategies to Enhance Oncolytic Virotherapy.* Front Oncol, 2017. **7**: p. 114.
46. Baxby, D., *Poxviruses*, in *Medical Microbiology*, S. Baron, Editor. 1996: Galveston (TX).
47. Jenner, E., *Edward Jenner. his Life. his Work, and his Writings.* Br Med J, 1902. **2**(2166): p. 1-17.
48. Fenner, F., *Smallpox and its eradication*. History of international public health. 1988, Geneva: World Health Organization. xvi, 1460 p.
49. Sanchez-Sampedro, L., et al., *The evolution of poxvirus vaccines.* Viruses, 2015. **7**(4): p. 1726-803.
50. Le Boeuf, F. and J.C. Bell, *United virus: the oncolytic tag-team against cancer!* Cytokine Growth Factor Rev, 2010. **21**(2-3): p. 205-11.
51. Moss, B. and P.L. Earl, *Overview of the vaccinia virus expression system.* Curr Protoc Protein Sci, 2001. **Chapter 5**: p. Unit5 11.
52. Puhlmann, M., et al., *Thymidine kinase-deleted vaccinia virus expressing purine nucleoside phosphorylase as a vector for tumor-directed gene therapy.* Hum Gene Ther, 1999. **10**(4): p. 649-57.
53. Zeh, H.J. and D.L. Bartlett, *Development of a replication-selective, oncolytic poxvirus for the treatment of human cancers.* Cancer Gene Ther, 2002. **9**(12): p. 1001-12.
54. Buller, R.M., et al., *Decreased virulence of recombinant vaccinia virus expression vectors is associated with a thymidine kinase-negative phenotype.* Nature, 1985. **317**(6040): p. 813-5.
55. Vanderplasschen, A., et al., *Extracellular enveloped vaccinia virus is resistant to complement because of incorporation of host complement control proteins into its envelope.* Proc Natl Acad Sci U S A, 1998. **95**(13): p. 7544-9.

56. McCart, J.A., et al., *Systemic cancer therapy with a tumor-selective vaccinia virus mutant lacking thymidine kinase and vaccinia growth factor genes.* Cancer Res, 2001. **61**(24): p. 8751-7.
57. Thorne, S.H., et al., *Rational strain selection and engineering creates a broad-spectrum, systemically effective oncolytic poxvirus, JX-963.* J Clin Invest, 2007. **117**(11): p. 3350-8.
58. Moss, B., *Poxvirus DNA replication.* Cold Spring Harb Perspect Biol, 2013. **5**(9).
59. Cono, J., et al., *Smallpox vaccination and adverse reactions. Guidance for clinicians.* MMWR Recomm Rep, 2003. **52**(RR-4): p. 1-28.
60. De Clercq, E., *Cidofovir in the treatment of poxvirus infections.* Antiviral Res, 2002. **55**(1): p. 1-13.
61. Reeves, P.M., et al., *Disabling poxvirus pathogenesis by inhibition of Abl-family tyrosine kinases.* Nat Med, 2005. **11**(7): p. 731-9.
62. Yang, G., et al., *An orally bioavailable antipoxvirus compound (ST-246) inhibits extracellular virus formation and protects mice from lethal orthopoxvirus Challenge.* J Virol, 2005. **79**(20): p. 13139-49.
63. Zhang, Q., et al., *Eradication of solid human breast tumors in nude mice with an intravenously injected light-emitting oncolytic vaccinia virus.* Cancer Res, 2007. **67**(20): p. 10038-46.
64. Felsenfeld, G. and M. Groudine, *Controlling the double helix.* Nature, 2003. **421**(6921): p. 448-53.
65. Dasso, M., S. Dimitrov, and A.P. Wolffe, *Nuclear assembly is independent of linker histones.* Proc Natl Acad Sci U S A, 1994. **91**(26): p. 12477-81.
66. Harp, J.M., et al., *Asymmetries in the nucleosome core particle at 2.5 A resolution.* Acta Crystallogr D Biol Crystallogr, 2000. **56**(Pt 12): p. 1513-34.
67. Kornberg, R.D., *Structure of chromatin.* Annu Rev Biochem, 1977. **46**: p. 931-54.
68. Jenuwein, T. and C.D. Allis, *Translating the histone code.* Science, 2001. **293**(5532): p. 1074-80.
69. Waddington, C.H., *The epigenotype. 1942.* Int J Epidemiol, 2012. **41**(1): p. 10-3.
70. Holliday, R., *DNA methylation and epigenetic inheritance.* Philos Trans R Soc Lond B Biol Sci, 1990. **326**(1235): p. 329-38.
71. Russo, V.E.A., R.A. Martienssen, and A.D. Riggs, *Epigenetic mechanisms of gene regulation*. Cold Spring Harbor monograph series,. 1996, Plainview, N.Y.: Cold Spring Harbor Laboratory Press. xii, 692 p.
72. Turner, B.M., *Histone acetylation and an epigenetic code.* Bioessays, 2000. **22**(9): p. 836-45.
73. Turner, B.M., *Defining an epigenetic code.* Nat Cell Biol, 2007. **9**(1): p. 2-6.
74. Baylin, S.B., *DNA methylation and gene silencing in cancer.* Nat Clin Pract Oncol, 2005. **2 Suppl 1**: p. S4-11.
75. Ellis, L., P.W. Atadja, and R.W. Johnstone, *Epigenetics in cancer: targeting chromatin modifications.* Mol Cancer Ther, 2009. **8**(6): p. 1409-20.

76. Esteller, M., *DNA methylation and cancer therapy: new developments and expectations.* Curr Opin Oncol, 2005. **17**(1): p. 55-60.
77. Esteller, M., *Epigenetics in cancer.* N Engl J Med, 2008. **358**(11): p. 1148-59.
78. Acharya, M.R., et al., *Rational development of histone deacetylase inhibitors as anticancer agents: a review.* Mol Pharmacol, 2005. **68**(4): p. 917-32.
79. Kouzarides, T., *Histone acetylases and deacetylases in cell proliferation.* Curr Opin Genet Dev, 1999. **9**(1): p. 40-8.
80. Mahlknecht, U. and D. Hoelzer, *Histone acetylation modifiers in the pathogenesis of malignant disease.* Mol Med, 2000. **6**(8): p. 623-44.
81. Minucci, S. and P.G. Pelicci, *Histone deacetylase inhibitors and the promise of epigenetic (and more) treatments for cancer.* Nat Rev Cancer, 2006. **6**(1): p. 38-51.
82. Choi, J.H., et al., *Expression profile of histone deacetylase 1 in gastric cancer tissues.* Jpn J Cancer Res, 2001. **92**(12): p. 1300-4.
83. Halkidou, K., et al., *Upregulation and nuclear recruitment of HDAC1 in hormone refractory prostate cancer.* Prostate, 2004. **59**(2): p. 177-89.
84. Zhu, P., et al., *Induction of HDAC2 expression upon loss of APC in colorectal tumorigenesis.* Cancer Cell, 2004. **5**(5): p. 455-63.
85. Witt, O., et al., *HDAC family: What are the cancer relevant targets?* Cancer Lett, 2009. **277**(1): p. 8-21.
86. Thiagalingam, S., et al., *Histone deacetylases: unique players in shaping the epigenetic histone code.* Ann N Y Acad Sci, 2003. **983**: p. 84-100.
87. Martin, C. and Y. Zhang, *The diverse functions of histone lysine methylation.* Nat Rev Mol Cell Biol, 2005. **6**(11): p. 838-49.
88. Zhang, Y. and D. Reinberg, *Transcription regulation by histone methylation: interplay between different covalent modifications of the core histone tails.* Genes Dev, 2001. **15**(18): p. 2343-60.
89. Lindemann, R.K., B. Gabrielli, and R.W. Johnstone, *Histone-deacetylase inhibitors for the treatment of cancer.* Cell Cycle, 2004. **3**(6): p. 779-88.
90. Bolden, J.E., M.J. Peart, and R.W. Johnstone, *Anticancer activities of histone deacetylase inhibitors.* Nat Rev Drug Discov, 2006. **5**(9): p. 769-84.
91. Richon, V.M., et al., *A class of hybrid polar inducers of transformed cell differentiation inhibits histone deacetylases.* Proc Natl Acad Sci U S A, 1998. **95**(6): p. 3003-7.
92. Kramer, O.H., M. Gottlicher, and T. Heinzel, *Histone deacetylase as a therapeutic target.* Trends Endocrinol Metab, 2001. **12**(7): p. 294-300.
93. Marks, P.A. and W.S. Xu, *Histone deacetylase inhibitors: Potential in cancer therapy.* J Cell Biochem, 2009. **107**(4): p. 600-8.
94. Qian, D.Z., et al., *Targeting tumor angiogenesis with histone deacetylase inhibitors: the hydroxamic acid derivative LBH589.* Clin Cancer Res, 2006. **12**(2): p. 634-42.
95. Johnstone, R.W., *Histone-deacetylase inhibitors: novel drugs for the treatment of cancer.* Nat Rev Drug Discov, 2002. **1**(4): p. 287-99.

96. Peart, M.J., et al., *Identification and functional significance of genes regulated by structurally different histone deacetylase inhibitors.* Proc Natl Acad Sci U S A, 2005. **102**(10): p. 3697-702.
97. Kim, J.H., J.H. Shin, and I.H. Kim, *Susceptibility and radiosensitization of human glioblastoma cells to trichostatin A, a histone deacetylase inhibitor.* Int J Radiat Oncol Biol Phys, 2004. **59**(4): p. 1174-80.
98. Yu, C., et al., *Histone deacetylase inhibitors promote STI571-mediated apoptosis in STI571-sensitive and -resistant Bcr/Abl+ human myeloid leukemia cells.* Cancer Res, 2003. **63**(9): p. 2118-26.
99. Yu, C., et al., *The proteasome inhibitor bortezomib interacts synergistically with histone deacetylase inhibitors to induce apoptosis in Bcr/Abl+ cells sensitive and resistant to STI571.* Blood, 2003. **102**(10): p. 3765-74.
100. Sanders, T.H., R.W. McMichael, Jr., and K.W. Hendrix, *Occurrence of resveratrol in edible peanuts.* J Agric Food Chem, 2000. **48**(4): p. 1243-6.
101. Lyons, M.M., et al., *Resveratrol in raw and baked blueberries and bilberries.* J Agric Food Chem, 2003. **51**(20): p. 5867-70.
102. Soleas, G.J., E.P. Diamandis, and D.M. Goldberg, *Resveratrol: a molecule whose time has come? And gone?* Clin Biochem, 1997. **30**(2): p. 91-113.
103. Gronbaek, M.N., et al., *[Beer, wine, spirits and mortality. Results from a prospective population study].* Ugeskr Laeger, 2001. **163**(21): p. 2946-9.
104. Kopp, P., *Resveratrol, a phytoestrogen found in red wine. A possible explanation for the conundrum of the 'French paradox'?* Eur J Endocrinol, 1998. **138**(6): p. 619-20.
105. Renaud, S. and M. de Lorgeril, *Wine, alcohol, platelets, and the French paradox for coronary heart disease.* Lancet, 1992. **339**(8808): p. 1523-6.
106. Csiszar, A., *Anti-inflammatory effects of resveratrol: possible role in prevention of age-related cardiovascular disease.* Ann N Y Acad Sci, 2011. **1215**: p. 117-22.
107. Ungvari, Z., et al., *Resveratrol increases vascular oxidative stress resistance.* Am J Physiol Heart Circ Physiol, 2007. **292**(5): p. H2417-24.
108. Jang, M., et al., *Cancer chemopreventive activity of resveratrol, a natural product derived from grapes.* Science, 1997. **275**(5297): p. 218-20.
109. Park, S.J., et al., *Resveratrol ameliorates aging-related metabolic phenotypes by inhibiting cAMP phosphodiesterases.* Cell, 2012. **148**(3): p. 421-33.
110. Vingtdeux, V., et al., *AMP-activated protein kinase signaling activation by resveratrol modulates amyloid-beta peptide metabolism.* J Biol Chem, 2010. **285**(12): p. 9100-13.
111. Csaki, C., A. Mobasheri, and M. Shakibaei, *Synergistic chondroprotective effects of curcumin and resveratrol in human articular chondrocytes: inhibition of IL-1beta-induced NF-kappaB-mediated inflammation and apoptosis.* Arthritis Res Ther, 2009. **11**(6): p. R165.
112. Howitz, K.T., et al., *Small molecule activators of sirtuins extend Saccharomyces cerevisiae lifespan.* Nature, 2003. **425**(6954): p. 191-6.
113. Walle, T., et al., *High absorption but very low bioavailability of oral resveratrol in humans.* Drug Metab Dispos, 2004. **32**(12): p. 1377-82.

114. Biasutto, L., et al., *Resveratrol derivatives as a pharmacological tool.* Ann N Y Acad Sci, 2017.
115. Hodek, P., P. Trefil, and M. Stiborova, *Flavonoids-potent and versatile biologically active compounds interacting with cytochromes P450.* Chem Biol Interact, 2002. **139**(1): p. 1-21.
116. Bajpai, M., et al., *Phenolic contents and antioxidant activity of some food and medicinal plants.* Int J Food Sci Nutr, 2005. **56**(4): p. 287-91.
117. DuPont, M.S., et al., *Absorption of kaempferol from endive, a source of kaempferol-3-glucuronide, in humans.* Eur J Clin Nutr, 2004. **58**(6): p. 947-54.
118. Jaganathan, S.K. and M. Mandal, *Antiproliferative effects of honey and of its polyphenols: a review.* J Biomed Biotechnol, 2009. **2009**: p. 830616.
119. Park, J.S., et al., *Enzymatic preparation of kaempferol from green tea seed and its antioxidant activity.* J Agric Food Chem, 2006. **54**(8): p. 2951-6.
120. Slimestad, R., T. Fossen, and M.J. Verheul, *The flavonoids of tomatoes.* J Agric Food Chem, 2008. **56**(7): p. 2436-41.
121. Zhang, Y., et al., *Isolation and identification of strawberry phenolics with antioxidant and human cancer cell antiproliferative properties.* J Agric Food Chem, 2008. **56**(3): p. 670-5.
122. De Leo, M., et al., *Antiproliferative activity of Pteleopsis suberosa leaf extract and its flavonoid components in human prostate carcinoma cells.* Planta Med, 2006. **72**(7): p. 604-10.
123. Kim, K.S., et al., *Ginkgo biloba extract (EGb 761) induces apoptosis by the activation of caspase-3 in oral cavity cancer cells.* Oral Oncol, 2005. **41**(4): p. 383-9.
124. Leung, H.W., et al., *Kaempferol induces apoptosis in human lung non-small carcinoma cells accompanied by an induction of antioxidant enzymes.* Food Chem Toxicol, 2007. **45**(10): p. 2005-13.
125. Marfe, G., et al., *Kaempferol induces apoptosis in two different cell lines via Akt inactivation, Bax and SIRT3 activation, and mitochondrial dysfunction.* J Cell Biochem, 2009. **106**(4): p. 643-50.
126. Mutoh, M., et al., *Suppression of cyclooxygenase-2 promoter-dependent transcriptional activity in colon cancer cells by chemopreventive agents with a resorcin-type structure.* Carcinogenesis, 2000. **21**(5): p. 959-63.
127. Lopez-Sanchez, C., et al., *Blood micromolar concentrations of kaempferol afford protection against ischemia/reperfusion-induced damage in rat brain.* Brain Res, 2007. **1182**: p. 123-37.
128. Butler, L.M., et al., *Suberoylanilide hydroxamic acid, an inhibitor of histone deacetylase, suppresses the growth of prostate cancer cells in vitro and in vivo.* Cancer Res, 2000. **60**(18): p. 5165-70.
129. Hsu, C.C., et al., *Suberoylanilide hydroxamic acid represses glioma stem-like cells.* J Biomed Sci, 2016. **23**(1): p. 81.
130. Hodges-Gallagher, L., et al., *Inhibition of histone deacetylase enhances the anti-proliferative action of antiestrogens on breast cancer cells and blocks tamoxifen-induced proliferation of uterine cells.* Breast Cancer Res Treat, 2007. **105**(3): p. 297-309.

131. Garcia-Manero, G., et al., *Phase 1 study of the histone deacetylase inhibitor vorinostat (suberoylanilide hydroxamic acid [SAHA]) in patients with advanced leukemias and myelodysplastic syndromes.* Blood, 2008. **111**(3): p. 1060-6.
132. Ramalingam, S.S., et al., *Carboplatin and Paclitaxel in combination with either vorinostat or placebo for first-line therapy of advanced non-small-cell lung cancer.* J Clin Oncol, 2010. **28**(1): p. 56-62.
133. Archin, N.M., et al., *Interval dosing with the HDAC inhibitor vorinostat effectively reverses HIV latency.* J Clin Invest, 2017.
134. Contreras, X., et al., *Suberoylanilide hydroxamic acid reactivates HIV from latently infected cells.* J Biol Chem, 2009. **284**(11): p. 6782-9.
135. Kelly, W.K., et al., *Phase I study of an oral histone deacetylase inhibitor, suberoylanilide hydroxamic acid, in patients with advanced cancer.* J Clin Oncol, 2005. **23**(17): p. 3923-31.
136. Kelly, W.K. and P.A. Marks, *Drug insight: Histone deacetylase inhibitors--development of the new targeted anticancer agent suberoylanilide hydroxamic acid.* Nat Clin Pract Oncol, 2005. **2**(3): p. 150-7.
137. Dashwood, R.H., M.C. Myzak, and E. Ho, *Dietary HDAC inhibitors: time to rethink weak ligands in cancer chemoprevention?* Carcinogenesis, 2006. **27**(2): p. 344-9.
138. Eager, R.M. and J. Nemunaitis, *Clinical development directions in oncolytic viral therapy.* Cancer Gene Ther, 2011. **18**(5): p. 305-17.
139. Harrington, K.J., et al., *Phase I/II study of oncolytic HSV GM-CSF in combination with radiotherapy and cisplatin in untreated stage III/IV squamous cell cancer of the head and neck.* Clin Cancer Res, 2010. **16**(15): p. 4005-15.
140. Harrington, K.J., et al., *Clinical trials with oncolytic reovirus: moving beyond phase I into combinations with standard therapeutics.* Cytokine Growth Factor Rev, 2010. **21**(2-3): p. 91-8.
141. Heo, J., et al., *Sequential therapy with JX-594, a targeted oncolytic poxvirus, followed by sorafenib in hepatocellular carcinoma: preclinical and clinical demonstration of combination efficacy.* Mol Ther, 2011. **19**(6): p. 1170-9.
142. Köllhofer, L., et al., *Improvement of therapeutic anti-cancer strategies by combination of oncolytic vaccinia virus GLV-1h68 with epigenetically modulating agents.* Z Gastroenterol, 2014. **52**(08).
143. Baust, J.G., D. Gao, and J.M. Baust, *Cryopreservation: An emerging paradigm change.* Organogenesis, 2009. **5**(3): p. 90-6.
144. Skehan, P., et al., *New colorimetric cytotoxicity assay for anticancer-drug screening.* J Natl Cancer Inst, 1990. **82**(13): p. 1107-12.
145. Moravec R, R.T., Promega Corporation, *The CellTiter-Blue cell viability assay: Monitoring cell viability using a fluorescent redox indicator dye.* Cell Notes, 2003. **5**(5): p. 3.
146. Riss T., M.R., Promega Corporation, *Simplifying Cytotoxicity Screening. Introducing CellTiter-Blue Cell Viability Assay.* Promega Notes, www.promega.com, 2003. **Number 83**: p. 10-13.

147. Mosmann, T., *Rapid colorimetric assay for cellular growth and survival: application to proliferation and cytotoxicity assays.* J Immunol Methods, 1983. **65**(1-2): p. 55-63.
148. Ulmer, D.D., B.L. Vallee, and W.E. Wacker, *Metalloenzymes and myocardial infarction. II. Malic and lactic dehydrogenase activities and zinc concentrations in serum.* N Engl J Med, 1956. **255**(10): p. 450-6.
149. Ke, N., et al., *The xCELLigence system for real-time and label-free monitoring of cell viability.* Methods Mol Biol, 2011. **740**: p. 33-43.
150. Nicoletti, I., et al., *A rapid and simple method for measuring thymocyte apoptosis by propidium iodide staining and flow cytometry.* J Immunol Methods, 1991. **139**(2): p. 271-9.
151. Ruf, B., et al., *Combination of the oral histone deacetylase inhibitor resminostat with oncolytic measles vaccine virus as a new option for epi-virotherapeutic treatment of hepatocellular carcinoma.* Mol Ther Oncolytics, 2015. **2**: p. 15019.
152. Ascierto, M.L., et al., *Permissivity of the NCI-60 cancer cell lines to oncolytic Vaccinia Virus GLV-1h68.* BMC Cancer, 2011. **11**: p. 451.
153. Ehrig, K., et al., *Growth inhibition of different human colorectal cancer xenografts after a single intravenous injection of oncolytic vaccinia virus GLV-1h68.* J Transl Med, 2013. **11**: p. 79.
154. Baek, S.J., L.C. Wilson, and T.E. Eling, *Resveratrol enhances the expression of non-steroidal anti-inflammatory drug-activated gene (NAG-1) by increasing the expression of p53.* Carcinogenesis, 2002. **23**(3): p. 425-34.
155. Feng, M., et al., *Resveratrol Treatment Inhibits Proliferation of and Induces Apoptosis in Human Colon Cancer Cells.* Med Sci Monit, 2016. **22**: p. 1101-8.
156. Fouad, M.A., et al., *Resveratrol inhibits proliferation, angiogenesis and induces apoptosis in colon cancer cells: calorie restriction is the force to the cytotoxicity.* Hum Exp Toxicol, 2013. **32**(10): p. 1067-80.
157. Li, H., et al., *2,3',4,4',5'-Pentamethoxy-trans-stilbene, a resveratrol derivative, inhibits colitis-associated colorectal carcinogenesis in mice.* Br J Pharmacol, 2010. **160**(6): p. 1352-61.
158. Li, J., et al., *Resveratrol promotes regression of renal carcinoma cells via a renin-angiotensin system suppression-dependent mechanism.* Oncol Lett, 2017. **13**(2): p. 613-620.
159. Zhang, D., et al., *Resveratrol Sensitizes Renal Cell Carcinoma Cells to Trail-Induced Apoptosis.* Journal of Urology, 2014. **191**(4): p. E376-E377.
160. Shi, T., et al., *Effects of resveratrol on gene expression in renal cell carcinoma.* Cancer Biol Ther, 2004. **3**(9): p. 882-8.
161. Tsunoda, T., et al., *Resveratrol induces luminal apoptosis of human colorectal cancer HCT116 cells in three-dimensional culture.* Anticancer Res, 2014. **34**(8): p. 4551-5.
162. Sanna, V., et al., *Single-step green synthesis and characterization of gold-conjugated polyphenol nanoparticles with antioxidant and biological activities.* Int J Nanomedicine, 2014. **9**: p. 4935-51.
163. Howells, L.M., et al., *Phase I randomised double-blind pilot study of micronized resveratrol (SRT501) in patients with hepatic metastases -*

safety, pharmacokinetics and pharmacodynamics. Cancer prevention research (Philadelphia, Pa.), 2011. **4**(9): p. 1419-1425.
164. de Vries, K., M. Strydom, and V. Steenkamp, *Bioavailability of resveratrol: Possibilities for enhancement.* Journal of Herbal Medicine, 2017.
165. Docherty, J.J., et al., *Resveratrol inhibition of herpes simplex virus replication.* Antiviral Res, 1999. **43**(3): p. 145-55.
166. Palamara, A.T., et al., *Inhibition of influenza A virus replication by resveratrol.* J Infect Dis, 2005. **191**(10): p. 1719-29.
167. Cao, S., et al., *Suppression of Poxvirus Replication by Resveratrol.* Front Microbiol, 2017. **8**: p. 2196.
168. Jaramillo-Carmona, S., et al., *Combination of Quercetin and Kaempferol enhances in vitro Cytotoxicity on Human Colon Cancer (HCT-116) Cells.* Records of Natural Products, 2014. **8**(3): p. 262-271.
169. Kalyani, C., M.L. Narasu, and Y.P. Devi, *SYNERGISTIC GROWTH INHIBITORY EFFECT OF FLAVONOL–KAEMPFEROL AND CONVENTIONAL CHEMOTHERAPEUTIC DRUGS ON CANCER CELLS.* 2017, 2017: p. 5.
170. Song, W.B., et al., *Kaempferol induces cell cycle arrest and apoptosis in renal cell carcinoma through EGFR/p38 signaling.* Oncology Reports, 2014. **31**(3): p. 1350-1356.
171. Zhou, Z.X., et al., *Pharmacokinetic evaluation of the interaction between oral kaempferol and ethanol in rats.* Acta Pharmaceutica, 2016. **66**(4): p. 563-568.
172. Amoros, M., et al., *Synergistic effect of flavones and flavonols against herpes simplex virus type 1 in cell culture. Comparison with the antiviral activity of propolis.* J Nat Prod, 1992. **55**(12): p. 1732-40.
173. Dharmendra Dave, S.W., Ashish Agrawal, Swapnil Goyal, Kaplish Dave, Santosh Singh Rana, *Antimicrobial Activity of Methanolic Extracts Of Cassia tora root.* INTERNATIONAL JOURNAL OF PHARMACEUTICAL AND BIOLOGICAL ARCHIVES, 2010. **2**(1): p. 3.
174. Dong, W., et al., *A dual character of flavonoids in influenza A virus replication and spread through modulating cell-autonomous immunity by MAPK signaling pathways.* Sci Rep, 2014. **4**: p. 7237.
175. Robin, V., et al., *Antipoliovirus flavonoids from Psiadia dentata.* Antivir Chem Chemother, 2001. **12**(5): p. 283-91.
176. Schwarz, S., et al., *Kaempferol derivatives as antiviral drugs against the 3a channel protein of coronavirus.* Planta Med, 2014. **80**(2-3): p. 177-82.
177. Bressan, A., et al., *Induction of a less aggressive phenotype in human colon carcinoma HCT116 cells by chronic exposure to HDAC inhibitor SAHA.* Oncol Rep, 2010. **24**(5): p. 1249-55.
178. Barua, I.S., et al., *PO-0976: Mechanisms of normal tissue toxicity from SAHA, an HDAC inhibitor and radiosensitizer.* Radiotherapy and Oncology. **123**: p. S540.
179. Tavares, T.S., et al., *Gene microarray analysis of human renal cell carcinoma: the effects of HDAC inhibition and retinoid treatment.* Cancer Biol Ther, 2008. **7**(10): p. 1607-18.

180. Park, K.C., et al., *The novel histone deacetylase inhibitor, N-hydroxy-7-(2-naphthylthio) hepatonomide, exhibits potent antitumor activity due to cytochrome-c-release-mediated apoptosis in renal cell carcinoma cells.* BMC Cancer, 2015. **15**: p. 19.
181. Lange, F., et al., *Biological and molecular effects of small molecule kinase inhibitors on low-passage human colorectal cancer cell lines.* Biomed Res Int, 2014. **2014**: p. 568693.
182. Boot, A., et al., *Characterization of novel low passage primary and metastatic colorectal cancer cell lines.* Oncotarget, 2016. **7**(12): p. 14499-509.
183. Norden, D.M., et al., *Storage Conditions and Passages Alter IL-6 secretion in C26 adenocarcinoma cell lines.* MethodsX, 2015. **2**: p. 53-58.
184. Pastor, D.M., et al., *Primary cell lines: false representation or model system? a comparison of four human colorectal tumors and their coordinately established cell lines.* Int J Clin Exp Med, 2010. **3**(1): p. 69-83.
185. Geraghty, R.J., et al., *Guidelines for the use of cell lines in biomedical research.* Br J Cancer, 2014. **111**(6): p. 1021-46.
186. Riss T, M.R., *Introducing the CytoTox-ONE homogeneous membrane integrity assay.* Promega Notes, www.promega.com, 2002. **82**: p. 15-18.
187. Lauer, U.M., et al., *Phase I Study of Oncolytic Vaccinia Virus GL-ONC1 in Patients with Peritoneal Carcinomatosis.* Clin Cancer Res, 2018.
188. Krug, L.M., et al., *Phase I study of intra-pleural administration of GL-ONC1, an oncolytic vaccinia virus, in patients with malignant pleural effusion.* Journal of Clinical Oncology, 2015. **33**(15_suppl): p. 7559-7559.
189. Garcia-Manero, G., et al., *Phase II trial of vorinostat with idarubicin and cytarabine for patients with newly diagnosed acute myelogenous leukemia or myelodysplastic syndrome.* J Clin Oncol, 2012. **30**(18): p. 2204-10.
190. Chang, H.M., et al., *Induction of interferon-stimulated gene expression and antiviral responses require protein deacetylase activity.* Proc Natl Acad Sci U S A, 2004. **101**(26): p. 9578-83.
191. Hongxun Wang, S.J.R., Jian Qiao., *495. Combination Therapy for Breast Cancer Using Oncolytic Viruses and Histone Deacetylase Inhibitors.* Molecular Therapy, 2010. **18**: p. S191-S192.
192. Bridle, B.W., et al., *HDAC inhibition suppresses primary immune responses, enhances secondary immune responses, and abrogates autoimmunity during tumor immunotherapy.* Mol Ther, 2013. **21**(4): p. 887-94.
193. Shulak, L., et al., *Histone deacetylase inhibitors potentiate vesicular stomatitis virus oncolysis in prostate cancer cells by modulating NF-kappaB-dependent autophagy.* J Virol, 2014. **88**(5): p. 2927-40.
194. Otsuki, A., et al., *Histone Deacetylase Inhibitors Augment Antitumor Efficacy of Herpes-based Oncolytic Viruses.* Mol Ther, 2008. **16**(9): p. 1546-1555.
195. White, M.C. and A.R. Frampton, Jr., *The histone deacetylase inhibitor valproic acid enhances equine herpesvirus type 1 (EHV-1)-mediated*

oncolysis of human glioma cells. Cancer Gene Ther, 2013. **20**(2): p. 88-93.
196. Cody, J.J., J.M. Markert, and D.R. Hurst, *Histone deacetylase inhibitors improve the replication of oncolytic herpes simplex virus in breast cancer cells.* PLoS One, 2014. **9**(3): p. e92919.
197. Wennier, S.T., J. Liu, and G. McFadden, *Bugs and drugs: oncolytic virotherapy in combination with chemotherapy.* Curr Pharm Biotechnol, 2012. **13**(9): p. 1817-33.
198. Foloppe, J., et al., *Targeted delivery of a suicide gene to human colorectal tumors by a conditionally replicating vaccinia virus.* Gene Ther, 2008. **15**(20): p. 1361-71.
199. Yu, Y.A., et al., *Regression of human pancreatic tumor xenografts in mice after a single systemic injection of recombinant vaccinia virus GLV-1h68.* Mol Cancer Ther, 2009. **8**(1): p. 141-51.
200. Bourgeois-Daigneault, M.C., et al., *Neoadjuvant oncolytic virotherapy before surgery sensitizes triple-negative breast cancer to immune checkpoint therapy.* Sci Transl Med, 2018. **10**(422).
201. Samson, A., et al., *Intravenous delivery of oncolytic reovirus to brain tumor patients immunologically primes for subsequent checkpoint blockade.* Sci Transl Med, 2018. **10**(422).
202. Nakashima, H., T. Nguyen, and E.A. Chiocca, *Combining HDAC inhibitors with oncolytic virotherapy for cancer therapy.* Oncolytic Virother, 2015. **4**: p. 183-91.
203. Flemington, E.K., *Herpesvirus lytic replication and the cell cycle: arresting new developments.* J Virol, 2001. **75**(10): p. 4475-81.

10. Publication List

10.1 Abstracts/Posters

1. L Köllhofer, J Beil, A Berger, I Smirnow, A Schenk, S Venturelli, NP Malek, T Auth, T Yu, AA Szalay, UM Lauer (2014). **Improvement of therapeutic anti-cancer strategies by combination of oncolytic vaccinia virus GLV-1h68 with epigenetically modulating agents.** *Z Gastroenterol 2014; 52 - KG178*

2. L Köllhofer, J Beil, A Berger, I Smirnow, A Schenk, NP Malek, S Berchtold, S Venturelli, Ulrich M. Lauer (2014). **Improvement of therapeutic anti-cancer strategies by combination of oncolytic vaccinia virus GLV-1h68 with the epigenetically modulating agent SAHA.** *Poster presentation at Forschungskolloqium der Medizinischen Fakultät Tübingen.*

10.2 Oral presentations

1. L Köllhofer, S Venturelli, UM Lauer (2014). **Improvement of therapeutic anti-cancer strategies by combination of oncolytic vaccinia virus GLV-1h68 with epigenetically modulating agents.** Oral presentation at *69. Jahrestagung der Deutschen Gesellschaft für Gastroenterologie, Verdauungs- und Stoffwechselkrankheiten mit Sektion Endoskopie.*

11. Erklärung zum Eigenanteil der Dissertationsschrift

Die Arbeit wurde in der Medizinischen Universitätsklinik, Abteilung für Innere Medizin VIII, Klinische Tumorbiologie, unter Betreuung von Herrn Prof. Dr. med. Ulrich M. Lauer durchgeführt.

Die Konzeption der Studie erfolgte durch Herrn Prof. Dr. med. Ulrich M. Lauer (Leiter der Forschungsgruppe „Virotherapie“) in Zusammenarbeit mit Herrn Dr. med. Dr. rer. nat. S. Venturelli (Stv. Direktor Abteilung für Vegetative und Klinische Physiologie), Frau Dr. rer. nat. J. Beil (wiss. Mitarbeiterin) und Frau Dr. med. S. Berchtold (Laborleiterin und wiss. Mitarbeiterin).

Sämtliche Versuche - mit unten stehenden Ausnahmen - wurden (nach Einarbeitung durch Frau I. Smirnow, MTA, Frau A. Schenk, MTA sowie Dr. rer. nat. M. Burkard, wiss. Mitarbeiter) von mir eigenständig durchgeführt.

Die Erstellung der Viruswachstumskurven in den Abschnitten 3.6.1.4 und 3.6.3.4 (abgebildet in den Figures 25 und 39) wurden von Frau I. Smirnow durchgeführt. Frau Dr. S. Berchtold hat die Daten für die Viruswachstumskurven ausgewertet.

Die statistische Auswertung der Experimente, mit Ausnahme der von Frau Dr. med. S. Berchtold erstellten Viruswachstumskurven, wurde eigenständig von mir durchgeführt.

Ich versichere, das Manuskript selbstständig (nach Anleitung durch Herrn Prof. Dr. med. Ulrich M. Lauer, Herrn Dr. med. Dr. rer. nat. S. Venturelli, Frau Dr. rer. nat. J. Beil und Frau Dr. med. S. Berchtold) verfasst zu haben und keine weiteren als die von mir angegebenen Quellen verwendet zu haben.

Stuttgart, den 23. April 2019

_____

Luisa Köllhofer

12. Danksagung

An erster Stelle möchte ich mich bei meinem Doktorvater Herrn Prof. Dr. med. Ulrich M. Lauer für die exzellente Betreuung und Unterstützung bedanken. Seinem persönlichen Engagement habe ich das einjährige Promotionsstipendium des Interdisziplinären Zentrums für Klinische Forschung Tübingen (IZKF) zu verdanken. Darüber hinaus danke ich ihm für die freundliche Aufnahme in seine Arbeitsgruppe, sowie seinem unermüdlichen Interesse an meiner Arbeit und den fast wöchentlichen Datenbesprechungen mit konstruktiven Anregungen während meiner experimentellen Phase.

Nicht weniger gilt mein Dank meinen insgesamt drei Betreuern, Dr. med. Dr. rer. nat. Sascha Venturelli, Dr. rer. nat. Julia Beil und Dr. med. Susanne Berchtold, die mir in jeder Situation mit bedingungsloser Hilfsbereitschaft und wertvollen Ratschlägen zur Seite standen und sich für gründliche Durchsichten von Präsentationen, Doktorarbeitskapiteln sowie den zahlreichen Besprechungen meiner Ergebnisse Zeit nahmen.

Weiterhin möchte ich mich bei der gesamten AG Lauer sowie AG Venturelli für die wunderschöne Zeit, den harmonievollen Kaffeepausen und der außerordentlichen Hilfsbereitschaft sowie Unterstützung bei zahlreichen Experimenten danken. Ein besonderer Dank gilt Frau Irina Smirnow, die mich unter effektiver Anleitung mit viel Geduld und Zeitaufwand in die Welt der Zellkulturen und Viren einführte.

Des Weiteren bedanke ich mich bei meinen Mitstreitern Verena May, Milena Meinhardt, Franziska Herster, Benjamin Ruf, Can Yurttas und Eike Binz.

Abschließend möchte ich meiner Familie sowie meinen Freunden danken, die während des Studiums und der Doktorarbeit eine unersetzbare Stütze waren und stets ein offenes Ohr für mich hatten. Mein ganz besonderer Dank aber gilt meinen Eltern, Ludwig und Ursula Köllhofer, die mir meinen bisherigen Lebensweg ermöglichten und denen ich diese Arbeit widme.